EVALUATION AND PERFORMANCE PREDICTION OF COOLING TOWER SPRAY ZONES

by

D.J. Viljoen

Thesis presented in partial fulfilment of the requirements for the degree M.Sc. Engineering at the University of Stellenbosch.

Supervisor: H.C.R. Reuter

Department of Mechanical Engineering
University of Stellenbosch
December 2006

DECLARATION

I, the undersigned, hereby declare that the work contained in this thesis is my own original work and that I have not previously in its entirety or in part submitted it at any university for a degree.

Signature:

Date:

SUMMARY

Cooling tower spray nozzle performance characteristics such as the water distribution onto the fill material, air side pressure drop, pump head, drop size distribution and heat transfer in the spray zone were investigated experimentally and theoretically. The aim was to evaluate and simulate the performance characteristics of new and existing types of cooling tower spray nozzles with emphasis on the spray zone. Two medium and two low pressure type spray nozzles were tested and the results analysed. Single nozzle water distribution data obtained from tests was used to predict the water distribution obtained from four evenly spaced nozzles by superposition. The results were compared to data obtained from corresponding four nozzle tests. Computer codes and CFD models were developed to predict the drop trajectories, water distribution, total heat transfer and pressure drop for single nozzles and four nozzle grids. This was compared to correlated data found in literature. The performance characteristics expected from an ideal nozzle was discussed and compared to actual nozzle performance characteristics.

OPSOMMING

Koeltoring sproeier-karakteristieke soos die water verdeling op die pakkings-materiaal, lugvloei drukverlies, pomphoogte, druppelgrootte verdelings en warmteoordrag in die sproeisone is eksperimenteel en teoreties ondersoek. Die doel was om sproeier-karakteristieke van nuwe en bestaande koeltoring sproeiers te evalueer en te simuleer met die klem op die sproeisone. Twee medium- en twee laedruk koeltoring sproeiers is getoets en die resultate ondersoek. Enkel sproeier water verdelings soos gemeet in toetse is gebruik om die water verdeling vir vier uniform gespasieerde sproeiers te bepaal deur middel van superposisie. Die resultate is vergelyk met ooreenstemmende vier sproeier toetse. Rekenaar kodes en BVM simulasies is ontwikkel om druppel trajekte, water verdelings, totale warmteoordrag en drukverliese vir enkel sowel as vier sproeier roosters te voorspel. Die resultate is vergelyk met gekorreleerde data gevind in die literatuur. Die sproeier-karakteristieke van ’n ideale sproeier is bespreek en vergelyk met die sproeier-karakteristieke van werklike sproeiers.

ACKNOWLEDGEMENTS

I would like to thank the following persons for their help and support:
Mr. H. Reuter for his guidance in this project.
Heinrich and Darren for their help with the experimentation, calibrations and the installation of components.
All the technical personnel for their assistance and willingness to always help with anything, especially Mr. Cobus Zietsman.
My parents, family and friends for their support and encouragement.
Darren and all the colleagues in the labs for interesting stories and “braaie”.
My heavenly father for the abilities he gave me.

TABLE OF CONTENTS

NOMENCLATURE

List of symbols

A	Area, m^2
C	Coefficient
c_p	Specific heat at constant pressure, J/kgK
c_v	Specific heat at constant volume, J/kgK
D	Diffusion coefficient, m^2/s
d	Diameter, m
F	Force, N
G	Mass velocity, kg/m^2s
g	Gravity acceleration, m/s^2
H	Head, m
h	Heat transfer coefficient, W/m^2K or Nozzle height, m
h_D	Mass transfer coefficient, m/s
h_d	Mass transfer coefficient, kg/m^2s
i	Enthalpy, J/kg
K	Pressure loss coefficient
k	Thermal conductivity, W/mK
L	Length, m or Vertical height, m or Nozzle spacing, m
m	Mass, kg
$\dot{m}$	Mass flow rate, kg/s
p	Pressure, Pa
Q	Flow rate, m^3/s or l/s, or Heat transfer rate, W
R	Gas constant, J/kgK
r	Radius, m
T	Temperature, K or ˚C
t	Time, s
U	Total internal energy, J
V	Volt,V, or Volume, m^3
v	Velocity, m/s
w	Humidity ratio, kg/kg dry air

List of Greek symbols

α	Thermal diffusivity, $k/\rho c_p$
Δ	Differential
θ	Angle, $^\circ$
μ	Dynamic viscosity, kg/ms
ρ	Density, kg/m^3
σ	Surface tension, N/m
Φ	Angle, $^\circ$
φ	Relative humidity, %

List of subscripts

a	Ambient or Air
B	Buoyancy
buc	Bucket
c	Convection
cup	Measurement cup
cyl	Measurement cylinder
D	Drag
d	Drop
f	Fluid
fr	Frontal
G	Global co-ordinate system
g	Gas
i	Inlet
L	Local co-ordinate system
m	Mean
n	Nozzle
o	Outlet
p	Pressure transducer
pl	Plenum
RR	Rosin Rammler
s	Saturation

Sm	Sauter mean
sp	Sprayer
t	Throat or Total
v	Vapour or Venturi
w	Water
wb	Wetbulb

LIST OF FIGURES

LIST OF TABLES

1. INTRODUCTION

1.1 Background

In many refrigeration, chemical, process, combustion and power generation systems, surplus heat needs to be rejected to the environment. The most efficient way to do this is to use available water from lakes, rivers and the sea to remove the process heat via a heat exchanger and then to return the water back to its source at a higher temperature. Due to environmental and conservation laws and the shortage of such natural water resources, the alternative is to reject waste heat to the atmosphere. In areas where there is sustainable water supply at reasonable cost, evaporative or wet cooling towers are generally used, whereas air cooled heat exchangers are generally used in processes where fluids of 60 ˚C or higher are to be cooled, when no make up water is available or the cost of water is too high. A combination of wet and dry cooling systems is used to save water while avoiding the high cost of fully dry-cooling systems, and to ensure relatively low process fluid temperatures where necessary.

Cooling towers can also be classified into natural and mechanical draft cooling towers. In mechanical draft cooling towers, air is either forced through the tower by a fan known as forced draft or drawn through the tower by a fan known as induced draft. Natural draft cooling towers make use of the buoyancy effect, due to the density difference between the air inside and outside the tower, to create the draft in the cooling tower thus eliminating auxiliary fan power. Natural draft cooling towers are much larger than equivalent mechanical draft cooling towers and are generally used for large plants as their life cycle costs are lower.

This thesis restricts itself to the spray nozzles used in wet cooling towers. Figure 1.1 is a schematic of a natural draft wet cooling tower. Warm cooling water from some cooling process is pumped into the tower and distributed onto the fill by the spray nozzles. Depending on the type of fill, the water then runs or trickles down through the fill section after which it falls into the pond where the water is collected and pumped back to the process plant. During this whole process the water is cooled by the air by means of convective heat and mass transfer. The drift eliminators above the

spray nozzles prevent smaller drops from being entrained into the counterflowing air leaving the cooling tower. In mechanical draft wet cooling towers, the basic principle is the same except that the draft is created by a fan. In some cooling towers the rain zone and/or spray zone height may be decreased to reduce pumping head and thus pumping costs.

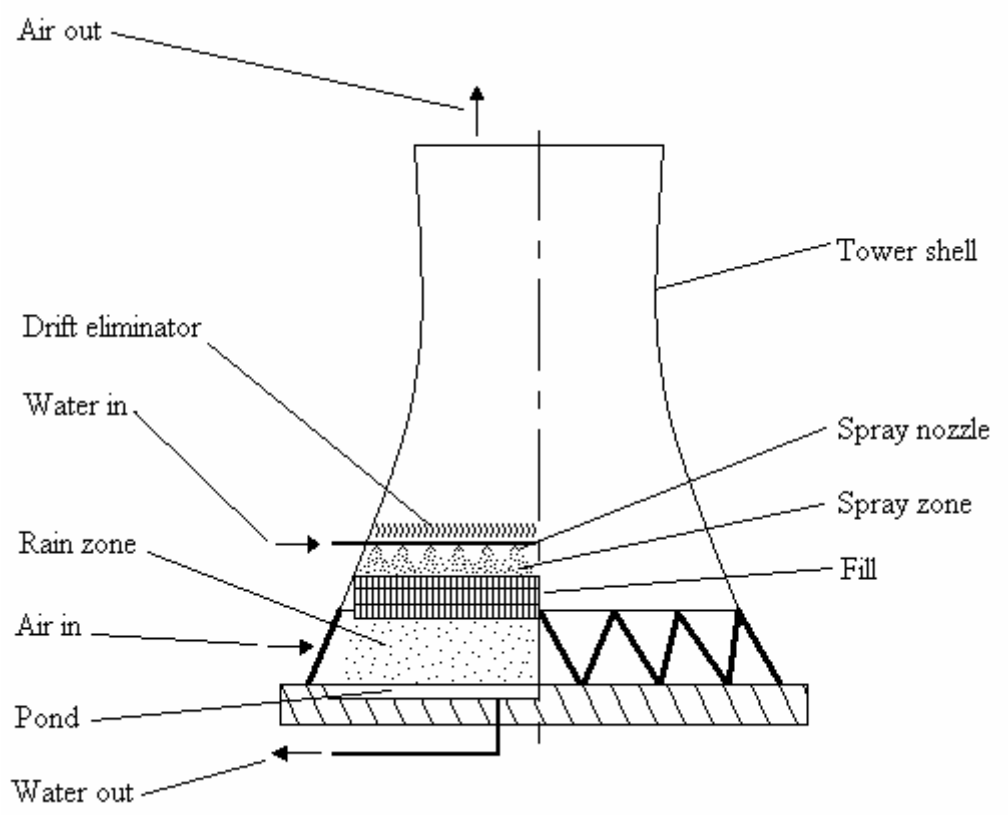

Figure 1.1 Schematic of a natural draft wet cooling tower.

In this thesis, cooling tower spray nozzle performance characteristics such as the water distribution onto the fill material, air side pressure drop, required pump head, drop size distribution and heat transfer in the spray zone are investigated experimentally and theoretically. The aim is to evaluate and simulate the performance characteristics of new and existing types of cooling tower spray nozzles with emphasis on the spray zone and not necessarily the physical design of the spray nozzles and water distribution systems.

Little is found in literature about the performance characteristics of the spray nozzles and the spray zone above the fill, although cooling towers are widely in use. This is of importance since the water distribution on the fill and drop size distribution in the

spray zone affects the performance of the cooling tower. The nozzle characteristics are influenced by different cooling tower operating conditions such as water and air flow rates as well as installation parameters such as nozzle spacing, height above the fill and direction of spray.

1.2 Objectives

In order to gain a better understanding of cooling tower spray nozzles and spray zone characteristics the following objectives were laid down for the project:

- Measure the pressure drop versus flow rate characteristic curves of different commercial spray nozzles.
- Measure the water distribution below different single nozzles and four nozzles arranged in a square grid for different nozzle heights and air and water flow rates.
- Measure the water drop size distribution of the spray generated by different nozzles.
- Develop a computer code that uses single nozzle data to predict the water distributions of four nozzles arranged in a square grid with different nozzle spacing.
- Develop a computer code to model the drop conditions at the nozzle outlet and the drop trajectories to achieve a given water distribution and to determine the heat and mass transfer between single drops and the air.
- Develop a CFD model to simulate the spray zone of wet cooling towers.
- Describe the characteristics of an ideal nozzle and compare these to the characteristics of real nozzles.

1.3 Scope of work

To meet the project objectives an experimental test set-up was built and water and drop size distributions measured for single nozzles and four nozzles arranged in a square grid under varying cooling tower operating conditions such as air and water flow rates and installation configurations such as nozzle height, spacing and direction of spray. From the experimental data the effect of these variable parameters on the

nozzle characteristics could be determined. Numerical and CFD models to simulate the spray from these nozzles were developed, based on the experimental data. The models were used to simulate different cooling tower operating conditions and installation configurations, these results were compared to corresponding experimental data to determine the validity of modelling spray nozzle characteristics numerically.

1.4 Motivation

By doing this project an improved understanding of spray nozzle characteristics in the cooling tower environment could be gained and documented to provide a basis for the development of individual spray nozzles as well as spray nozzle systems in cooling tower installations. This will help to achieve the maximum performance from the spray zone above the fill and in the cooling tower as a whole.

1.5 Literature review

According to Thacker (1997), spray nozzles used to spray the water onto the fill can be classified according to water inlet pressure. Mechanical draft cooling towers normally use medium pressure spray nozzles with pressures ranging from 15 to 100 kPa. Thacker (1997) designed a pressure-swirl or simplex atomizer. There are two basic types of pressure swirl atomizers characterized by their spray pattern on the fill, namely hollow cone and full cone nozzles. The hollow cone nozzle concentrates most of the drops on the periphery of a conical spray sheet producing a ring shaped water distribution on the fill. The full cone nozzle also produces a conical spray sheet, but produces a fairly uniform distribution of drops within the cone and onto the fill. Both the hollow and full cone nozzles use some type of swirler to set the fluid entering the nozzle from the supply pipe into a swirling motion. The spin chamber of the nozzle is conically shaped and as the diameter decreases the rotational velocity of the fluid increases. This spinning sheet then exits the nozzle through the orifice after which the sheet is broken up into drops. The full cone nozzle also has a central jet spraying down into the centre of the spinning sheet, breaking up the orderly flow of the sheet, creating a more uniform water distribution. The study focuses on the modelling and design of pressure swirl atomizers and the design parameters that influence the water

distribution and nozzle pressure drop. The designs were evaluated by measuring the nozzle pressure drop and water distribution below each nozzle.

Nonnenmacher and Piesche (2000) also simulated a hollow cone pressure swirl nozzle numerically and divide the processes involved into the following: flow inside the nozzle, sheet contour, sheet break up and ligament break up into drops. They also predicted the Sauter mean diameter of the drops produced by the nozzle. Comparing experimental data to their numerical results shows good agreement. The study focused on simulating the nozzle itself and did not simulate the spray after leaving the nozzle. A photograph of a medium pressure full cone spray nozzle is shown in Figure G.1.

Natural draft cooling towers generally use low pressure spray nozzles for pressures ranging from 5 to 15 kPa to minimise pumping head. Tognotti et al. (1991) discusses the drop break up process of a few low pressure nozzles. These low pressure nozzles spray a central jet of water onto a nozzle or diffuser plate. These nozzle plates are shaped to form consecutive cones or parturitions and have apertures which cut and break up the liquid sheet to form ligaments and water drops. They measured Sauter mean diameters between 4 to 6.5 mm for these nozzles. Figure G.1 and G.2 shows photographs of low pressure spray nozzles.

Fay and Hesse (1984) investigated the performance and operational characteristics of spraying upwards and compare it to the case of downward directed sprayers. According to them the continuing goal of tower design should involve the efficient and uniform water distribution of water onto the fill material. A poor distribution of water also causes a poor distribution of airflow and a reduction in performance. The required heat and mass transfer in wet cooling towers is obtained by the combined inter action of the three contributors namely spray, fill and rain zone. They state that an extremely uniform water distribution can be obtained by up spray and that with the right installation the pumping head of up spray is virtually identical to that of down spray. In a case study, the fill depth for up spray was 0.15 m less than for down spray with the same performance. The accessibility of an up spraying cooling tower is also better and easier to inspect. It is also possible to add additional layers of fill without changing the water distribution significantly, this is however not the case with down spray.

In a paper by Bellagamba et al. (1988) it is stated that the water distribution on top of the fill is a key aspect to the performance of the whole cooling system. This is a function of nozzle design, nozzle installation, height of the spray zone and the structural cleanliness of the spray chamber. A two dimensional simulation done shows that drop size in the spray zone plays an important role in cooling tower performance.

In a paper by Tognotti et al. (1991) the results obtained experimentally show that correlations exist between the behaviour of single nozzles and nozzle arrangements in cooling towers. The uniformity of the water distribution is strongly related to nozzle installation pattern and the operative conditions. The Sauter mean diameter also increases for nozzles placed in grid formation with varying operating conditions due to coalescence of drops when overlapping of trajectories occur.

Moussiopoulos and Ernst (1987) developed an algorithm for numerically modelling spray cooling that allows predictions of the thermal performance of spray cooling ponds in the case of zero wind velocity to be made. Spray ponds consist of a water pond into which warm process water is sprayed by means of up spraying nozzles. The natural draft of the warmer rising air or wind cools the drops by means of heat and mass transfer. For their numerical model they modelled their drops by means of the Sauter mean diameter. The performance predicted in zero wind velocity was in good agreement with results obtained from field measurements.

Li and Kawano (1995) simulate the drop movement emitted from a noncircular nozzle used in the irrigation industry. These nozzles emit a coherent jet of water and not individual drops. To simulate the drop movement they introduced the concept of “apparent drag coefficient” which includes nozzle shape, size, discharge coefficient, drop diameter, and pressure on the water drop motion.

No literature could be found on modelling spray generated by cooling tower spray nozzles to provide a means to determine heat and mass transfer from the spray zone as well as to investigate the effect of different operating and installation parameters in cooling towers on the nozzle’s performance.

2. EXPERIMENTAL WORK

2.1 Introduction

It was found that there was a shortage of literature regarding the effect of the water distribution system on cooling tower performance considering the nozzle type, nozzle orientation, water distribution and drop size as well as measurement techniques to measure these. Thacker (1997) tested medium pressure cooling tower spray nozzles using a system of cups to determine the water distribution under a single spray nozzle with different orifice openings and swirlers. These tests were conducted without investigating the effect of airflow on the water distribution. Tognotti et al. (1991) used photographic techniques to determine the water jet sheet as well as the water drop size distribution and specific flow rate measurements to determine the water distribution of a grid of spray nozzles in a cooling tower. According to this study the uniformity of the water distribution is strongly related to the nozzle installation pattern and the operating conditions.

For this thesis, water drop size distributions and water distributions needed to be measured in order to validate CFD and numerical simulations of the spray zone performance. Furthermore the effect that a change in water flow rate, counterflow air velocity, nozzle spacing and nozzle height above the fill has on the water distributions produced by a grid of cooling tower spray nozzles were to be determined. A counterflow wet cooling tower test facility was designed and built in which the different operating parameters could be varied and the corresponding water distribution and drop size distribution measured accordingly. In the following section the design criteria of the experimental apparatus, description of experimental apparatus, measurement techniques, instrumentation and test procedures are discussed.

2.2 Design criteria for the experimental apparatus

The experimental apparatus consists of an induced draft wet cooling tower test rig, a spray nozzle system, a water distribution measurement system and a water drop size measurement system, each with its own specific design requirements as follows:

2.2.1 Cooling tower test rig

- The air flow rate is to be variable and monitored continuously.
- The water flow rate is to be variable and monitored continuously.
- The water and ambient air dry bulb temperatures are to be monitored continuously.
- There should be sufficient space to install the water distribution system inside the test rig.
- Surplus spray water from the spray nozzles must be collected by the test section bypass channel system and returned to the pond.
- It must be possible to install fill material below the spray nozzles.

2.2.2 Spray nozzle system

- Each spray nozzle in the grid is to be supplied with water at the same flow rate and pressure.
- The nozzle height above the fill is to be adjustable.
- The nozzle spacing is to be adjustable.
- The nozzles are to be invertible to spray either upward or downward.
- The nozzles are to be interchangeable.
- Sufficient support must be provided to keep nozzles in place.
- The nozzles must be easily accessible in order to change and adjust them.

2.2.3 Water distribution measurement system

- The water distribution is to be measured at discrete points below the water distribution system to provide an evenly spaced measurement grid.
- The measurement grid must have a suitable resolution.
- Disturbance or interference from the measurement system must be negligible.
- Adjustment to the position of the measurement system must not interrupt testing.

2.2.4 Water drop size measurement system

- Digital photography must be used to measure the drop size distribution.
- Interference to the air flow and splashing due to measurement equipment must be negligible.
- Good photographic quality of digital drop size images is required.

2.3 Description of the experimental apparatus

2.3.1 Cooling tower test rig

The induced draft test rig shown schematically in Figure 2.1, basically consists of a vertical rectangular wind tunnel which is suitable for the installation and performance testing of different types of water distribution systems, fill material configurations and rain zone heights. An axial flow fan draws air into the system via a rounded inlet. The air moves upwards through the rain zone, fill, water distribution and drift eliminator sections and enters the inlet nozzle of a venturi flow meter. In the nozzle the air is accelerated and the pressure difference between the plenum and nozzle throat is measured to determine the air flow rate. In the diffuser section of the nozzle some static pressure recovery takes place before the air enters the fan and is discharged to the atmosphere.

Water is pumped from the pond to the spray nozzle system by means of centrifugal pumps. To measure the water flow rate another venturi flow meter located between the flow control valve and the spray nozzle system is used. The pressure difference over the flow meter is measured with an electronic pressure transducer. The water is sprayed into the test section and falls downwards in counterflow air, passing through the spray, fill and rain zone sections before returning to the pond for recirculation through the system. In order to eliminate boundary effects in the rain zone, a portion of the water sprayed into the test section bypasses the rain zone. This water is collected in channels which drain to a bypass tank with which the flow rate is measured using a stopwatch. The fan speed is controlled by a variable speed drive which allows the air flow rate through the test facility to be changed. The water flow rate delivered to the spray nozzle system is controlled by means of a flow control valve located downstream of the pumps. Appendix A describes the calibration of the measurement equipment for the water and air flow rates through the test facility.

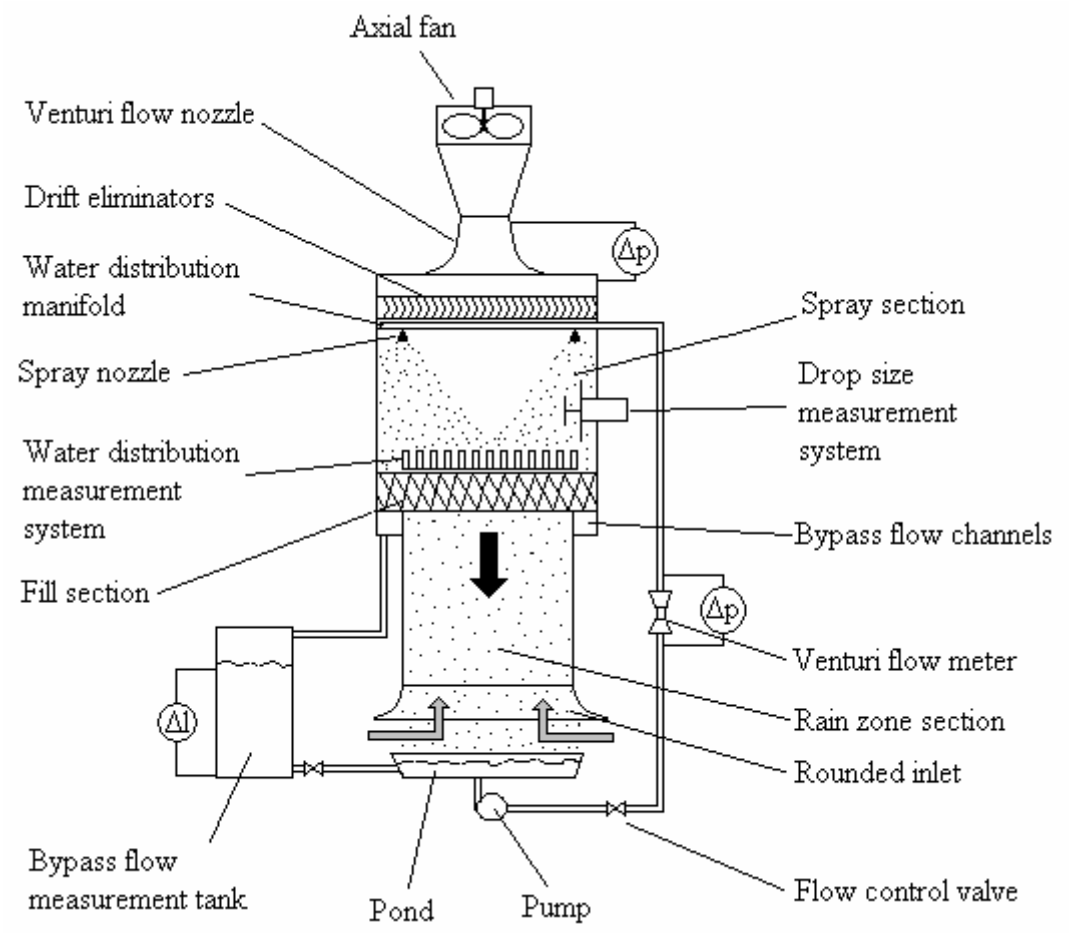

Figure 2.1 Schematic of the induced draft test facility.

2.3.2 Spray nozzle system

The spray nozzle system consists of between one and four water spray nozzles, distribution pipes needed to distribute water evenly to the nozzles and a pipe support frame to keep the system in place inside the spray section, as shown in Figure 2.2. Water enters the system from the side, and depending on the test set-up, either flows through a single pipe to one spray nozzle or through a T-piece connected to two distribution pipes, each supplying water to two spray nozzles. The water passes through the spray nozzles and is then sprayed into the test section. The system allows nozzles spacing and height above the fill to be adjustable. The nozzle spacing can be adjusted by installing different lengths of piping to distribute water to the spray nozzles. The nozzle height can be adjusted by placing spacers of different heights below the fill material and thus changing the nozzle to fill height. Honeycomb flow straighteners are placed inside the pipes to minimize the effect of flow disturbance from the elbows on nozzle performance. Pressure tapping points are used to measure

the pressure upstream of each nozzle. In some of the tests only a quarter of the total nozzle flow rate passes through the rain zone test section. The remaining flow is sprayed into the bypass water collecting channels and drains to the bypass water tank. Figure 2.2 shows the spray, fill and bypass channel zones in the cooling tower test rig.

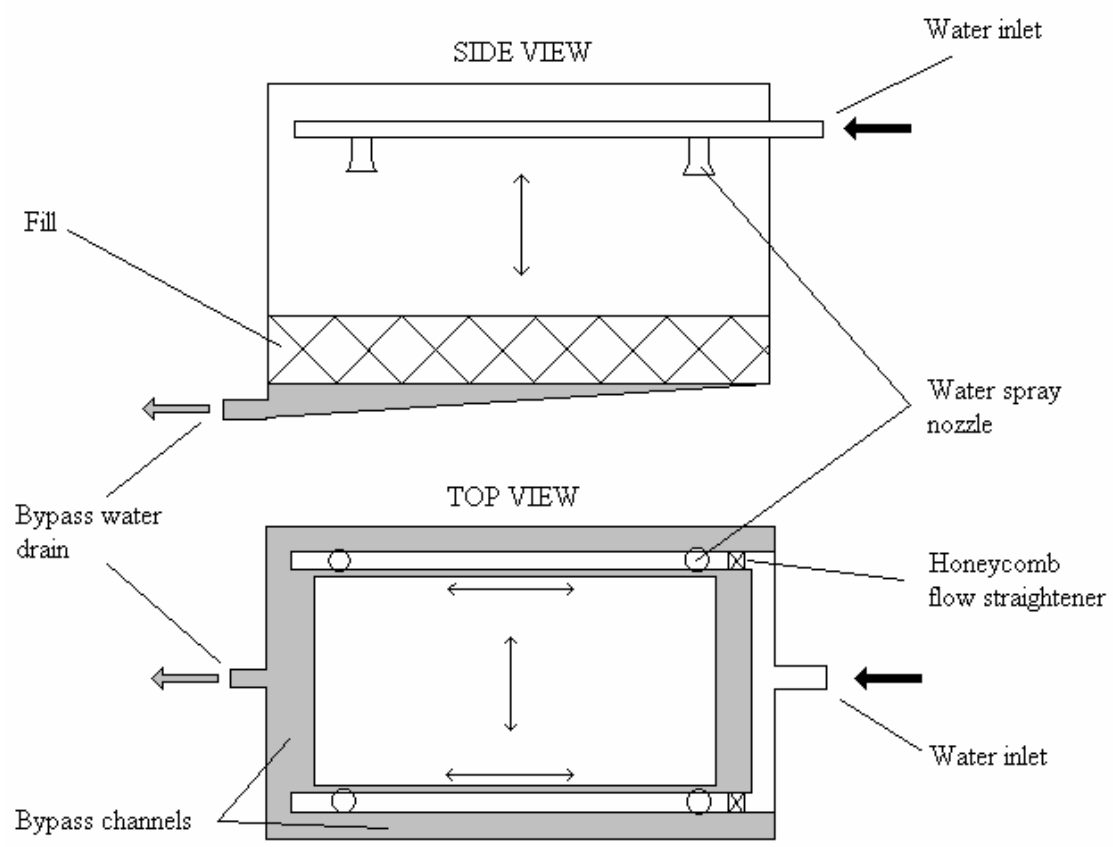

Figure 2.2 Spray, fill and bypass water zones.

2.3.3 Water distribution measurement system

The water distribution below the medium pressure spray nozzles is measured by means of the water distribution measurement system shown in Figure 2.3. The system consisted of 17 measuring cups, each with a diameter of 40 mm, which are evenly spaced on a beam at a centre to centre distance of 60 mm as shown in Figure 2.5. The beam is moved through the test section on a guide rail. The reason for selecting a 40 mm measuring cup diameter is explained in Appendix E. Honeycomb is placed inside the measuring cups to prevent the water from splashing out during testing. The water from the measuring cups drain through plastic pipes to a rake of measurement cylinders where the water is collected over a certain period of time to determine the flow rate. The water distribution measurement system was designed to minimize the effect of flow disturbances on the drop trajectories. This was done by using a

cylindrical beam to house the measuring cups, placing the guide rails in the bypass channels outside the air stream and using thin pipes to drain the water from the measuring cups to the measurement cylinders thus reducing the blockage of the air stream.

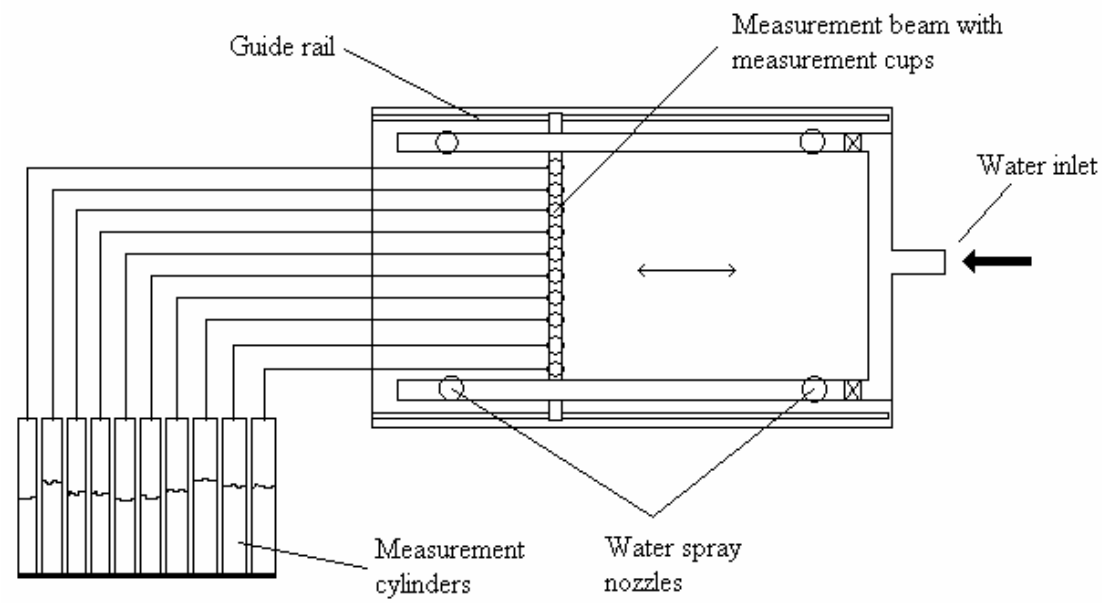

Figure 2.3 Water distribution measurement system.

The water distribution produced by the low pressure spray nozzles can not be measured with the measurement beam and therefore a series of larger containers with catchment area dimensions of 0.12 x 0.2 m are placed on a plank in the test section. This plank can be moved radially with the nozzle acting as centre point. The volume of water collected over a measured period of time in each container, is measured individually by taking the containers out of the test section and weighing them to determine the volume of water and flow rate into them. Due to this set-up the low pressure nozzles can not be tested under counterflow air conditions as this set-up causes air flow disturbances.

2.3.4 Water drop size measurement system

The water drop size measurement system is used to measure the size distribution of drops coming from the spray nozzles as shown in Figure 2.4. This equipment and accompanying software to analyse the data was developed by Terblanche (2005) at the University of Stellenbosch. During testing, drops were photographed at a distance of 0.7 m and 1.25 m from the spray nozzle. The equipment used to photograph the

drops at a distance of 1.25 m consists of a camera placed inside a pipe with a screen attached at a fixed focal length of 0.55 m. The pipe can be inserted into the rain zone test section and the falling water drops digitally photographed under counterflow conditions. The system is designed in such a way that a plate shields the section in front of the screen from the airflow disturbances caused by the pipe and therefore the trajectory of the water drops falling past the screen are not influenced. To photograph the drops at a distance of 0.7 m from the nozzle without airflow conditions, the background plate is placed in the rain zone and the digital camera placed at the focal length of 0.55 m as shown in Figure 2.6. Since there is no airflow, the pipe and shielding plate is removed and the drops photographed without disturbance. The digital photographs are then analysed with the help of a program that calculates the drop diameters and drop size distributions.

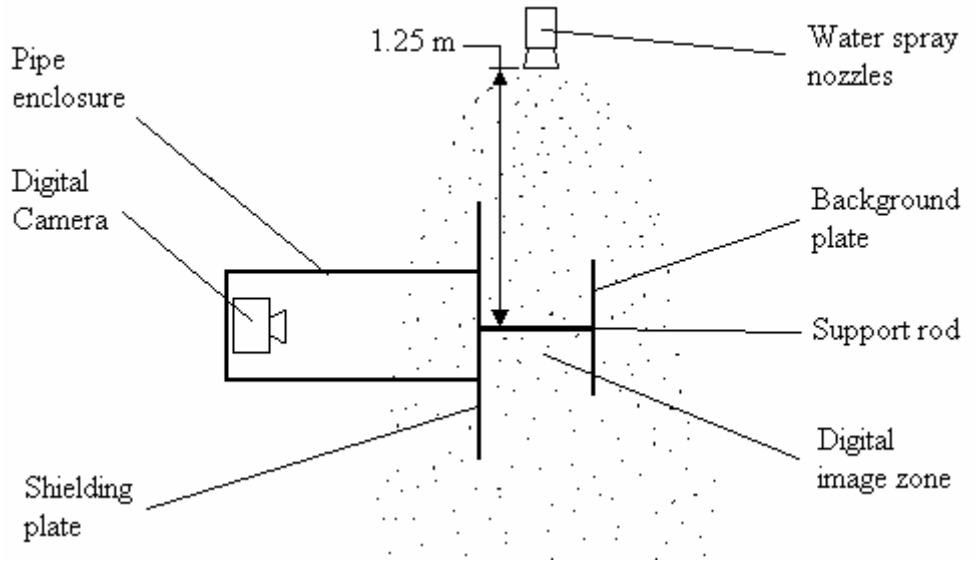

Figure 2.4 Water drop size measurement equipment set-up at 1.25 m from the nozzle.

2.4 Measurement techniques and instrumentation

In order to achieve the project objectives, water distribution tests and drop size distribution tests were conducted at different water flow rates, air flow rates, spray nozzle heights and spray nozzle spacings. The measurement techniques and instrumentation used for the water flow, air flow, water distribution and water drop size distribution measurements are discussed in this section.

2.4.1 Water and air flow rate measurements

To control the air flow rate through the induced draft test facility, a fan with a frequency inverter type variable speed drive is used. Before entering the fan the air passes through the flow nozzle of a venturi shown in Figure 2.1. The pressure difference between the plenum and the nozzle throat is measured using a Betz micro water manometer. This pressure difference is then used to determine the air flow rate through the system. To control the air flow rate, the fan speed is adjusted manually until the measured and required air flows are the same. The calibration of the venturi is discussed in Appendix A.

To control the water flow rate, a butterfly valve and venturi flow meter are used. It can be seen from Figure 2.1 that water is pumped from the pond by the centrifugal pump through the venturi to the spray nozzle system and then falls back to the pond under gravity. The butterfly valve is used to regulate and the venturi to measure the water flow rate. The static pressure difference between the upstream pipe and the venturi throat is measured by means of an electronic pressure transducer, which is then used to determine the water flow rate to the spray nozzle system. The calibration curves of the venturi and the pressure transducer as well as the pressure transducer specifications are presented in Appendix A. To control the water flow rate, the data from the pressure transducer is monitored by a data logger and converted to flow rate by a computer programme. The butterfly valve is adjusted manually until the desired flow rate is obtained.

2.4.2 Water distribution tests

The water distribution of two medium and two low pressure cooling tower spray nozzles was to be measured at different air flow rates, water flow rates, nozzle heights and nozzle spacings. Thacker (1997) tested medium pressure cooling tower spray nozzles using a system of cups to determine the water distribution under a single spray nozzle. His measurement cups were spaced at a centre to centre distance of 80 mm and had a diameter of 45 mm. His tests were done under no air flow conditions.

To measure the water distribution under the medium pressure spray nozzles, a measurement beam and a rake of measurement cylinders was used as shown in Figure 2.3. The measurement beam consists of a single row of 17 measurement cups with a

diameter of 40 mm and a centre to centre spacing of 60 mm. The edges of these cups were sharpened to reduce splashing of drops from the edges. Honeycombs were placed inside the cups to prevent water splashing from the cups. Figure 2.5 is a schematic of a section of the beam showing two measurement cups.

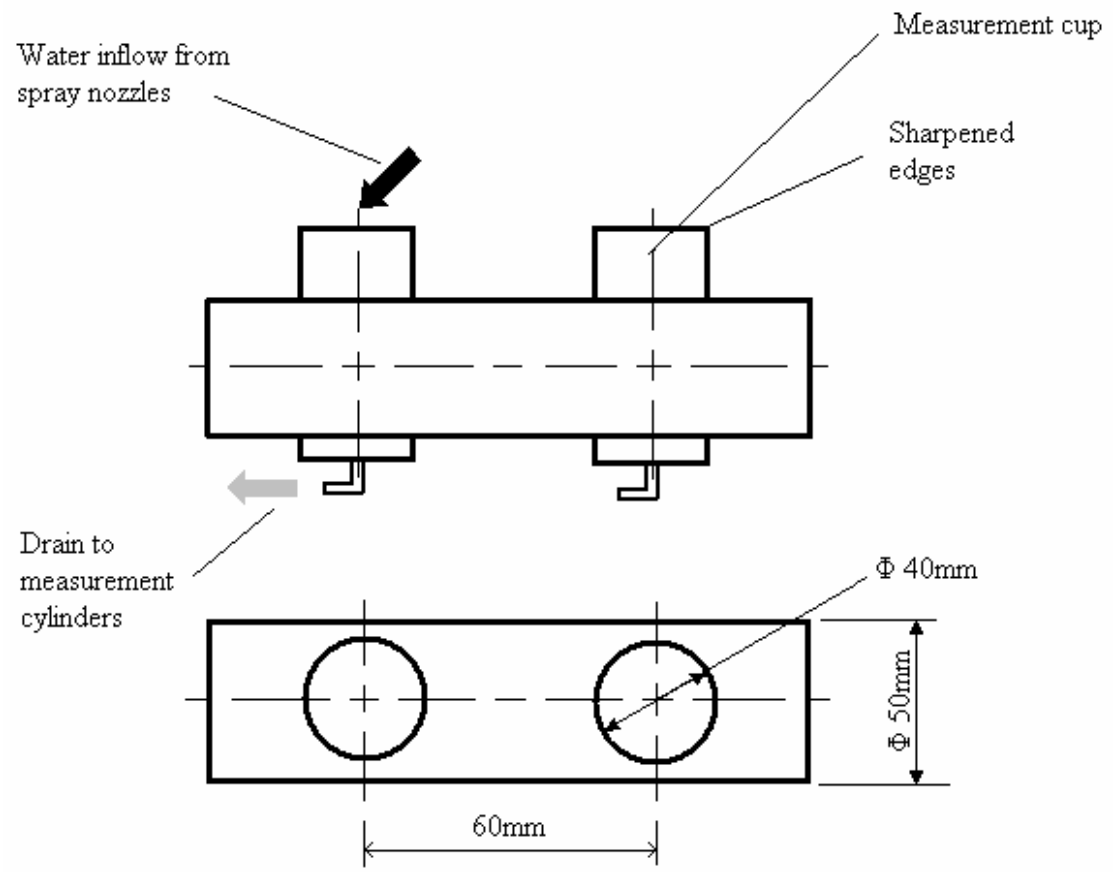

Figure 2.5 Section of the water distribution measurement beam showing two cups.

The beam was placed underneath the spray nozzles on a rail supported on the fill material. By means of two push rods, extending to the outside of the test section, the beam could be moved along the rail. Moving the beam in increments of 60 mm a 60 x 60 mm measurement grid was obtained. During testing, water from the spray nozzles is sprayed into the test section and caught by the measurement cups. The water then drains under gravity to the measurement cylinders at a lower level. The measurement cylinders are allowed to fill for a measured period of time. The volume of water in each cylinder is measured which is used to determine the mass velocity by means of equation (2.1). A sample calculation is given in Appendix D.

$$G_w = \frac{V_{cyl}\rho_w}{A_{cup}\Delta t}\ ,kg/m^2s \qquad (2.1)$$

To measure the water distribution for the low pressure nozzles, larger containers with catchment area dimensions of 0.12 x 0.2 m, are placed on a wooden plank. Moving the plank and containers radially around the nozzle centre, the water distribution can be obtained when the sprayers are tested in the up spray configuration. The containers are placed at the fill height to represent the water distribution on the fill. Before testing, the nozzle is covered to prevent water from spraying into the test section. The containers are placed adjacent to one another onto the plank and the cover is removed. The time is recorded to fill the containers to a certain level and the nozzle covered again. By removing the containers and measuring the volume of water in each container the mass velocity can be determined by means of equation (2.2). The measurement resolution is improved by moving the plank radially by half a container width.

$$G_w = \frac{V_{buc}\rho_w}{A_{buc}\Delta t}\ ,kg/m^2s \qquad (2.2)$$

2.4.3 Drop size distribution tests

The water drop size distribution was measured for different types of spray nozzles, tested individually under varying water flow rates and distances from the spray nozzles, to determine the effect of water flow rate and drop travel distance on the drop size distribution.

Tognotti et al. (1991) used high speed photographic techniques to determine the water jet umbrella as well as the water drop size distribution at different positions under a grid of spray nozzles in a cooling tower. They used a macro lens that had a depth of field of 50 mm at the best focal point of the lens. The drops could then be photographed, classified and counted for each flow configuration in order to evaluate the drop size distribution.

To measure the water drop size distribution, digital images are taken of the nozzle spray using a digital camera. A computer programme is then used to do image processing and to extract the drop size distribution data. This equipment and software was developed at the University of Stellenbosch as part of a B.Eng undergraduate final year project (Terblanche, 2005).

To capture the digital drop images at a distance of 1.25 m from the spray nozzle outlet, the drop size measurement system was inserted into the rain zone test section as shown schematically in Figure 2.4. Figure 2.1 shows the location of the equipment in the induced draft test facility. For the second set of tests conducted at a distance of 0.7 m from the spray nozzle, the pipe and shielding plate shown in Figure 2.4 were removed, since they were obstructions causing splashing and flow disturbances when placed in close proximity to the spray nozzles. Of the set-up shown in Figure 2.4, only the background plate was used, placed ± 0.1 m from the periphery of the spray zone and aligned in the direction of the drop trajectories shown in Figure 2.6. The drops were photographed against the background plate similar to the previous tests. The calibration of this equipment is discussed and presented in Appendix A.

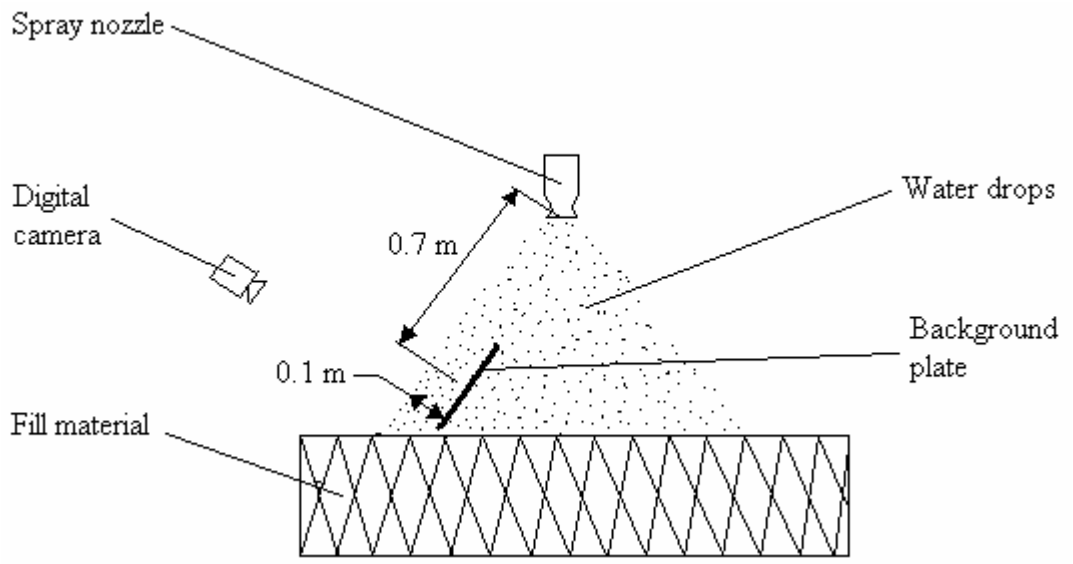

Figure 2.6 Water drop size measurement equipment set-up at 0.7 m from the nozzle.

For the drop size analysis, the digital images were imported into an image processing computer programme. The programme recognises the drops and defines the edges around them, numbering each drop. The area surrounded by an edge is determined in terms of pixels. From calibration values in terms of mm/pixels, the area of each drop is determined, from which the drop diameter is calculated.

2.5 Test procedure

The test procedure followed for the tests described above are provided in this section.

2.5.1 Water distribution test procedure

The water distribution tests were done using the water distribution measurement system as described in section 2.3.3. The test procedure for the medium pressure spray nozzles is as follows:

1. Install the spray nozzle in the required position in the spray section of the test rig.
2. Place the measurement beam in the test section and connect the plastic tubing to the measurement cups.
3. Close up the spray section.
4. Start the pump and set the desired water flow by means of the control valve.
5. Start the axial fan and set the desired air flow by means of the frequency inverter drive.
6. Allow the water temperature to stabilize.
7. Record the air and water temperatures as well as the atmospheric pressure.
8. Calculate air density.
9. Reset the air flow to the desired air flow rate.
10. Allow the water flowing from the measurement cups to the measurement cylinders to stabilize.
11. Place the measurement cylinders under the plastic tubing and start the stop watch.
12. Remove the measurement cylinders and stop the stop watch.
13. Move the measurement beam to next position.
14. Measure the water volume in measurement cylinders.
15. Repeat from no.10 until all points required for a specific test has been measured.

The test procedure for the low pressure spray nozzles is as follows:

1. Install the spray nozzle in the required position in the spray section of the test rig.
2. Start the pump and set the desired water flow by means of the control valve.
3. Record the air and water temperatures as well as the atmospheric pressure.
4. Cover the spray nozzle with the cover.
5. Place the containers on the plank in the test section.
6. Remove the cover and start the stop watch.

7. Replace the cover over the spray nozzle and stop the stop watch.
8. Measure water volume in containers.
9. Repeat from no.5 until all points required for a specific test have been measured.

2.5.2 Water drop size distribution test procedure

The water drop size distribution tests were done using the water drop size measurement systems as described in section 2.3.4. The test procedure is as follows:

1. Install the spray nozzle in the required position in the spray section of the test rig.
2. Install the drop size measurement equipment in the test section.
3. Start the pump and set the desired water flow by means of the control valve.
4. Record the air and water temperature as well as the atmospheric pressure.
5. Switch the digital camera on, fully extend the zoom lens and set to fill flash.
6. Insert digital camera into the pipe of the drop size measurement equipment.
7. Ensure that there is no splashing from background plate, if there is adjust the alignment of the background plate.
8. Take digital images.
9. Process images using the image processing programme (Terblanche, 2005).

2.6 Conclusion

The design requirements for the cooling tower test rig and spray nozzle system given in section 2.2 were met. The water distribution measurement system used to measure the medium pressure nozzle water distributions met the design requirements but the system used for the low pressure nozzles could not be used in counterflow air conditions since the air flow was disturbed by the equipment. The drop size measurement systems used to measure the drop size distributions could not be used in counterflow air and in close proximity to the nozzle outlet, since the equipment disturbed the air flow and caused splashing on the background plate. It would be advisable to redesign this equipment to prevent these problems, especially when measuring in close proximity to the nozzle. The test procedures described ensured the repeatability of the tests.

3. EXPERIMENTAL RESULTS OF NOZZLE TESTS

3.1 Introduction

In this section the experimental data obtained from the water distribution and drop size distribution tests, using the experimental apparatus, measurement techniques and procedures described in Chapter 2, are presented. Different medium and low pressure cooling tower spray nozzles were tested in single and grid configuration and the repeatability and accuracy of the data is investigated. The main objective is to determine the effect that water flow rate, air velocity and height above the fill material have on the drop size distribution, water distribution and drop trajectories produced by the different nozzles. The data is furthermore required as input data for the nozzle spray simulation codes as well as the CFD simulations presented in chapters to follow.

3.2 Flow characteristics

3.2.1 Flow characteristics of single medium pressure spray nozzles

Tests were conducted on two full cone medium pressure spray nozzles. According to the manufacturer's data sheet, the small nozzle, hereafter referred to as no.1, requires a pressure head of between 1.5 and 7 m of water to achieve corresponding flow rates of between 2.22 and 4.86 l/s. The other medium pressure nozzle, referred to as no.2, requires a pressure head of 1.5 to 6 m of water for flow rates of between 3.33 and 7.22 l/s. Figure 3.1 shows the flow characteristic curves obtained from the manufacturer's data sheets and experimental data.

3.2.2 Flow characteristics of single low pressure spray nozzles

Tests were conducted on two low pressure cooling tower spray nozzles. According to the manufacturer, these nozzles require a pressure head of between of 0.5 and 1.5 m water. The first spray nozzle has a 25 mm orifice and was tested at a pressure head of 1 m which corresponds to a flow rate of 1.6 l/s and will hereafter be referred to as nozzle no.3. The second spray nozzle has a 34 mm orifice and was also tested at a pressure head of 1 m which corresponds to a flow rate of 3.15 l/s and will hereafter be referred to as nozzle no.4. For nozzle no.4 the manufacturers flow rate was 19%

higher than the measured flow rate. No manufacturer's flow rate data was available for nozzle no.3.

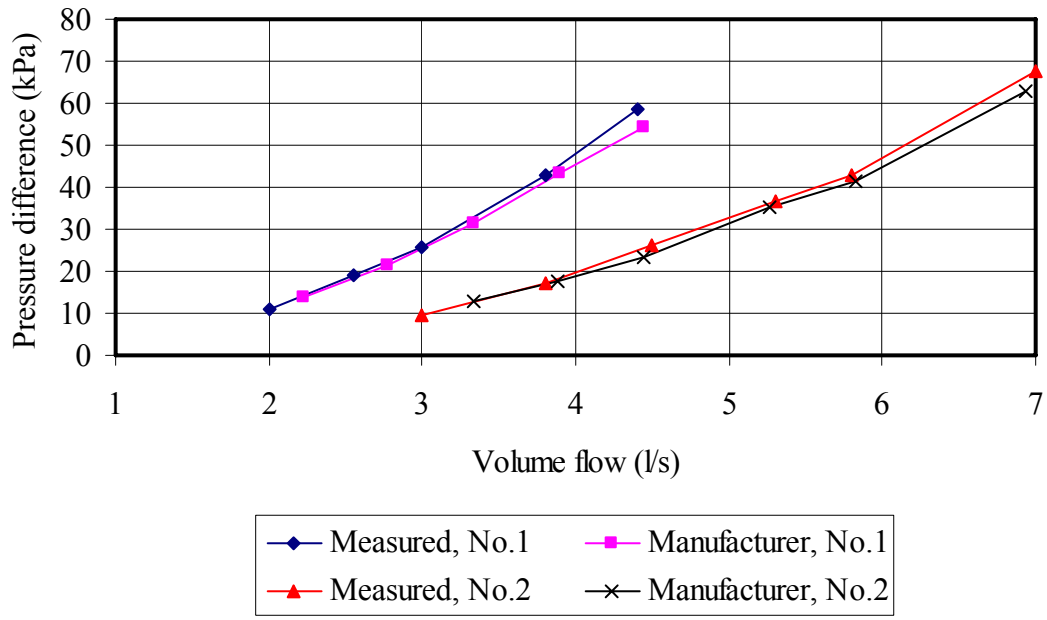

Figure 3.1 Medium pressure spray nozzle flow characteristics.

3.3 Water distribution of single medium and low pressure nozzles

The water distribution tests were conducted by employing the experimental apparatus, techniques and procedures described in Chapter 2.

3.3.1 Water distribution of single medium pressure spray nozzles

The water distribution was tested for both medium pressure nozzles at the water flow rates, counterflow air velocities and heights above the fill material as given in Tables 3.1 and 3.2. The water distribution tests were all done with one layer of cross fluted fill material.

Table 3.1 Test conditions for spray nozzle no.1.

Test no.		1	2	3	4	5	10	11	12	13
Water flow rate	l/s	4.38	3.08	3.08	4.38	4.38	3.08	3.08	4.38	4.38
Air velocity	m/s	0	0	3	3	2	0	3	0	3
Nozzle height	m	0.47	0.47	0.47	0.47	0.47	0.35	0.35	0.35	0.35

Table 3.2 Test conditions for spray nozzle no.2.

Test no.		6	7	8	9
Water flow rate	l/s	4.38	4.38	6.8	6.8
Air velocity	m/s	0	3	0	3
Nozzle height	m	0.47	0.47	0.47	0.47

An approximation of the drop axial velocity coming from the spray nozzle orifice could be made by dividing the water volume flow rate by the nozzle orifice area as given by equation (3.1). Figure G.1 shows nozzle no.1 (red nozzle) and the nozzle orifice diameter.

$$v_{axial} = \frac{Q_w}{A_t}, \text{ m/s} \qquad (3.1)$$

This will be the minimum velocity of a drop leaving the nozzle outlet throat, since the swirl and radial components are neglected. This is useful when analysing the experimental data as well as for initial values for the simulation programs. It can be seen from Table 3.3 that when the corresponding water flow rates of nozzles no.1 and 2 are compared, the velocity of nozzle no.1 is higher, as its outlet area is smaller.

Table 3.3 Water axial velocities at nozzle throat.

Nozzle no.		1	1	2	2
Water flow rate	l/s	3.08	4.38	4.38	6.8
v_{axial}	m/s	5.8	8.3	4.7	6.3

The measured water distribution quadrants of the two tested nozzles are presented in Figures 3.2 and 3.3.

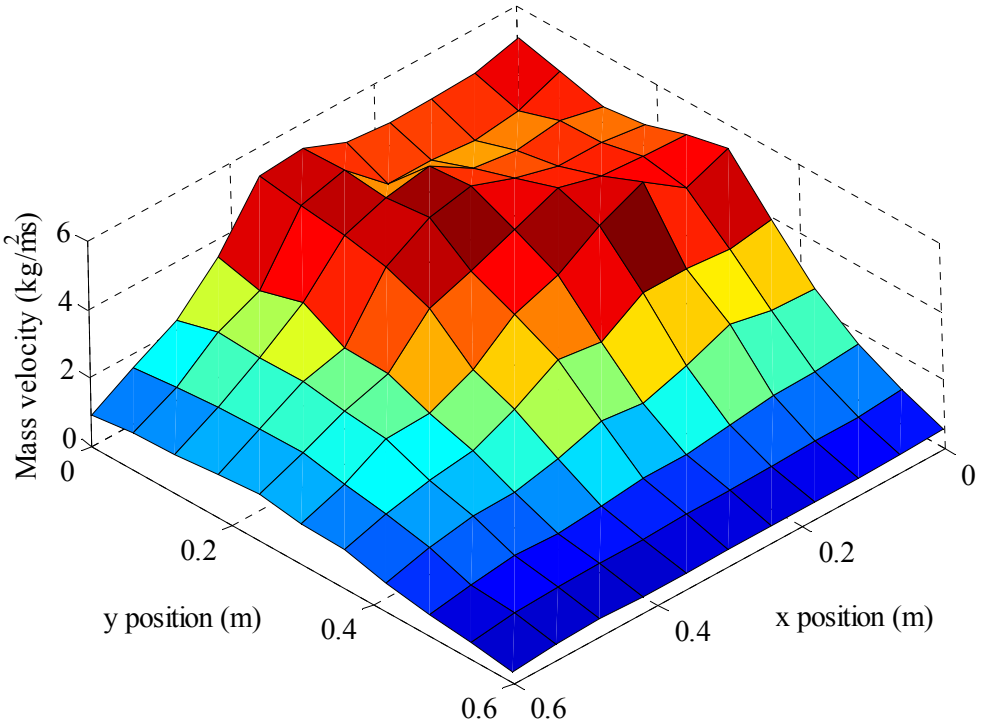

Figure 3.2 Water distribution of nozzle no.1 for Test no.1.

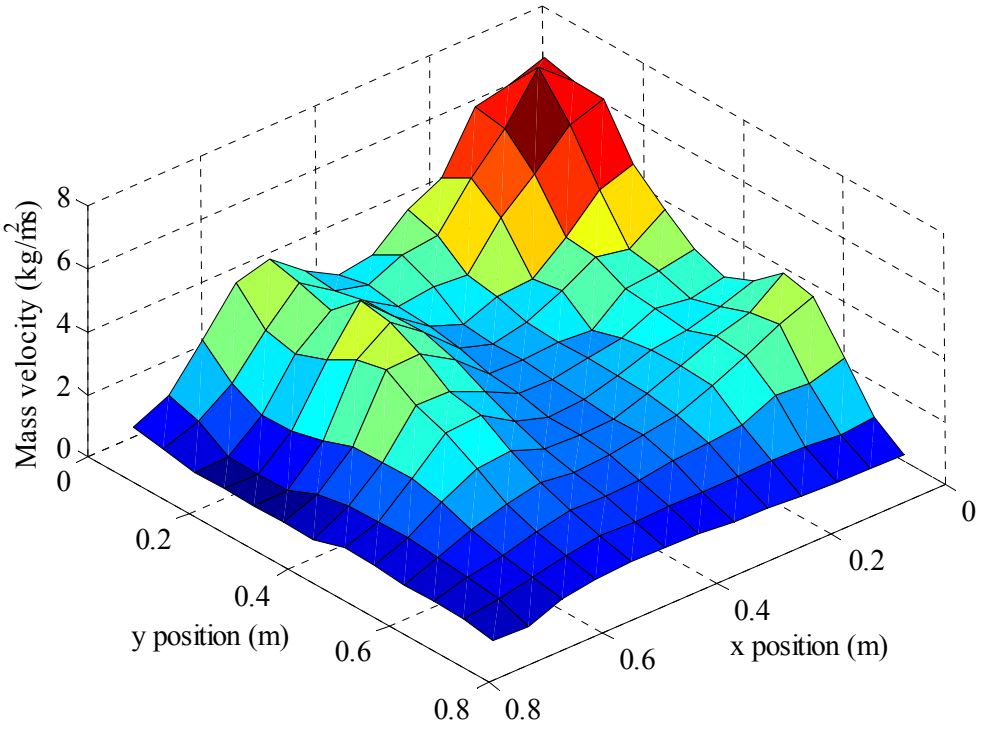

Figure 3.3 Water distribution of nozzle no.2 for Test no.6.

To simplify the data analysis, water distributions measured are presented along the x, y and k axis as shown in Figure 3.4.

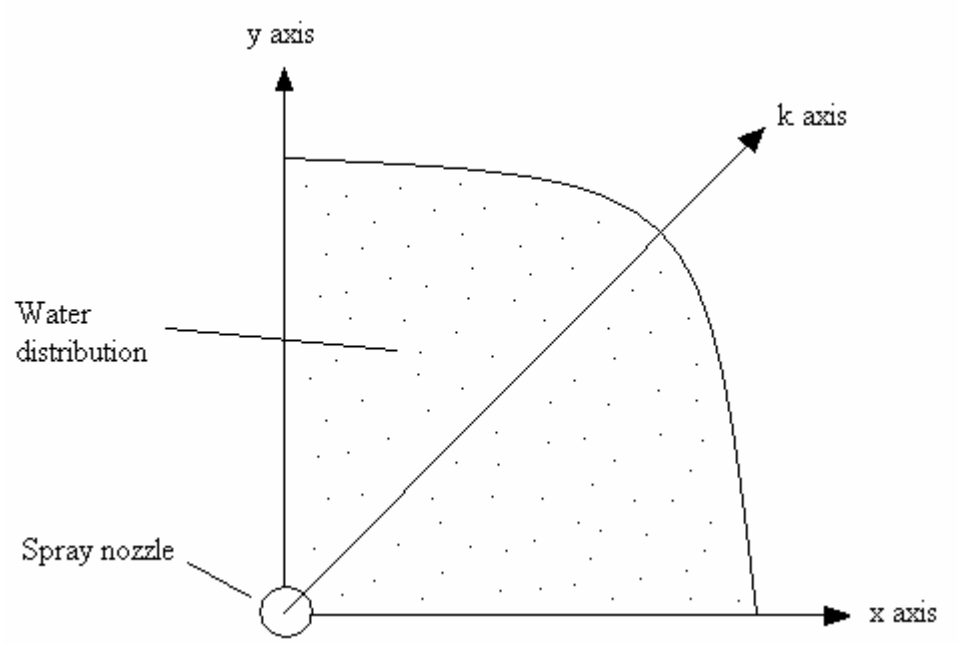

Figure 3.4 Axes along which water distributions are presented.

No literature could be found on the effect that counterflow air has on the water distribution from the spray nozzles, which could be important to the performance of the cooling tower. When determining the effect of counterflow air velocity all variables were kept constant except for the air velocity which was varied.

Figure 3.5 shows no noticeable effect of counterflow air velocity on the water distribution of nozzle no.1 when comparing the data of Test no.2 and 3. It was expected that if there is an effect it would be most pronounced at the low water flow rates since the drops' contact time with the counterflow air is longer. However no significant difference in the water distribution could be seen considering the measuring uncertainty discussed in section 3.3.3.

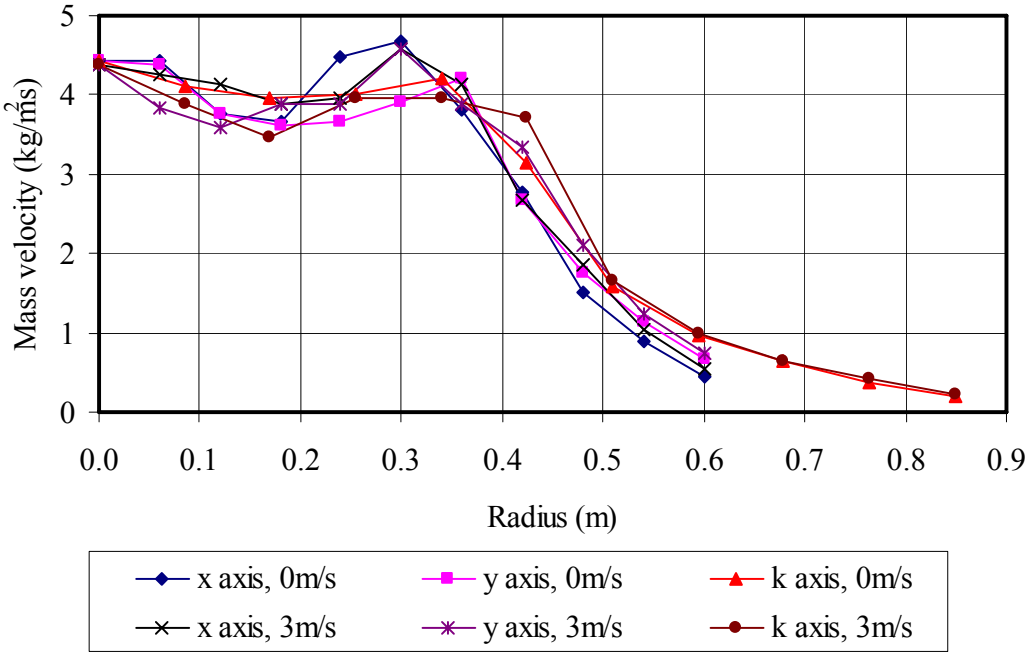

Figure 3.5 Water distribution of nozzle no.1 at different air velocities.

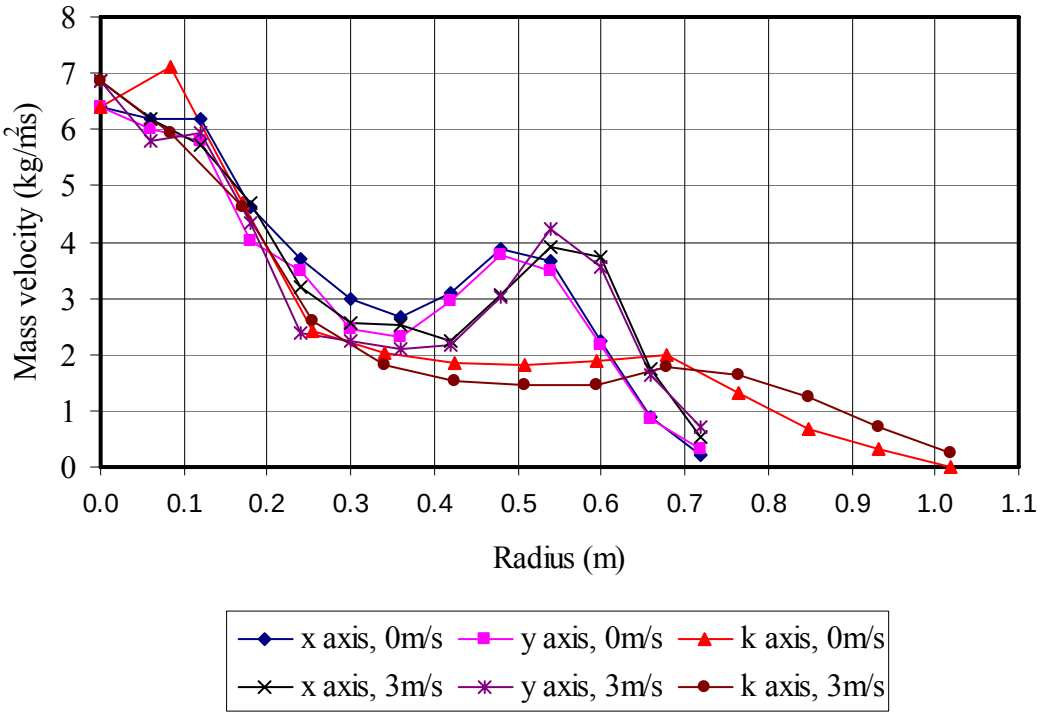

Figure 3.6 Water distribution of nozzle no.2 at different air velocities.

Figure 3.6 shows a noticeable effect of counterflow air velocity on the water distribution of nozzle no.2 when comparing the data of Test no.6 and 7. It can be seen that the peak in the water distribution at a radius of 0.5 m was shifted radially outward

in the order of 10% by the counterflow air and subsequently the trough was lowered. This trend was most significant with the lower water flow rate, explained by the longer contact period between the spray and the air due to the lower drop velocities.

The nozzle height above the fill has a direct influence on the area covered by a nozzle and therefore the rain density of the water distribution under the nozzle at the fill level, thus having an influence on the nozzle spacing required in the cooling tower. When determining the effect of spray nozzle height, all the other variables were kept constant except the nozzle height which was varied.

Figure 3.8 shows the effect of nozzle height on the water distribution of nozzle no.1 at a low water flow rate using the data of Test no.2 and 10. It can be seen that the area sprayed by the nozzle at a height of 0.47 m is larger than the area sprayed by the nozzle at a height of 0.35 m. In Figure 3.7 it is shown that if a straight line is drawn through the peak at a radius 0.25 m for the nozzle height of 0.35 m and the peak at a radius 0.33 m for a nozzle height of 0.47 m, the radius will be 0 m at the nozzle height. This indicates that the spray is conical and that the drop trajectories are virtually straight.

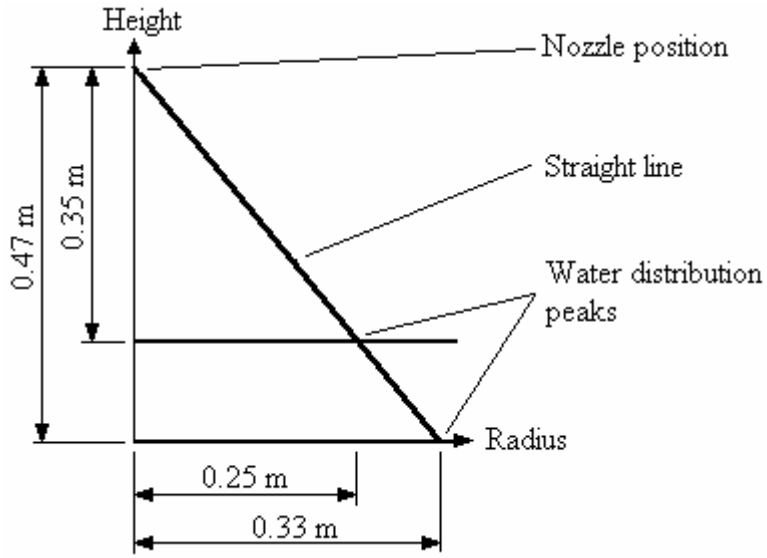

Figure 3.7 Schematic of a straight line through the water distribution peaks.

The mass velocity for the nozzle height of 0.47 m is lower than that for the nozzle height of 0.35 m since the area sprayed is bigger. Looking at the peaks at 0.25 m and

0.33 m it can be seen that there is an increase in area of 43% and a decrease in the mass velocity of 40%.

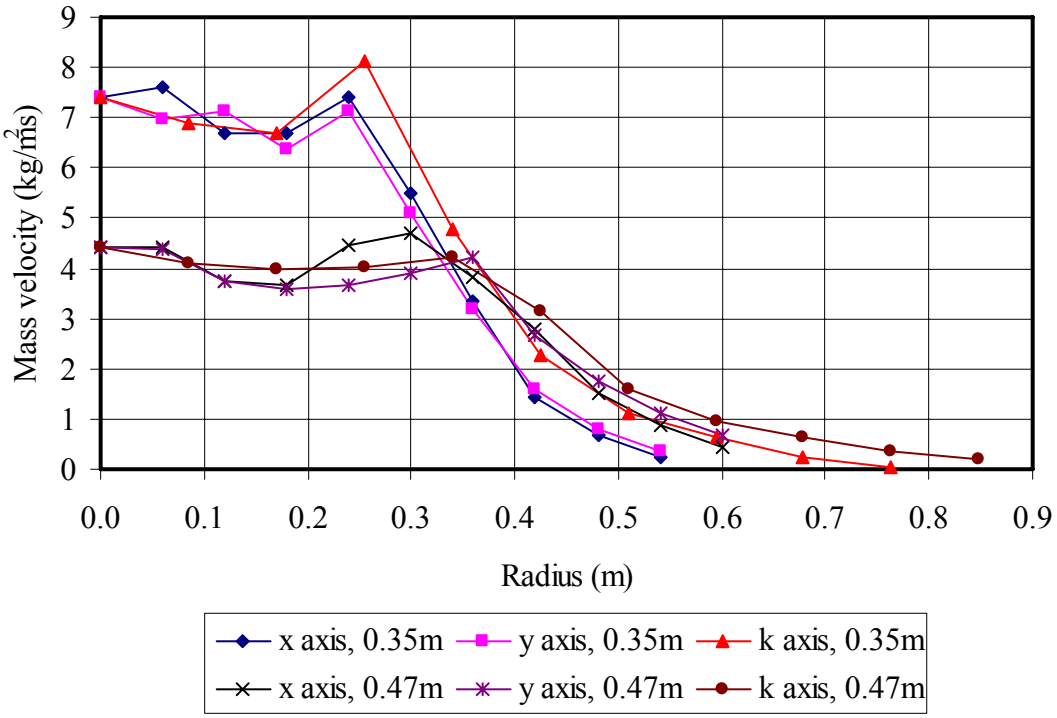

Figure 3.8 Water distribution of nozzle no.1 for low water flow rate at different heights.

When comparing the effect of nozzle height on the water distribution of nozzle no.1 at a higher water flow rate using the data of Test no.1 and 12, the same trend was observed. Again it was found that the drop trajectories were virtually straight. From the corresponding peaks at different nozzle heights it could be seen that there was an increase in area of 39% and a decrease in the mass velocity of 42%.

Cooling towers have different sizes and flow requirements, which means that spray nozzle water flow rate differs. This can have an influence on the water distribution and therefore affect the performance of the cooling tower. When determining the effect of water flow rate, all the variables were kept constant except for water flow rate which was varied.

Figure 3.9 shows the effect of varying water flow rate on the water distribution of nozzle no.1 using the data of Test no.10 and 12. It can be seen that the higher flow

rate is offset from the lower flow rate and that the same water distribution trend is followed with the peaks at the same radius. When integrating the water distributions of Test no.10 and 12, flow rates of 3.5 and 4.4 l/s was obtained respectively. Since the area sprayed by the nozzles stays reasonably the same the higher flow rate should be offset from the lower flow rate by the ratio between the two flow rates which is equal to 1.3.

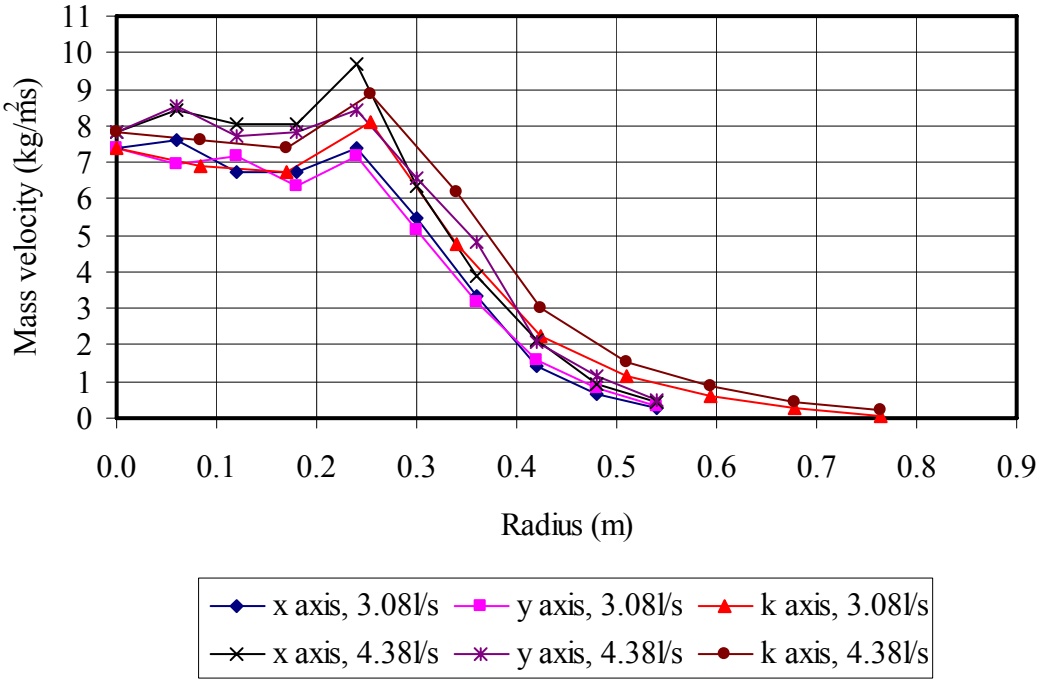

Figure 3.9 Water distribution of nozzle no.1 for different water flow rates.

Figure 3.10 shows the effect of varying water flow rate on the water distribution of nozzle no.2 using the data of Test no.6 and 8. It can again be seen that the higher flow rate is offset from the lower flow rate and that the same water distribution trend is followed with the peaks at the same radius. When integrating the water distributions of Test no.6 and 8, flow rates of 4.3 and 6.1 l/s were obtained respectively. The area sprayed by the nozzles again stays reasonably the same and therefore the higher flow rate should be offset from the lower flow rate by the ratio between the two flow rates which is equal to 1.4.

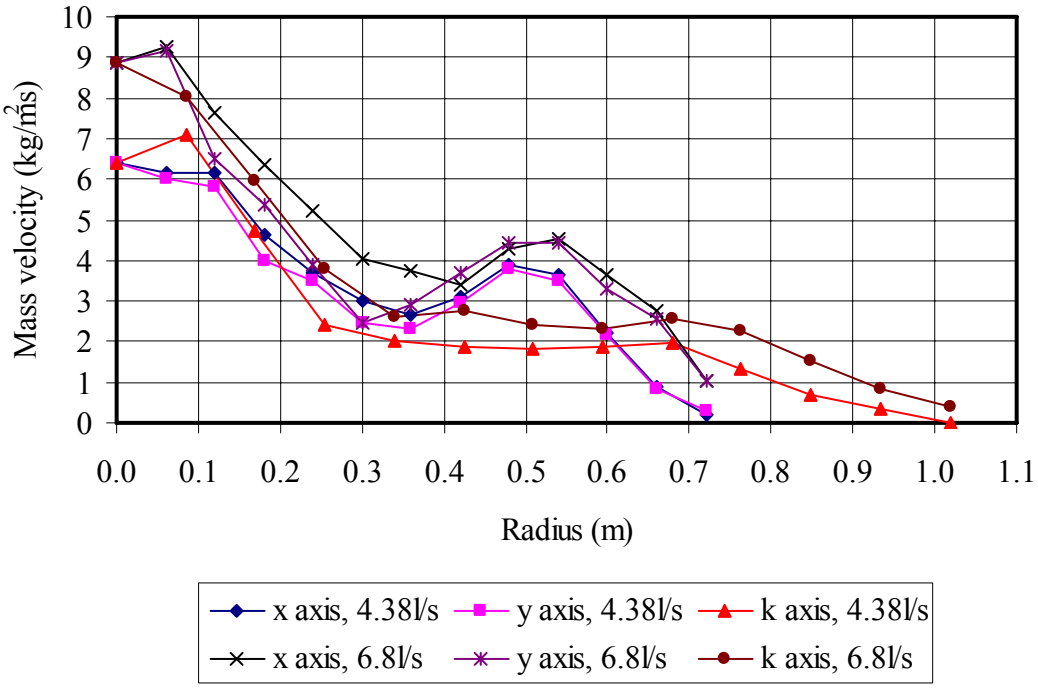

Figure 3.10 Water distribution for nozzle no.2 for different water flow rates.

3.3.2 Water distribution of single low pressure spray nozzles

No water distribution was measured for the two low pressure nozzles in the down spray arrangement since the area sprayed was too small to obtain a sufficiently fine measurement resolution. According to the manufacturers' data sheet the sprayers should be spaced 0.8 to 1.2 m apart at a height of 0.4 m above the fill material in the down spray configuration. At a nozzle height of 0.47 m the spray diameter was measured, using photographs, to be approximately 0.8 m on the fill.

The spray produced by these nozzles in the up spray configuration consists of numerous drop trajectories following a relative fixed path. The cups on the measurement beam used to measure the medium pressure nozzle water distributions was found to be to small and larger containers, placed on a plank as described in Chapter 2 were used to measure the water distribution.

The low pressure nozzles were both tested in up spray under no air flow conditions with a pressure head of 1 m water. The water distributions were measured at fill level with a nozzle height of 0 m (fill packed between the distribution pipes and the nozzle level with the fill). Table 3.4 gives the test conditions for nozzles no. 3 and 4.

Table 3.4 Test conditions for spray nozzles no.3 and 4.

Test no.		18	19
Nozzle no.		3	4
Water head	m	1	1
Water flow rate	l/s	1.6	3.15
Air velocity	m/s	0	0
Nozzle height	m	0	0

During testing it was found that the water distribution differed at different circumferential positions and this was due to the supports holding up the outer ring, having the effect of channelling the water and thus causing different water distributions over and between the supports. Figure 3.11 shows the supports holding the outer ring and the direction of the spray.

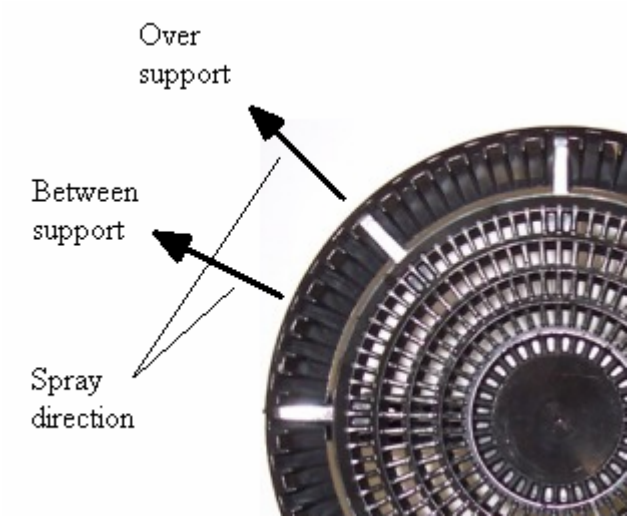

Figure 3.11 Supports holding up the outer ring.

Figure 3.12 shows the water distribution for nozzle no.3 using the data of Test no.18. Measurements could only be taken up to 0.195 m from the nozzle since the nozzle and supply pipe prevented closer measurements. The supports had the effect of reducing the mass velocity further away from the nozzle as well as shifting the peak mass velocity closer to the nozzle. The supports also had the effect of channelling the water causing more water to be sprayed between the supports than over them. This caused a non uniform water distribution radially as well as in the circumference of the spray region.

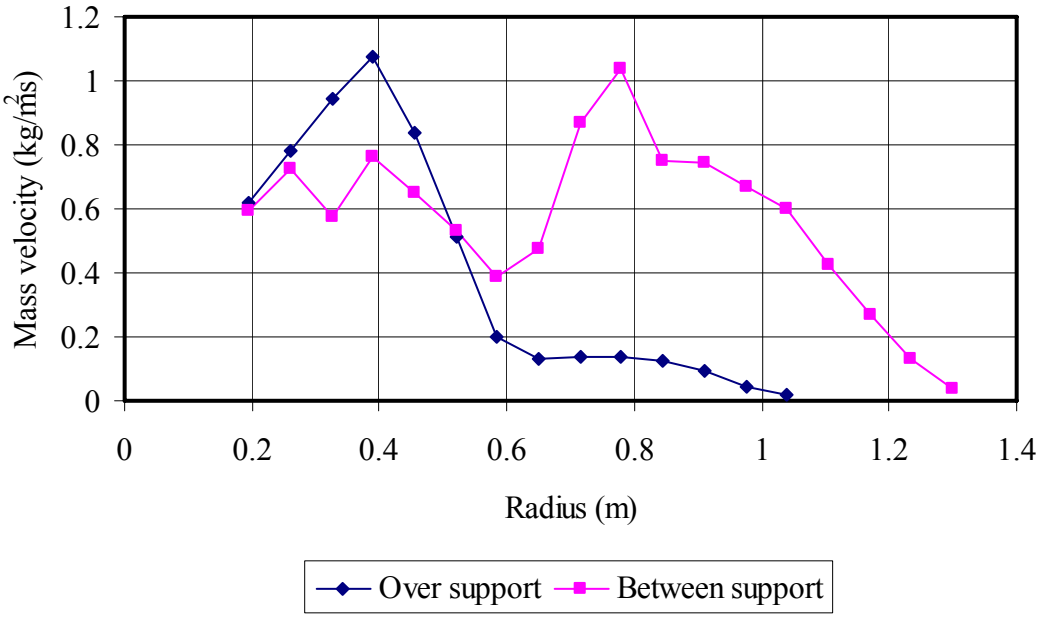

Figure 3.12 Water distributions over and between the supports for nozzle no.3.

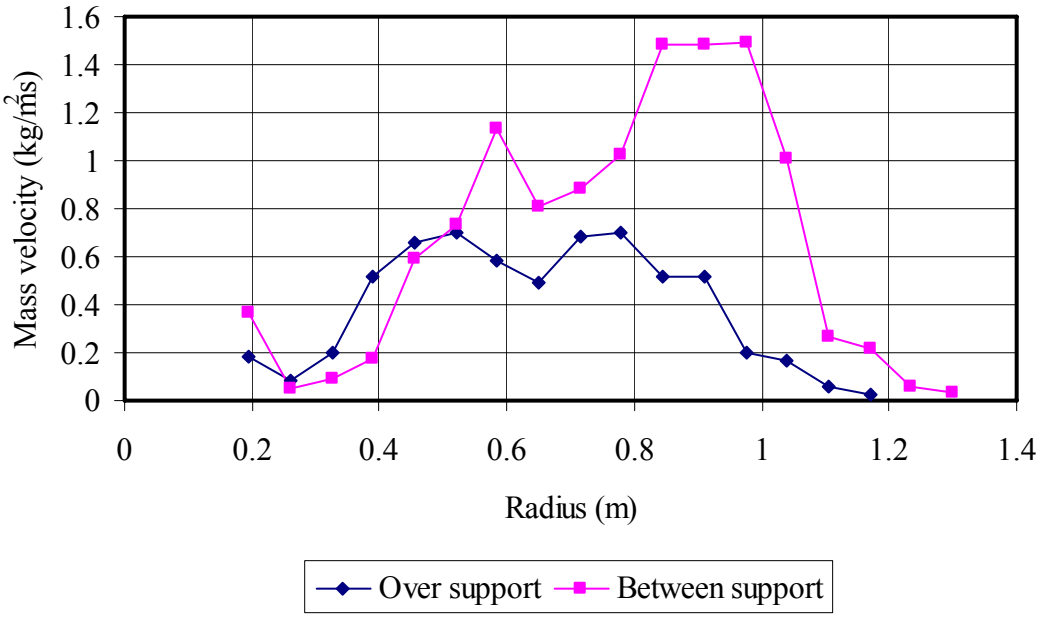

Figure 3.13 Water distributions over and between the supports for nozzle no.4.

Figure 3.13 shows the water distribution for nozzle no.4 using the data of Test no.19. Measurements could only be taken up to 0.195 m from the nozzle since the nozzle and supply pipe prevented closer measurements. Again the support had the effect of reducing the mass velocity further away from the nozzle as well as shifting the peak mass velocity closer to the nozzle. The supports also had the effect of channelling the water causing more water to be sprayed between the supports than over them, causing

a non-uniform water distribution radially as well as in the circumference of the spray region.

3.3.3 Repeatability of single medium and low pressure nozzle water distribution results

When analysing experimental data it is important to quantify or to obtain an indication of measurement uncertainty. A repeatability test was therefore done during each test for one position of the measurement beam or containers, by sampling the data twice and comparing the results. Figure 3.14 shows the deviation of the mass velocity measured for each cup on the measurement beam for the medium pressure nozzle water distribution tests.

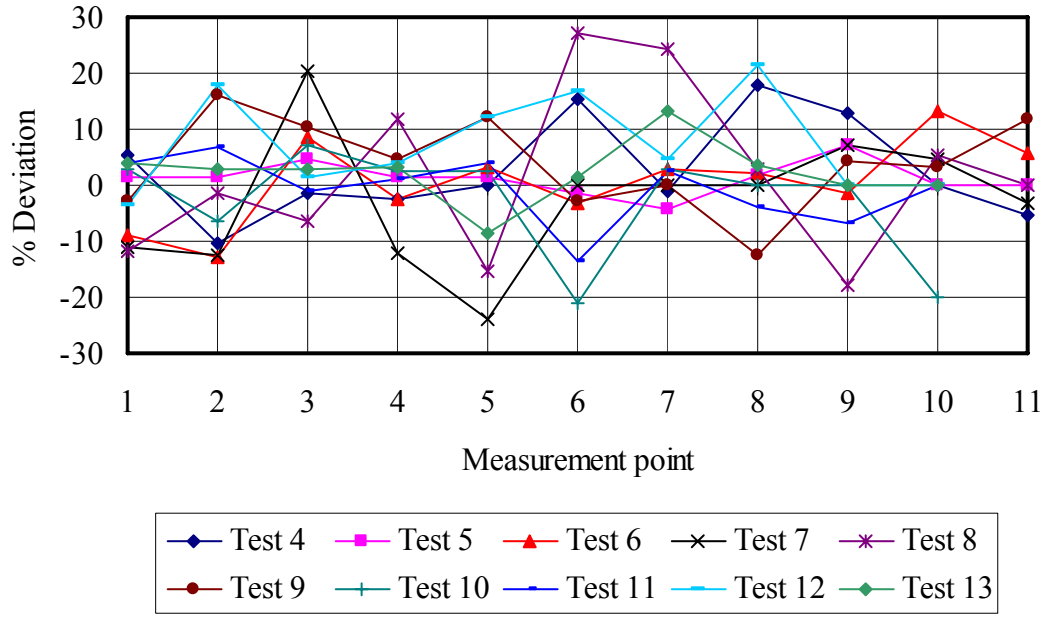

Figure 3.14 Repeatability of water distribution tests for medium pressure nozzles.

Of the data points shown in Figure 3.14, 74% of the points deviate within ±10%, with 95% of the points deviating within ±20% with a maximum deviation of 27%. These nozzles were observed to spray the water in fluctuating bursts of water. In Figure 3.15 the area of high density drops directly below the nozzle can be seen during one of these bursts. The deviation in the results could be explained by the randomness of individual drop trajectories and thus the spray produced by the nozzles.

Figure 3.15 Water burst from a medium pressure nozzle.

Another reason for the deviation can be attributed to slug flow in the flexible plastic tubing due to the small diameter and the long length of tubing in which the water has to flow horizontal over the fill material before draining vertically down to the measuring cylinders. In worst cases the error associated with this could be 15%.

A water mass balance was also done for each test. The flow rate was calculated by integrating the grid of measured points and comparing the results to the mass flow rate as measured with the venturi flow meter as given in Table 3.5.

Table 3.5 Mass balance for single medium pressure nozzles.

Test no.	1	2	3	4	5	6	7	8	9	10	11	12	13
Mass balance deviation, %	-4	7	12	-1	-4	-2	2	-11	-11	14	19	1	2

Since the medium pressure nozzles spray four identical quadrants, they therefore have two axes of symmetry. Using this symmetry, the accuracy of the data can be checked since the water distribution along the y and x axis should be the same within the measurement accuracy. The x and y axes are shown in Figure 3.4.

In worst cases the repeatability of the low pressure nozzle water distribution tests was found to be in the order of 50%. Plotting the two tests on the same graph it was however found that the same water distribution trend was followed. Reasons for the poor repeatability could be due to the manual placement of the containers into the test section, since the single streams of spray created by these nozzles were found to make a large difference in the water distribution with small movement of the containers. The fact that the measurement points taken were spaced half width meant that the tests had to be broken up and the pump restarted between the different stages of the test. No mass balance could be done for the low pressure spray nozzles since the water distribution varied radially as well as circumferentially with the edge of the spray zone being serrated.

3.4 Water drop size distribution of single medium and low pressure nozzles

The water drop size distribution tests were conducted by employing the experimental apparatus, techniques and procedures described in Chapter 2.

3.4.1 Mean diameters and Rosin Rammler diameter distribution

It was decided to use three different mean diameters to analyse the data obtained from the drop size distribution tests. The mean or arithmetic mean diameter is used for comparisons and evaporation studies according to the FLUENT documentation (2005). The mean diameter is defined by:

$$d_{dm} = \frac{\sum_{i=1}^{n} N_i \cdot d_i}{N} \qquad (3.2)$$

The Sauter mean diameter, d_{Sm} is defined as the sum of the drop volumes per interval divided by the sum of the drop surfaces per interval. The Sauter mean diameter is used for combustion, mass transfer and efficiency studies according to the FLUENT documentation (2005). Moussiopoulos and Ernst (1987) used the Sauter mean diameter to model the drop diameters when modelling spray pond sprays. The Sauter mean diameter is defined by:

$$d_{Sm} = \frac{\sum_{i=1}^{n} N_i \cdot d_i^3}{\sum_{i=1}^{n} N_i \cdot d_i^2} \tag{3.3}$$

The Rosin Rammler distribution curve is based on an exponential relationship that exists between the drop diameter, d and the mass fraction of drops with diameter greater than d, namely Y_d. The Rosin Rammler mean diameter, d_{RR} is defined as the diameter at which $Y_d = e^{-1} = 0.368$ and was also used in the data analysis process. The spread parameter n can be obtained by taking the mean of all the interval's spread parameters.

$$n = \frac{\ln(-\ln Y_d)}{\ln\left(d/d_{RR}\right)} \tag{3.4}$$

The Rosin Rammler distribution curve can now be defined as:

$$Y_d = e^{-\left(d/d_{RR}\right)^n} \tag{3.5}$$

Smaller water drops cool down faster than larger ones due to a larger surface to volume ratio. Thus to increase the heat transfer from a cooling tower spray nozzle it is desirable to have small water drops. To break up a drop into smaller drops the surface tension force of the drop needs to be broken. The pressure difference between the inside and outside of a spherical drop is balanced by a ring of surface tension forces which can be written as:

$$\Delta p = \frac{2\sigma}{r} \tag{3.6}$$

The smaller the drop radius the higher the surface tension force and the greater the energy input needed to break up the drop. In cooling towers, low and medium pressure spray nozzles are used with pressure heads ranging between 0.5 to 1.5 m and 1.5 to 8 m water respectively and it can thus be expected that the drops would be large since the required pump head is low compared to nozzles used for fogging.

3.4.2 Water drop size distribution analysis of single medium pressure spray nozzles

The no.1 and 2 medium pressure spray nozzles were tested to determine the drop size distribution for these nozzles as described in Chapter 2.

The drop size distribution data measured at a distance of 0.7 m from the outlet of spray nozzle no.1 at Test no.1 conditions is presented in Figures 3.16 and 3.17. It can be seen from Figure 3.16 that there are a large number of 1 and 2 mm drops.

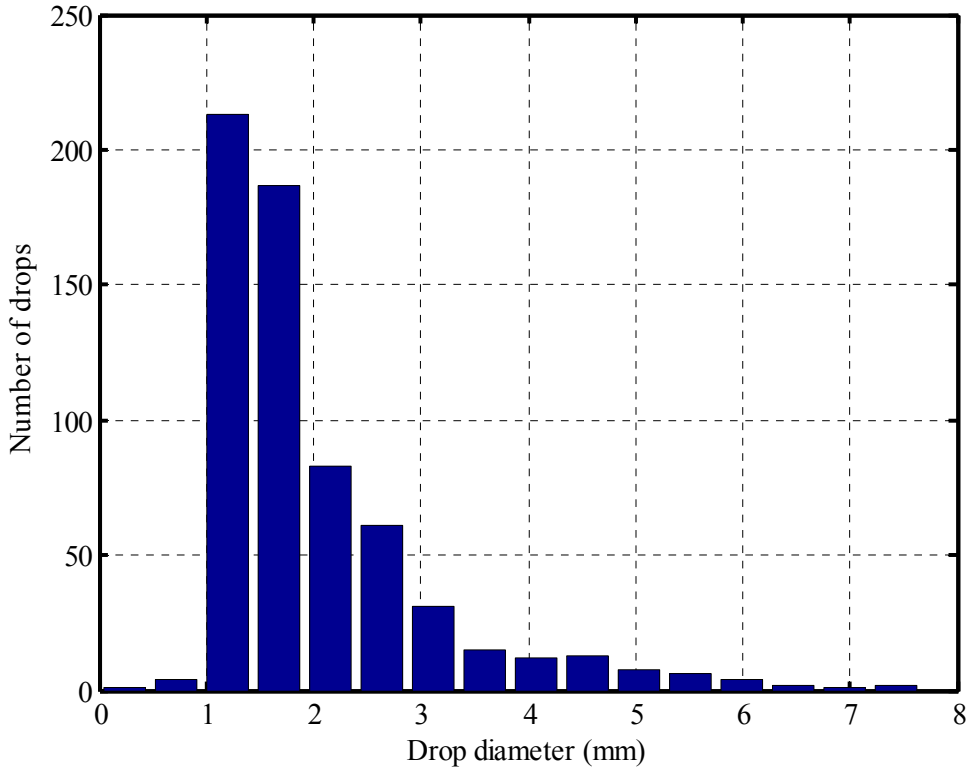

Figure 3.16 Water drop size distribution.

The cumulative mass fraction presented in Figure 3.17 however shows that these drop sizes only contribute 10% toward the total mass. Although the smaller drops cool down faster than the bigger drops they have a very small influence on the cooling of the total mass. The mean diameters are given in Table 3.6.

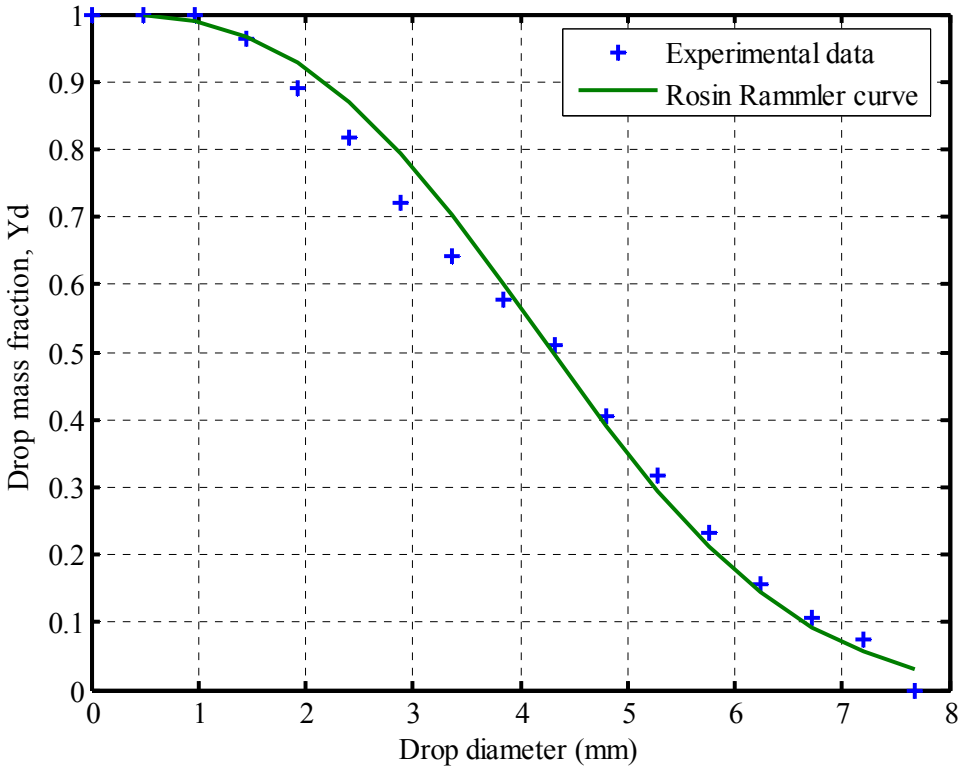

Figure 3.17 Cumulative mass fraction data and Rosin Rammler distribution curve.

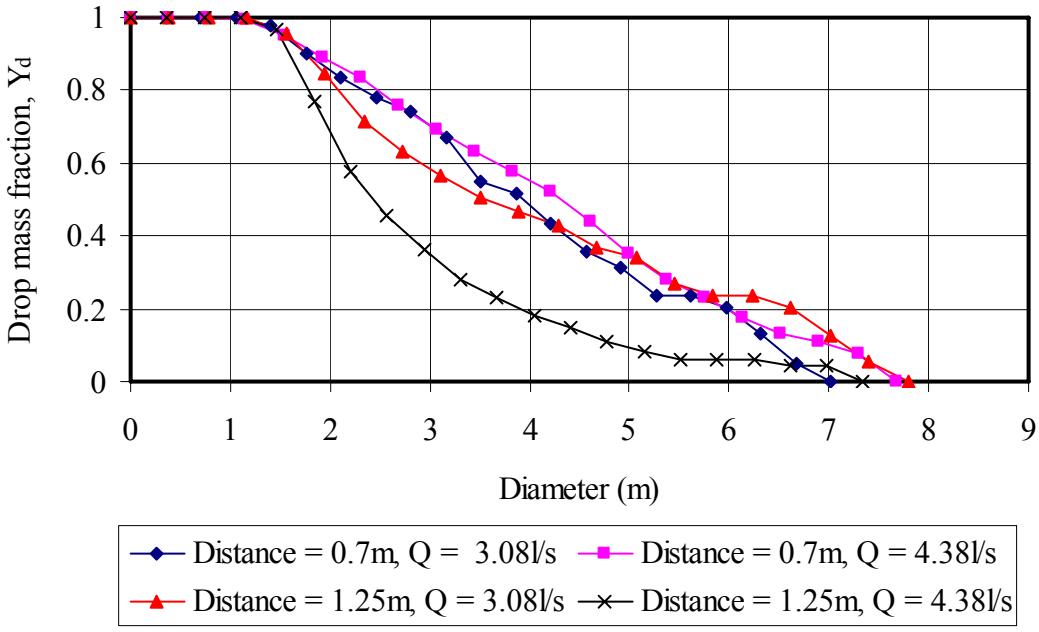

Figure 3.18 Cumulative drop mass fraction distribution curves for nozzle no.1.

In Figure 3.18 the cumulative mass fractions Y_d for nozzle no.1, measured at Test no.1 and 2 conditions is presented. It can be seen from the figure that the largest

quantity of smaller drops is observed at the higher water flow rate at a distance of 1.25 m. The reasons could be that the higher drop velocity and pressure drop associated with the higher flow rate could cause drops to break up. Increased travel distance of the drops could lead to even further drop break up. For nozzle no.2 similar trends could be observed.

The Sauter mean, arithmetic mean and the Rosin Rammler mean diameters for all the tested cases for nozzles no.1 and 2 are presented in Tables 3.6 and 3.7. In general it seems that the mean diameters decrease as the water flow rate increases, which can be attributed to the higher pressure difference over the nozzle and drop velocity. Furthermore there is a decrease in mean diameters as the distance from the nozzle increases which can be as a result of the larger drops falling faster than the smaller ones causing further drop break up.

Table 3.6 Mean diameters for no.1 full cone spray nozzle.

Water flow rate	l/s	3.08	4.38	3.08	4.38
Distance from nozzle	m	0.7	0.7	1.25	1.25
Sauter mean diameter	mm	3.26	3.38	3.12	2.43
Arithmetic mean diameter	mm	2.09	2.03	2.07	1.94
Rosin Rammler mean diameter	mm	4.5	4.9	4.7	2.9

Table 3.7 Mean diameters for no.2 full cone spray nozzle.

Water flow rate	l/s	4.38	6.8	4.38	6.8
Distance from nozzle	m	0.7	0.7	1.25	1.25
Sauter mean diameter	mm	3.25	3.11	3.05	2.89
Arithmetic mean diameter	mm	1.96	2.09	2.05	1.86
Rosin Rammler mean diameter	mm	5.2	4.6	4.5	4.2

3.4.3 Water drop size distribution analysis of single low pressure spray nozzles

Both the low pressure spray nozzles were photographed in up spray at a distance of 0.7 m from the nozzle outlet. Since the nozzles sprayed streams of water, only the drops in these streams could be photographed. Table 3.8 shows the Sauter mean, arithmetic mean and the Rosin Rammler mean diameters for nozzles no.3 and 4.

Table 3.8 Mean diameters for nozzles no.3 and 4.

Nozzle no.		3	4
Water flow rate	l/s	1.6	3.15
Distance from nozzle	m	0.7	0.7
Sauter mean diameter	mm	7.38	7.47
Arithmetic mean diameter	mm	3.24	3.13
Rosin Rammler mean diameter	mm	9.8	10.2

From the drop size distribution graph it was found that for nozzle no.3 there were a lot of small drops between 1 and 2 mm, but a number of large drops, in the order of 10 to 12 mm were also visible. From the cumulative mass fraction data it was found that 50% of the mass was contained in drops larger than 8.9 mm.

For nozzle no.4 it was also found that there were a lot of small drops between 1 and 2mm. There was however a number of large drops in the order of 14 to 16 mm and 50% of the mass were contained in drops larger than 8.8 mm.

3.4.4 Repeatability of single medium and low pressure spray nozzle drop size distributions

To ensure the repeatability of the water drop size distribution tests a number of photographs were taken for each test. The best three photographs were chosen based on clarity, least splashing on the background plate and least clustering of individual drops. The photos for each test were then analysed and averaged using the analysis program (Terblanche, 2005).

Figure 3.19 Water drops photographed in the spray zone.

3.5 Water distribution of four medium pressure spray nozzles

The water distribution from four spray nozzles arranged in a square grid was measured using the measurement beam as described in Chapter 2. Measurements were conducted in the spray region between the four nozzles as shown in Figure 3.20. The test conditions for nozzle no.1 are given in Table 3.9.

Table 3.9 Test conditions for four no.1 spray nozzles arranged in a square grid.

Test no.		14	15	16	17
Water flow rate	l/s	12.3	12.3	12.3	12.3
Air velocity	m/s	0	3	0	3
Nozzle height	m	0.47	0.47	0.35	0.35

Figure 3.20 shows the axes along which water distribution data is presented.

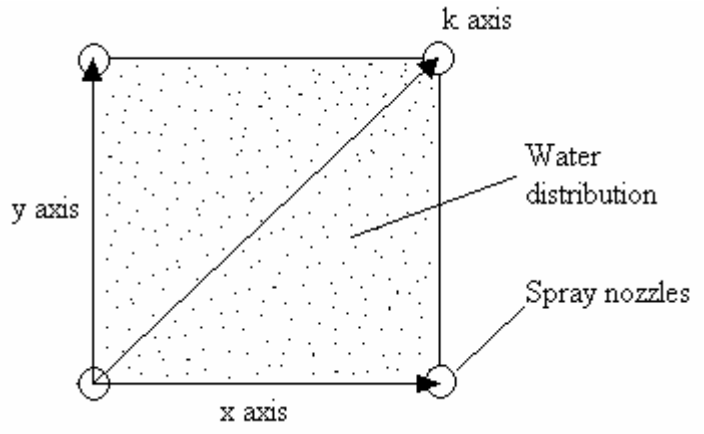

Figure 3.20 Axes along which water distributions are presented.

3.5.1 Water distribution of four medium pressure spray nozzles

Using the superpositioning code described in Chapter 4, it was determined that a nozzle spacing of 0.9 m at a nozzle height of 0.47 m would give a fairly uniform water distribution. The nozzles were therefore installed in this way and the water distributions measured. The effect of counterflow air on the water distribution was investigated by measuring the water distributions at the same water flow rate with and without counterflow air. Figure 3.21 shows water distribution data of Tests no.14 and 15.

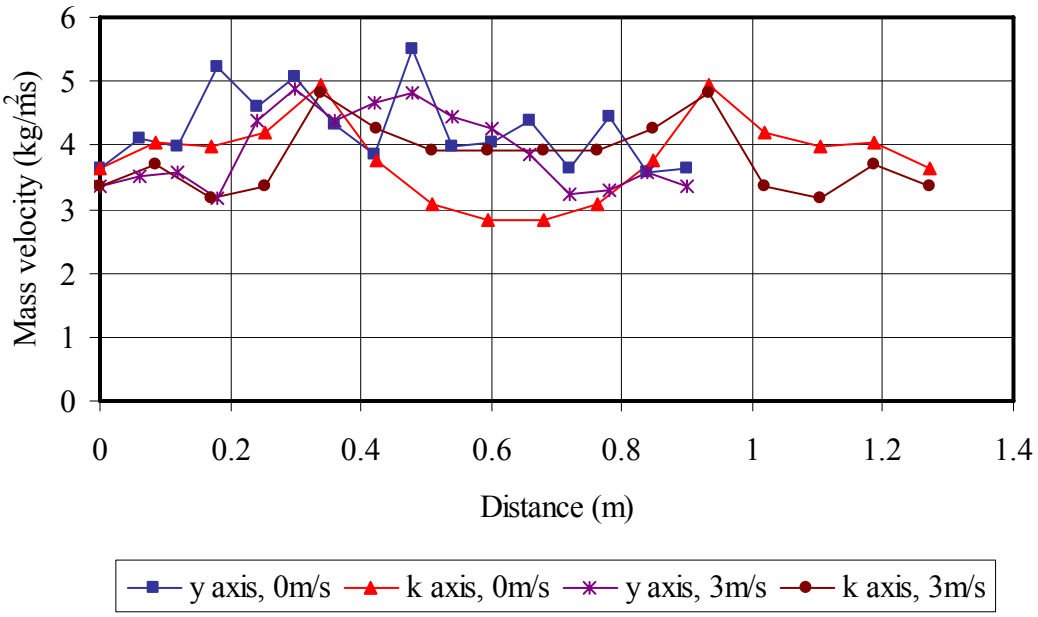

Figure 3.21 Measured water distribution data for four no.1 nozzles with and without counterflow air.

It can be seen along the y axis that the counterflow air had the effect of evening out the water distribution. The trough along the k axis was also levelled out by the counterflow air. This could be due to the higher air speeds through the path of least resistance between the overlapping water distributions, causing the individual nozzle water distributions to increase in diameter, causing a more uniform water distribution.

A similar trend was observed at a nozzle height of 0.35 m, using the data of Tests no.16 and 17.

3.5.2 Repeatability of water distribution tests for four medium pressure spray nozzles

For each of the four nozzle tests, one of the sets of measurements was repeated to determine the repeatability as shown in Figure 3.22. It can be seen that 75% of the points deviate within ±10% and that all of the points deviate within ±20% with a maximum deviation of 19%.

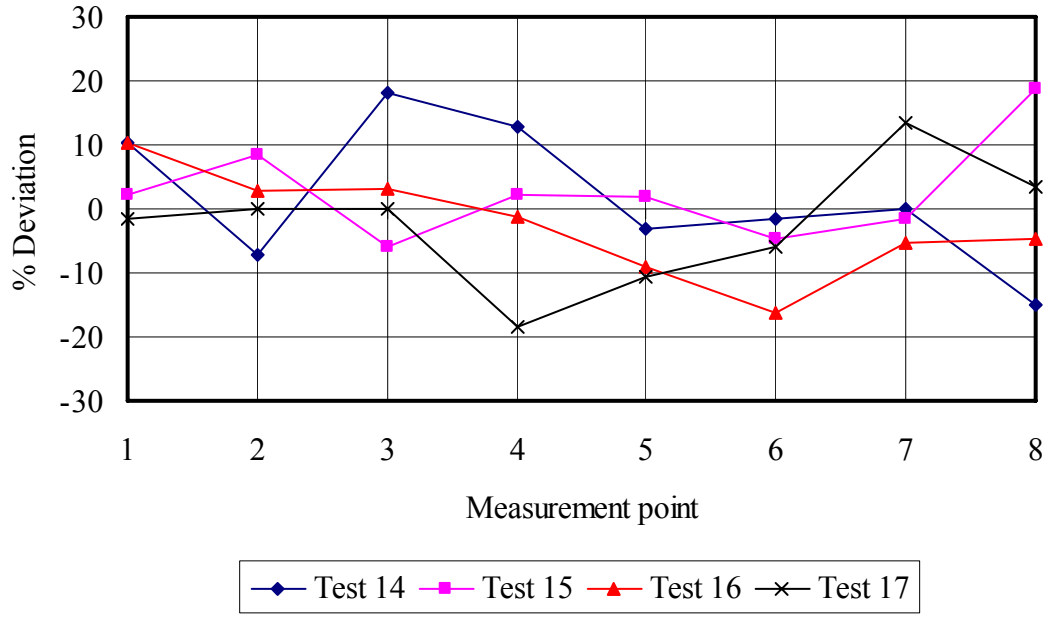

Figure 3.22 Repeatability of water distribution tests with four no.1 nozzles.

As with the single nozzle tests a mass balance was done for each test by integrating the grid of measured points and comparing it to the water flow rate as measured with the venturi flow meter. The mass balance deviation is shown in Table 3.10.

Table 3.10 Mass balance for four nozzles.

Test no.	14	15	16	17
Mass balance deviation %	6	6	4	5

3.6 Conclusion

Measured data showed that the effect of counterflow air velocity on the water distribution of the two medium pressure spray nozzles is small. The drop velocities from these nozzles are quite high and therefore the drop residence time is relatively short. The largest effect was observed at the lower drop velocity, where the peak in the water distribution moved radially outward by approximately 10 %. From these tests it can be concluded that by increasing the residence time of the drops by increasing the distance between the nozzle and fill material, spraying upward, reducing the drop size or reducing the drop velocity at the nozzle outlet, will increase the effect of the counterflow air on the water distribution in a cooling tower. Increasing the height of the medium pressure nozzles above the fill increases the area sprayed by the nozzle, but decreases the mass velocity proportionally. For these specific nozzles it was found that the drop trajectories are virtually straight due to the high drop velocities. For the medium pressure nozzles the water distribution trend as well as the spray diameter stays reasonably the same for different water flow rates but the mass velocity changes proportionately. Counterflow air had the effect of smoothing out the troughs and peaks in the water distribution of four medium pressure spray nozzles arranged in grid formation.

For the low pressure nozzles it was found that in up spray, concentric rings of water were sprayed with the inner ring trajectories passing through the outer ring trajectories. This could lead to possible collision and coalescence of drops causing larger drops. Water also flowed down over the nozzles sides and around the supply pipe, not being broken up into drops and therefore not having any significant effect on the heat transfer. The counterflow air velocity in natural draft cooling towers where these nozzles are used are in the order of 1.5 m/s and the airflow will therefore have

minimal effect on the water distribution of these nozzles since the drop diameters are large.

The water flow rate, required pressure head over the nozzle and distance from the nozzle all have an influence on the drop size distribution. Sauter mean diameters in the order of 3.3 mm were obtained for the medium pressure nozzles. Large drops of up to 16 mm are formed by the low pressure nozzles with Sauter mean diameters in the order of 7.4 mm. The Sauter mean diameter decreases as the pressure head over the nozzle and flow rate increase as well as with an increase in drop travel distance.

4. THEORETICAL MODELLING OF SPRAY NOZZLE PERFORMANCE

4.1 Introduction

For wet cooling towers to operate effectively and to reduce uncertainty when modelling cooling tower performance, it is important to distribute the water uniformly onto the fill material. To achieve this, the characteristics of spray nozzles and the correct nozzle heights above the fill and nozzle spacing are required. In this section a computer code is presented which predicts the water distribution produced by a grid of nozzles installed at a given spacing by superimposing single nozzle data. Furthermore three different computer codes based on different assumptions regarding the nozzle outlet conditions were developed to predict the effect of different operating and installation parameters on single nozzle water distributions. These computer codes solve the differential equations of motion and temperature change for a spherical drop by means of numerical integration.

4.2 Prediction of the water distribution of a grid of nozzles by means of superimposing single nozzle data

A computer code was developed which uses the water distribution data obtained from a single nozzle test to obtain the overall water distribution produced by a grid of nozzles by means of superposition. The distance between the nozzles can be varied to find the optimal nozzle spacing based on the most uniform water distribution obtained. As the code uses single nozzle data, it does not take into account the effects created by placing nozzles in grid formation. These effects include drop collision, drop coalescence and airflow disturbances caused by overlapping water distributions which in turn has an affect on the water distribution.

Single nozzle water distribution data and nozzle spacing was required as input data for the code. The water distribution data is available in the form of a matrix containing the mass velocities measured at all the points on a square Cartesian measurement grid as described in Chapter 2. The spray produced by the medium pressure nozzles was found to be symmetric around two axes. The code firstly generates the water distribution matrix for all four quadrants of a single nozzle in terms of a local co-

ordinate system (x and y coordinates) with its origin at the nozzle centre line. The overall water distribution produced by the overlapping sprays from four nozzles is then calculated by superimposing the water distribution data of the four single nozzles using equation (4.2). This was done by locating the nozzles in a global co-ordinate system (X an Y coordinates) by redefining the origin of the mass velocity co-ordinates for each nozzle in terms of the global co-ordinates and then summing the mass velocities to obtain an overall water distribution matrix in terms of the global co-ordinate system.

The mass velocity for the single nozzle in terms of local co-ordinates is defined by:

$$G_{wL}(x,y) = f(x,y) \qquad (4.1)$$

For a grid of m x n nozzles with nozzle spacing L, the water mass velocity is defined by:

$$G_{wG}(X,Y) = \sum_{i=0}^{m-1}\sum_{j=0}^{n-1} G_{wL}(X- iL, Y- jL) \qquad (4.2)$$

In order to compare the results of the code to measured data, single nozzle data for nozzle no.1 (Test no.2) was used to model the water distribution of 4 single nozzles spaced at 0.9 m, which provides a relatively uniform water distribution at a nozzle height of 0.47 m and flow rate of 12.3 l/s. Subsequently water distribution tests were conducted on four nozzles installed in the test facility as described in Chapter 2.

Figure 4.1 shows the results of Test no.14 and the code results based on Test no.2 data, both conducted without counterflow air. Comparing the measured to the calculated water distribution, it can be seen that the code predicts the same water distribution trends along both axes. Considering the measurement uncertainty there seems to be no visible influence of drop collision on the water distribution.

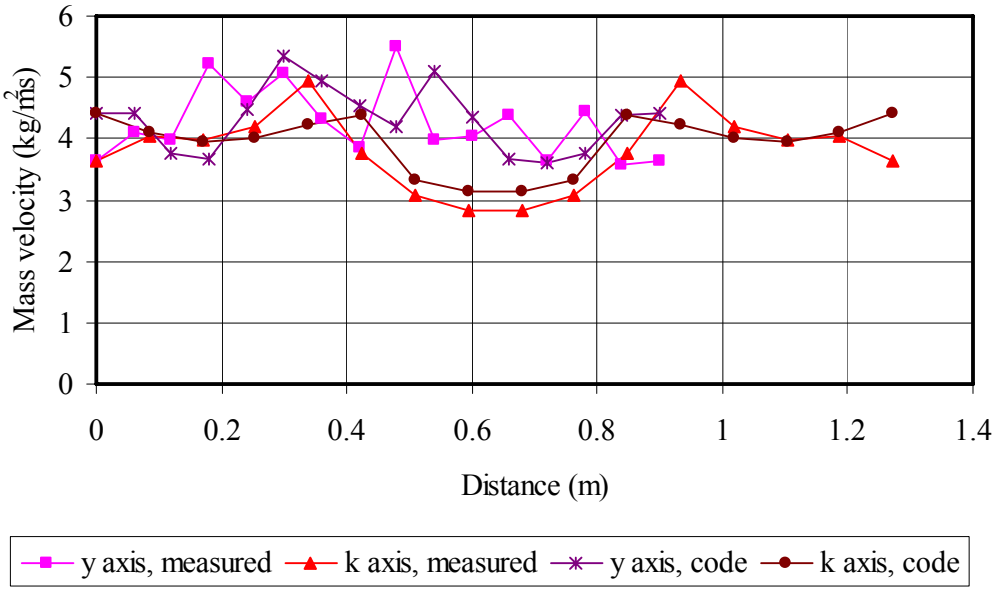

Figure 4.1 Predicted and measured water distribution of four nozzles without air flow.

Figure 4.2 shows the results of Test no.15 and the code results based on Test no.3 data. Both tests were done at an air velocity of 3 m/s. It can be seen that the code over predicts the mass velocity along the y axis between 0.3 – 0.6 m and under predicts it along the k axis between 0.5 – 0.75 m. An explanation for this could be higher air velocities through the path of least resistance in the overlapping section between the nozzles, causing higher drag here and thus flattening the peaks and raising the troughs, resulting in a more uniform water distribution.

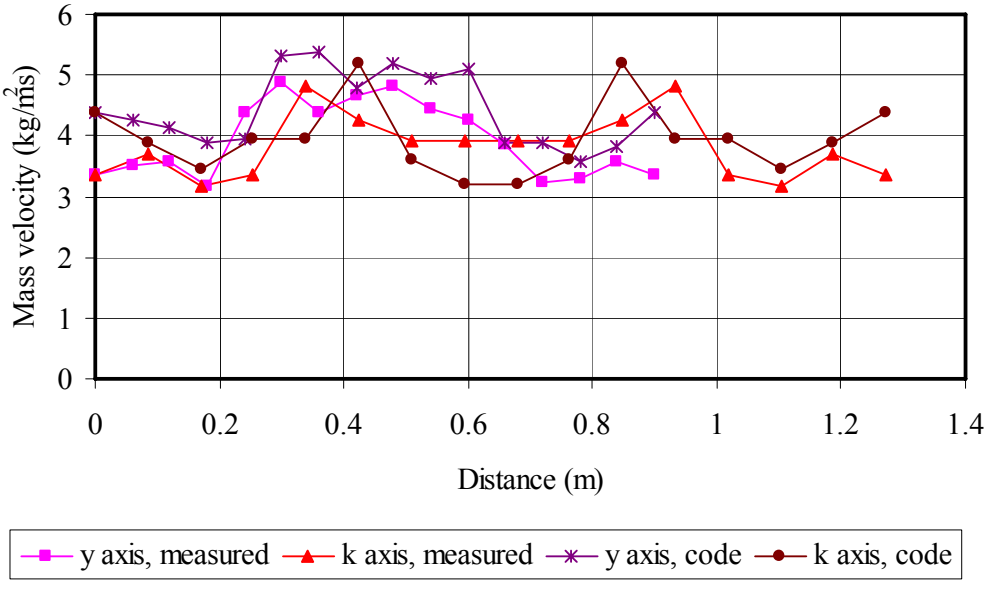

Figure 4.2 Predicted and measured water distribution of four nozzles in 3 m/s air.

According to the manufacturer of these specific spray nozzles, they should be installed at a height of 0.35 m above the fill material, spaced 1 m apart or at a height of 0.4 m spaced at 1.2 m. Figure 4.3 shows the calculated water distribution between four no.1 nozzles with a spacing of 0.9 m and a height of 0.35 m. It can be seen that the water distribution is not uniform and that large troughs exist between the nozzles. The presented data is from Test no.17.

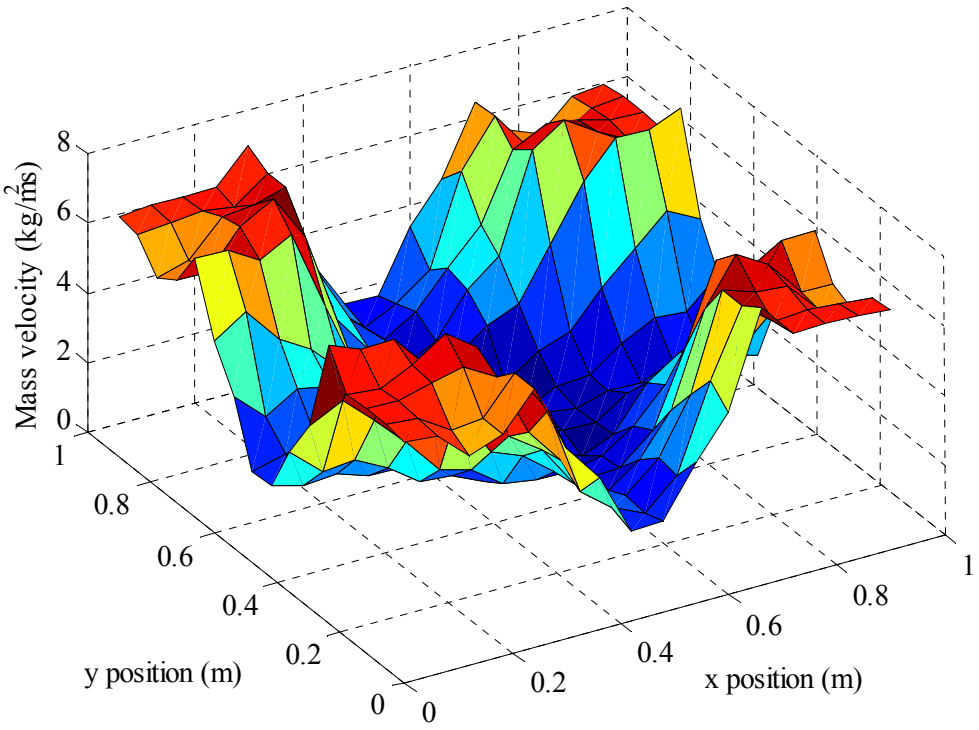

Figure 4.3 Water distribution of four no.1 nozzles spaced 0.9 m apart with a nozzle height of 0.35 m.

4.3 Spray simulation codes

Three different nozzle codes were developed to model the effect that varying cooling tower operating and installation parameters such as counterflow air velocity, water flow, nozzle height, spray direction and water temperature have on the water distribution and heat and mass transfer between the water and air in the spray zone. Being able to model these parameters will help to improve cooling tower performance. These models differ from each other with respect to the criteria at which the drops exit the nozzle orifice i.e. initial conditions of the spray. Calculating the

drop trajectory and temperature change of a single drop with given initial conditions formed the basis of all these codes. By applying different initial conditions, different spray patterns could be constructed and drop temperature changes calculated.

4.3.1 Governing equations for drop trajectory

To determine the drop trajectory of a single drop the following assumptions were made: the drop remains spherical; no drop break up occurs; the drop diameter remains constant; the drop falls in a two dimensional plane; the air velocity is vertically upwards. The forces acting on the drop are the aerodynamic drag force F_D, the buoyancy force F_B and the body force due to gravity mg. The relative air velocity over the drop v_{ad} is calculated using the drop velocity v_d and the vertical air velocity v_a. Figure 4.4 shows these forces and velocities acting on the drop.

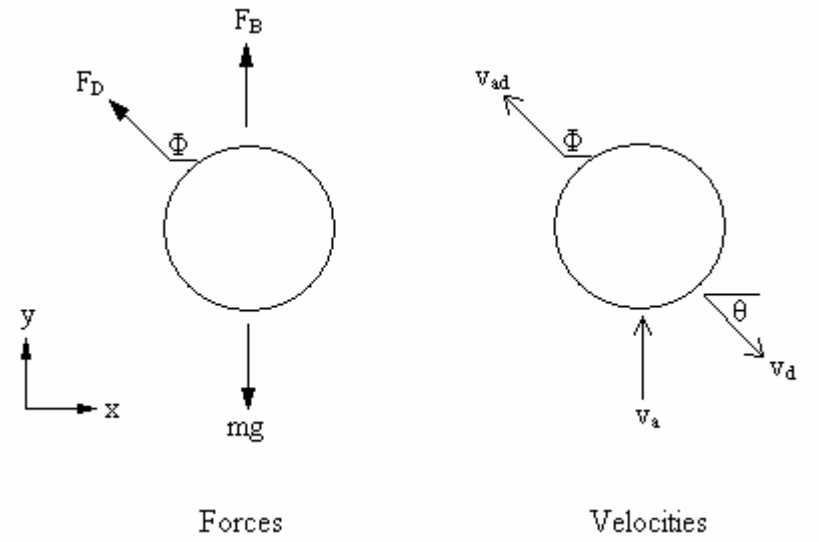

Figure 4.4 Forces and velocities acting on a spherical drop falling through air.

Due to drop initial conditions, the drop might have x and y velocity components, and thus the aerodynamic drag force will also have x and y components. Using Newton's second law the differential equations of motion in the x and y directions are given by:

x direction:

$$m_d \frac{dv_{dx}}{dt} = F_{Dx} \qquad (4.3)$$

y direction:

$$m_d \frac{dv_{dy}}{dt} = F_B + F_{Dy} - m_d g \tag{4.4}$$

For the first time step, the drop absolute velocity and the drop injection angle at the injection point is used to determine the drop absolute velocities in the x and y directions:

$$v_{dx} = v_d \cos(\theta) \tag{4.5}$$

$$v_{dy} = v_d \sin(\theta) \tag{4.6}$$

The relative air velocity over the drop is calculated from the x- and y drop absolute velocity components and the counterflow air velocity:

$$v_{ax} = -v_{dx} \tag{4.7}$$

$$v_{ay} = v_a - v_{dy} \tag{4.8}$$

$$v_{ad} = \left(v_{ax}^2 + v_{ay}^2\right)^{0.5} \tag{4.9}$$

The relative air velocity is used to calculate the Reynolds number:

$$Re = \frac{\rho_a v_{ad} d}{\mu_a} \tag{4.10}$$

A drag correlation by Turton and Levenspiel (1986) for Re $\leq$ 200000 is used to determine the drag coefficient:

$$C_D = \frac{24(1+0.173Re^{0.657})}{Re} + \frac{0.413}{(1+16300Re^{-1.09})} \tag{4.11}$$

The x- and y drop relative velocity components are then used to calculate the relative velocity angle:

$$\Phi = \operatorname{atan}\left(\frac{v_{ay}}{v_{ax}}\right) \tag{4.12}$$

The total drag force acting on the drop is then calculated from:

$$F_D = C_D A_{fr} \frac{1}{2} \rho_a v_{ad}^2 \tag{4.13}$$

The x and y drag components are determined from:

$$F_{Dx} = F_D \cos(\Phi) \tag{4.14}$$

$$F_{Dy} = F_D \sin(\Phi) \tag{4.15}$$

The buoyancy force acting on the drop is determined by calculating the body force of the air displaced by the drop:

$$F_B = \rho_a V_d g \tag{4.16}$$

Equations (4.3) and (4.4) are solved using a first order Euler integration scheme with respect to time to give drop velocity in the x and y direction for each time step. With the time step and the drop x and y velocities known, the drop displacement in the x and y directions are calculated at each time step.

$$x_d^{i+1} = x_d^i + \frac{v_{dx}^i + v_{dx}^{i+1}}{2} \cdot \Delta t \tag{4.17}$$

$$y_d^{i+1} = y_d^i + \frac{v_{dy}^i + v_{dy}^{i+1}}{2} \cdot \Delta t \tag{4.18}$$

From the drop x and y direction displacements respectively, the drop position could be plotted for each time step. Appendix C gives sample calculations for the drop trajectory calculations.

4.3.2 Governing equations for drop temperature change

To determine the drop temperature change, the following assumptions are made: the drop shape remains spherical; the drop diameter remains constant; the drop temperature is homogeneous; the relative humidity of air at the control surface remains 100%; the humidity ratio for ambient air remains constant; the ambient air temperature remains constant; the counterflow air velocity is vertically upwards. The Reynolds number defined by equation (4.10) is also used to calculate the drop temperature change. The change in total internal energy of the drop is due to mass

transfer and convective heat transfer across the control surface defined at the drop interface as shown in Figure 4.5.

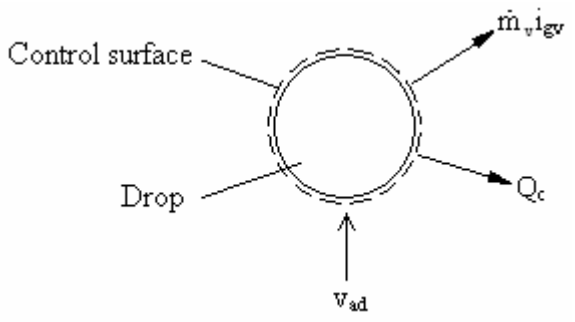

Figure 4.5 Control volume for a spherical drop falling through air.

From the first law of thermodynamics, an energy balance for a control volume in an unsteady flow process can be expressed by:

First law of thermodynamics:

$$\frac{dU}{dt} = \left(Q_c + W + \dot{m}_v i_{gv}\right)_{in} - \left(Q_c + W + \dot{m}_v i_{gv}\right)_{out} \tag{4.19}$$

For the control volume in Figure 4.5, using the product rule, equation (4.19) simplifies to:

$$\frac{dT_d}{dt} = \frac{\left(-\dot{m}_v i_{fgw} - Q_c\right)}{\left(m_d c_{vw}\right)} \tag{4.20}$$

To determine the temperature change of the drop the mass transfer $\dot{m}_v$ and convective heat transfer Q_c from the drop have to be calculated. Gilliland (1934) proposed a semi empirical equation for the diffusion coefficient in a mixture of air and water vapour given by:

$$D = \frac{0.3 \times 0.04357 \cdot T_a^{1.5}}{33.14 \cdot p_a} \tag{4.21}$$

The Schmidt number of air is defined by:

$$Sc_a = \frac{\mu_a}{\rho_a D} \tag{4.22}$$

Ranz and Marshall (1952) proposed a semi-empirical correlation for the Sherwood number for $2 \leq Re < 800$:

$$Sh = 2+0.6Re^{0.5}Sc_a^{0.33} \tag{4.23}$$

Clift et al. (1978) proposed the following correlations for the Sherwood number for $800 \leq Re < 2000$:

$$Sh = 1+\left(\left(1+\frac{1}{Re \cdot Sc_a}\right)^{\frac{1}{3}} Sc_a^{\frac{1}{3}}\right)(0.752Re^{0.472}) \tag{4.24}$$

and for $2000 \leq Re \leq 100000$:

$$Sh = 1+\left(\left(1+\frac{1}{Re \cdot Sc_a}\right)^{\frac{1}{3}} Sc_a^{\frac{1}{3}}\right) \cdot (0.44Re^{0.5}+0.034Re^{0.71}) \tag{4.25}$$

The humidity ratio at the drop surface is defined by:

$$w_d = \frac{0.622\varphi p_{vd}}{p_a - \varphi p_{vd}} \tag{4.26}$$

The mass transfer coefficient is calculated using the applicable Sherwood number and diffusion coefficient:

$$h_D = \frac{Sh \cdot D}{d} \tag{4.27}$$

Kröger (2004) gives the mass transfer coefficient where water is exposed to an air stream:

$$h_d \approx \frac{2h_D p_a}{R_v (w_d - w_\infty)(T_d + T_a)}\left(\frac{w_d}{(w_d + 0.622)} - \frac{w_\infty}{(w_\infty + 0.622)}\right) \tag{4.28}$$

With the mass transfer coefficient known, the mass transfer from the drop can be calculated using the difference between the air and drop humidity ratios:

$$\dot{m}_v = h_d A_d (w_d - w_\infty) \tag{4.29}$$

Ranz and Marshall (1952) give a correlation to determine the Nusselt number of free falling spherical liquid drops for Re < 800:

$$Nu = 2 + 0.6Re^{\frac{1}{2}}Pr_a^{\frac{1}{3}} \tag{4.30}$$

Miura et al. (1977) showed that the equation is valid for Re < 2000.

The heat transfer coefficient and convective heat transfer are defined as follows:

$$h_c = \frac{Nu \cdot k_a}{d} \tag{4.31}$$

$$Q_c = h_c A\left(T_d - T_a\right) \tag{4.32}$$

Equation (4.20) can be solved numerically using a first order Euler integration scheme with respect to time and the drop temperature calculated for each time step. Appendix C gives sample calculations for the drop temperature change calculations.

4.3.3 Modelling of velocity and temperature change for a single drop

In order to validate the numerical solution for drop trajectory and temperature change, the modelling results were compared to corresponding results obtained using the commercial CFD code, FLUENT (version 6.2.16). Two different scenarios were used to investigate this. In the first scenario, single drops of different diameters were injected at an initial speed and different initial angles into upward flowing air. In the second scenario single drops of different diameters with zero initial speed were injected vertically, at an angle of -90˚ from the horizontal, into upward flowing air. For both scenarios three different drop diameters were used namely 1, 3 and 5 mm. The initial conditions for all the simulations were as follows:

Ambient drybulb temperature	$T_a = 293$ K
Ambient wetbulb temperature	$T_{wb} = 286$ K
Atmospheric pressure	$p_a = 101325$ Pa
Drop temperature	$T_d = 313$ K
Counterflow air velocity	$v_a = 2.5$ m/s
Code time step	$\Delta t = 0.05$ s

The 2-D FLUENT simulations were done with the steady state solver and interaction with continuous phase activated. The heat transfer and two equation k-ε turbulence

model were also used. To simulate the mass transfer from the drop, species transport was activated and water and air chosen as active species. Once a converged solution was obtained for the continuous phase the discrete phase model with continuous phase interaction could be activated and the source terms set to update after every ten continuous phase iterations. The drop injections could then be defined.

Figure 4.6 shows the drop trajectories for the first scenario. To prevent the data from lying on top of each other the initial injection angle of the 1 mm drop is -60˚ from the horizontal, -50˚ for the 3 mm and -40˚ for the 5 mm drop. The spray height was simulated to be 2 m and the initial drop speed 2 m/s. The aim of this figure is not to show the difference between different drop diameters and injection angles but rather to compare the code and FLUENT simulations for corresponding conditions.

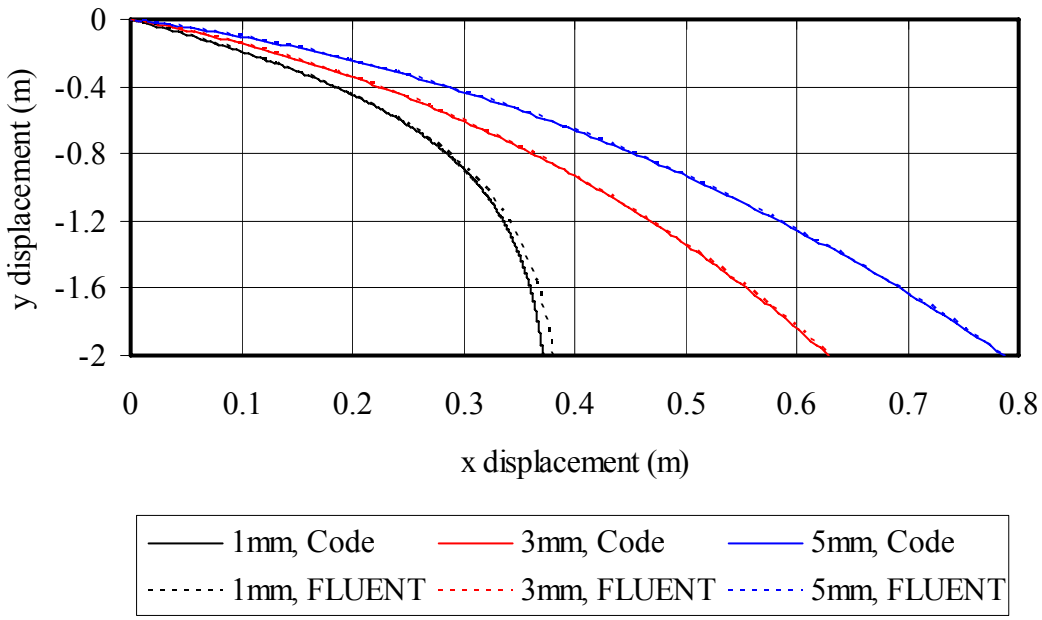

Figure 4.6 Drop trajectories calculated using FLUENT and code for different drop diameters.

Figure 4.6 shows that the code under predicts the drop trajectory for the 1 mm drop compared to FLUENT, by 2.5% whereas the 3 mm and 5 mm trajectories are the same for both the code and FLUENT.

For the second scenario, Figure 4.7 and 4.8 shows the drop velocities and temperatures as a function of time in 2.5 m/s counterflow air. The difference in

terminal velocity can be attributed to different drag correlations used by FLUENT. It can be seen that the terminal drop velocity for smaller drops is lower and is reached faster than bigger drops. Comparing the code and FLUENT results it can be seen that the three drop temperatures compare well and that smaller drops cool down much faster than the bigger drops.

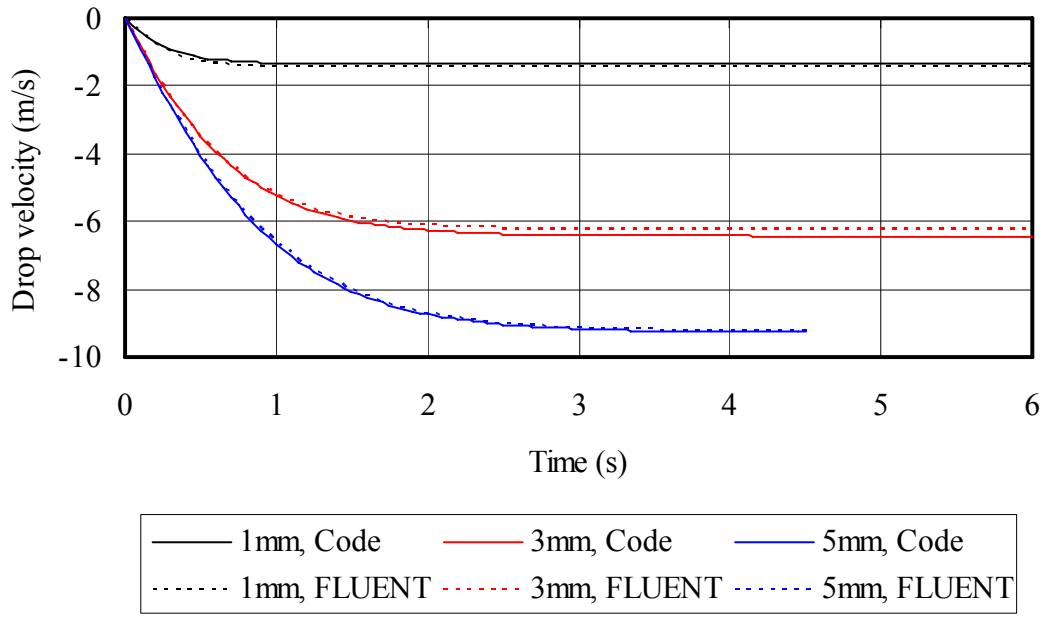

Figure 4.7 Drop vertical velocity as a function of time in 2.5 m/s counterflowing air.

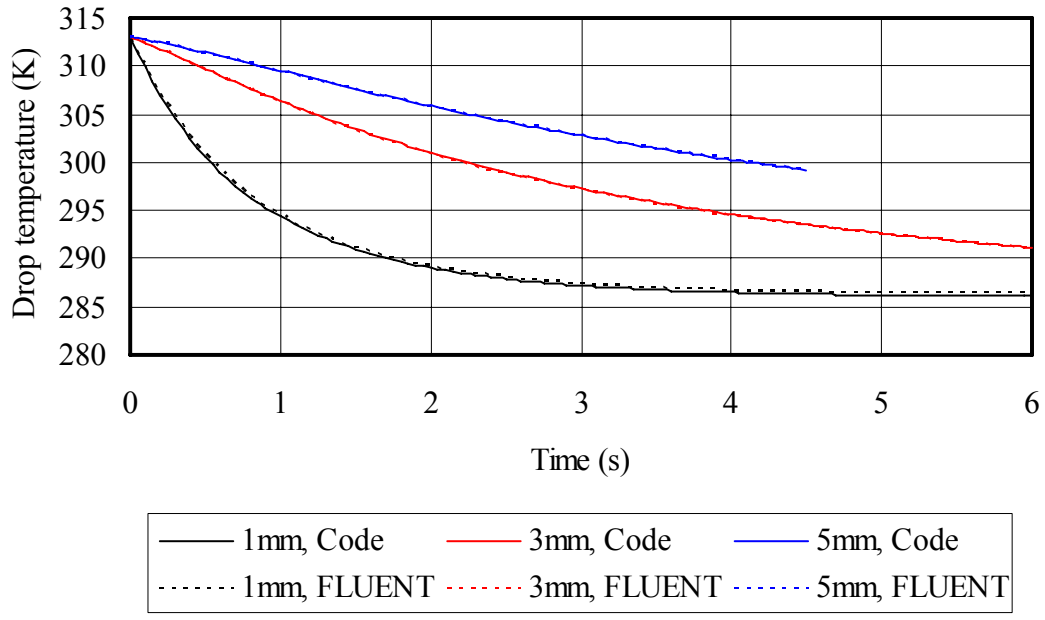

Figure 4.8 Drop temperature change as a function of time in 2.5 m/s counterflowing air.

4.3.4 Modelling of spray zones

The following additional assumptions are required to model sprays: all drop trajectories originate from a single point; there are no drop collisions; each drop exists and interacts with ambient air in the same way as a single drop; the ambient air temperature remains constant; the relative humidity of ambient air remains constant; the air speed remains uniform and constant; the drop diameter remains constant and the drop diameters are uniform.

The required user inputs to the code include the following: the ambient air temperature; the ambient air wetbulb temperature; the atmospheric pressure; the vertical air velocity; the drop diameter; the nozzle to fill height; the time step; the spray diameter; the number of spray trajectories and the mass velocity of each spray trajectory.

The spray diameter is sub divided into evenly spaced concentric rings. The number of rings is equal to the number of spray trajectories. The end position of each trajectory lies in one of the rings and the mass velocity of each trajectory is used to calculate the number of drops represented by each trajectory. The drop temperature change along each trajectory, as well as the total mass and energy transfer is then calculated. The different codes can be differentiated by the following criteria used to determine the drop trajectories. These criteria are:

1. Constant initial speed

The constant initial speed code, referred to as constant speed code hereafter, assumes that all the drop trajectories have the same initial drop speed given as input by the user. The code then iterates the initial angle of each trajectory until the required trajectory end positions on the fill are obtained.

2. Constant initial angle

The constant initial angle code, referred to as constant angle code hereafter, assumes that all the drop trajectories have the same initial angle given as input by the user. The code then iterates the initial velocity vector of each trajectory so that the required trajectory end position on the fill is obtained.

3. Constant y velocity at the fill

The constant y velocity at the fill level code, referred to as constant y velocity code hereafter, assumes that all the drop trajectories have the same y velocity component when entering the fill given as input by the user. The code then iterates the initial velocity vector and initial angle of each trajectory so that the trajectory end position on the fill is obtained, achieving the stated y velocity component.

Figure 4.9 shows the drop initial conditions at the nozzle outlet for the different codes, simulating Test no.6 conditions as discussed in the following section. The initial drop angle is measured downward from the horizontal plane.

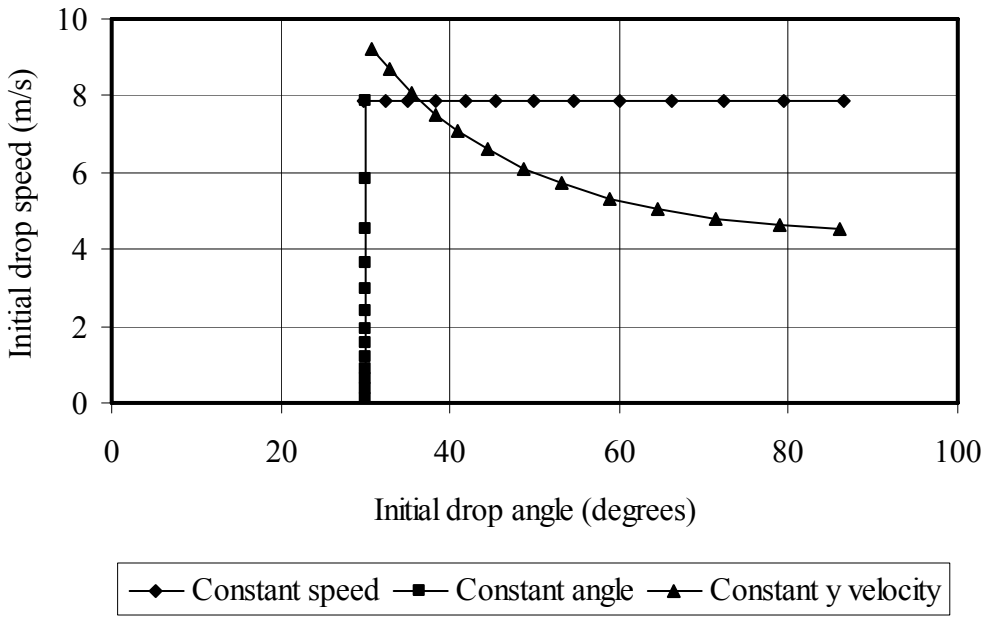

Figure 4.9 Drop initial angle and speed at nozzle outlet.

4.3.5 Comparison between code and single nozzle water distribution data

The results from the three different nozzle simulation codes were compared to measured single nozzle water distribution data. The validity of the modelling assumptions made, as well as the value of the codes in predicting spray nozzle water distributions under varying counterflow air conditions and nozzle heights was investigated.

Experimental data from tests conducted with the no.2 spray nozzle, at a flow rate of 4.38 l/s and vertical air speeds of 0 and 3 m/s, was used to evaluate the results

obtained from the three nozzle simulation tests. The experimental data of Test no.6 at 0 m/s was used to predict the water distribution at 3 m/s. The results are then compared to the experimental data at 3 m/s of Test no.7. A Sauter mean drop diameter of 3.25 mm, determined using the drop size distribution tests described in Chapter 2, was used to simulate the drops. Tests were conducted and simulated at a nozzle to fill height of 0.47 m

To simulate the water distribution with the constant y velocity code, the drop y velocity entering the fill had to be calculated. Using the drop y velocity at the nozzle exit, presented in Table 3.3, the drop y velocity entering the fill 0.47 m below the nozzle was calculated to be 5.2 m/s and used as input value into the code. To simulate the water distribution with the constant angle code, the spray angle of the actual nozzle was measured from a photograph taken, which was found to be -30˚ from the horizontal. This angle was used as input value into the code. To simulate the water distribution with the constant speed code, the drop injection speed of the outermost trajectory, as calculated with the constant angle code for a spray angle of -30˚ was used. The peripheral trajectories of the constant speed and constant angle codes will therefore be the same having a drop injection speed of 7.86 m/s. This drop injection speed was used as input into the code.

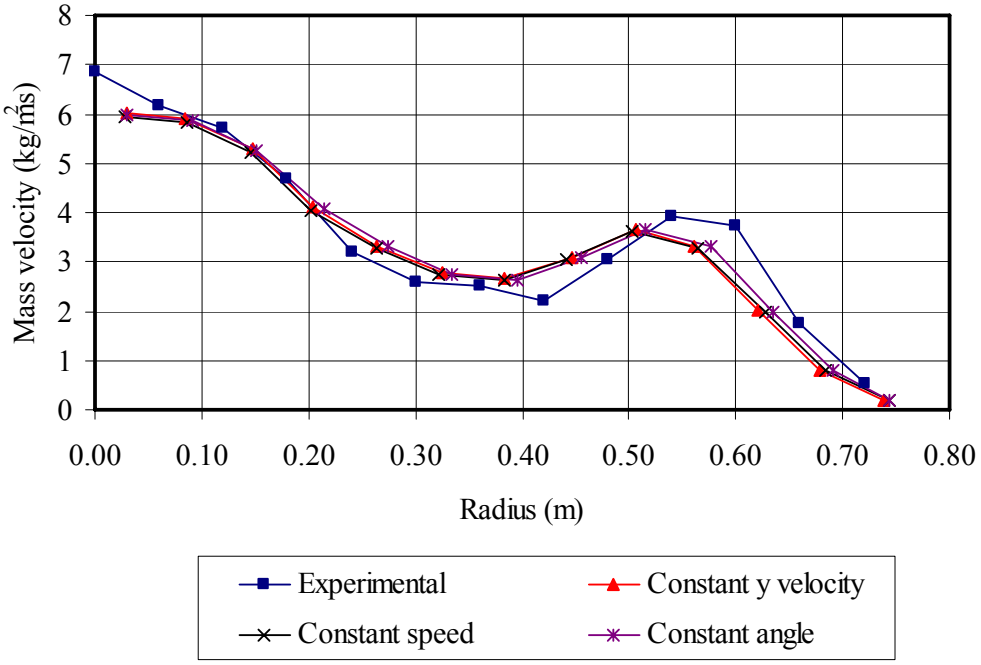

Figure 4.10 Predicted and measured water distribution in 3 m/s counterflow air.

From Figure 4.10 it can be seen that all three of the simulation codes under predict the effect of counterflow air on the water distribution. The outward radial movement of the peak in the water distribution at 0.54 m was under predicted in the order of 5%. The same trend is however followed by all three simulation codes. The reason that the code under predicts the water distribution can be attributed to the assumption that the air velocity profile remains uniform which differs from the real velocity profile due to interaction between the air and spray. Investigating the affect of diameter, the constant angle code and a diameter of 2.25 mm best represented the radial movement of the water distribution peak. This diameter is however 30% smaller then the measured Sauter mean diameter of 3.25 mm.

There were no water distribution data available for up spraying nozzles in counterflow air. Instead a hypothetical up spraying nozzle with the same water distribution as measured for Test no.6 was simulated using the three simulation codes. The spray height was simulated to be 1 m in no airflow conditions and the nozzle height at 0 m (fill packed between the distribution pipes). A Sauter mean diameter of 3.25 mm was used to simulate the drop diameter. The input values for the three codes were as follows: y drop velocity of 4.2 m/s for the constant y velocity code, initial angle of 78.7° for the constant angle code and initial drop speed of 4.8 m/s for the constant speed code. The effect of 3 m/s counterflowing air on the water distribution could then be investigated.

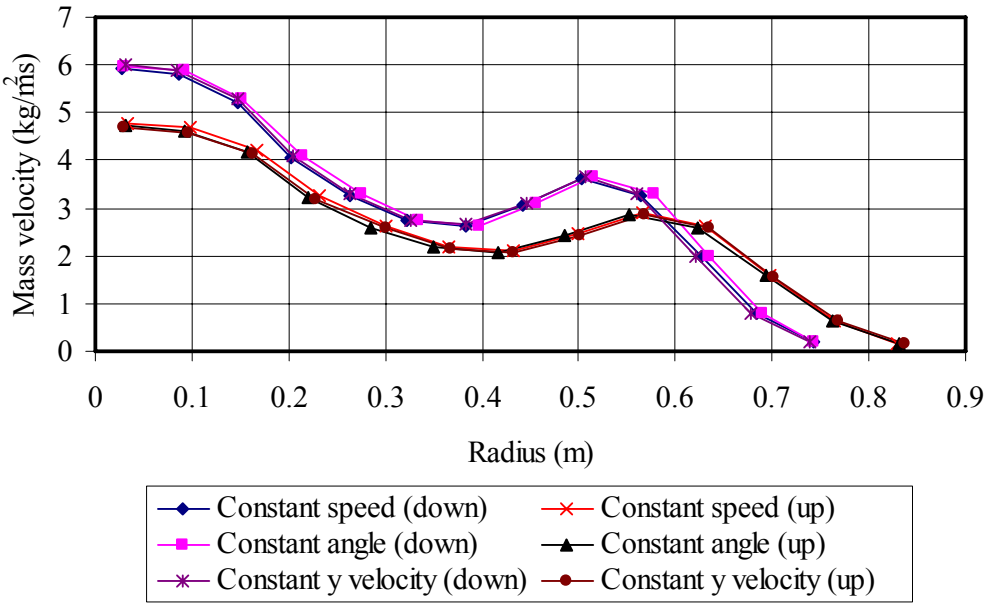

Figure 4.11 Predicted up and down spray water distributions in 3 m/s counterflow air.

Figure 4.11 shows the predicted water distributions, using the three simulation codes, for up and down spraying nozzles. From the figure it can be seen that the effect of counterflow air on the water distribution is more significant for up spray than for down spray, thus increasing the spray diameter by 10% more and lowering the water mass velocity more significantly than for down spray.

Experimental data from tests conducted with the no.1 nozzle at nozzle to fill heights of 0.35 and 0.47 m and a flow rate of 4.38 l/s were also simulated. The experimental data of Test no.12 at a height of 0.35 m was used to predict the water distribution at a height of 0.47 m. This was then compared to the experimental data of Test no.1 at a height of 0.47 m. A Sauter mean drop diameter of 3.4 mm was measured and used to simulate the drop diameter. The water distributions were simulated without counterflow air.

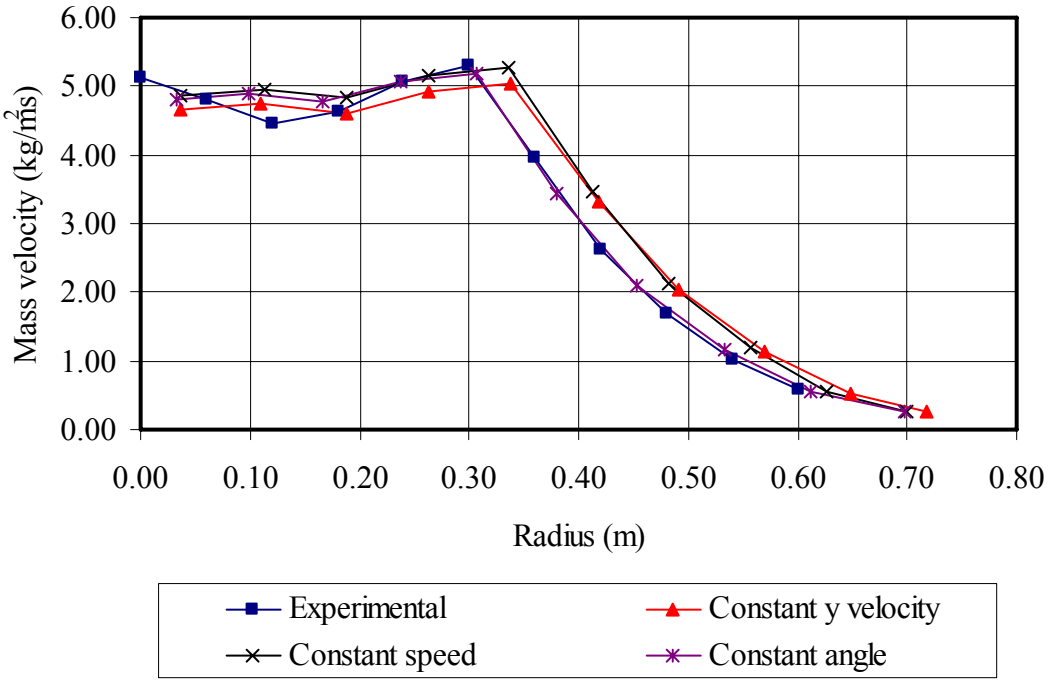

Figure 4.12 Predicted and measured water distribution at a spray nozzle height of 0.47m.

From Figure 4.12 it can be seen that the constant angle code predicts the effect of different nozzle heights best compared to the experimental data.

4.4 Conclusion

The presented data shows that it is possible to use superposition to predict, within reasonable measuring accuracy, the water distribution of a grid of four nozzles using single nozzle data. Collision of drops does not seem to have a large influence on the water distribution, but it was found that there are effects due to counterflow air that can not be predicted. The code for single drop trajectory and temperature change were discussed and found to compare within 2.5% to corresponding simulations done with FLUENT. Three different nozzle spray modelling codes were developed and the results obtained were compared to experimental data to determine the validity of these codes. The constant angle code was found to predict the effect of different nozzle heights best compared to experimental data. The effect of counterflow air on the outward radial movement of the water distribution peak was under predicted by 5% for all the simulation codes due to air flow effects not modelled. Comparing predicted water distributions for up and down spraying nozzles, it was found that the up spraying nozzles were affected more by counterflowing air and that the spray diameter increased by 10% more than for down spray. The constant angle code best predicted the water distributions, but it is assumed that the constant speed code is the closest representation of the spray produced by an actual nozzle.

5. CFD SIMULATIONS

5.1 Introduction

The commercial CFD code FLUENT (version 6.2.16) was used to simulate the spray from spray nozzles using different modelling approaches and the results were compared to experimental data. The spray model developed was used to simulate single nozzles as well as nozzles in grid arrangement in both up spray and down spray configurations. The pressure drop and Merkel numbers were calculated and compared to correlations from literature based on experimental data.

5.2 Modelling of single nozzle spray

The advantage of modelling spray using FLUENT rather than the codes developed, was that FLUENT models the interaction between the drops and the continuous phase, thus affecting the continuous phase temperature, velocity and humidity ratio to give a more realistic simulation. All FLUENT simulations were conducted at two different air conditions shown in Table 5.1 Test condition no.1 simulates nozzles spraying into typical ambient conditions when there are no fill and rain zones present. Test condition no.2 simulates typical conditions encountered above the fill material in a cooling tower. For both the test conditions the initial water temperature was 313 K.

Table 5.1 Input conditions for FLUENT simulations.

Test condition	No. 1	No. 2
Ambient drybulb temperature	T_a = 293 K	T_a = 305 K
Ambient wetbulb temperature	T_{wb} = 286 K	T_{wb} = 305 K
Ambient pressure	p_a = 101325 Pa	p_a = 101325 Pa
Drop initial temperature	T_d = 313 K	T_d = 313 K
Water mass flow rate per nozzle	$\dot{m}$ = 4.5 kg/s	$\dot{m}$ = 4.5 kg/s

The grid independence for temperature and pressure was achieved for all practical purposes for a cell size of 50x50x50 mm. Since the number of cells used in the simulations was small, it was decided to use a cell size of 40x40x40 mm. For all the

3-D simulations the same model for solving the flow field was used to be consistent. The steady state segregated implicit solver was used with the standard two equation k-ε turbulence model activated to solve for turbulence. The coupled heat transfer solver was used to solve for heat transfer and the species transport model was activated with active species selected as air and water. The material properties were left to the default settings except for the following properties listed in Table 5.2 and the vapour pressure correlated by equation (5.1).

$$p_v = 2.816513\times10^{-6}T^5 - 3.582071\times10^{-3}T^4 + 1.839788T^3 - 4.766325\times10^{2}T^2 + 6.223929\times10^{4}T - 3.274958\times10^{6}, \text{Pa} \quad (275\text{K} \le T \le 325\text{K}) \tag{5.1}$$

Table 5.2 Default properties changed in FLUENT.

	Unit	Test condition no.1	Test condition no.2
Thermal conductivity of air	W/mK	0.026	0.027
Thermal conductivity of water	W/mK	0.61	0.61
Dynamic viscosity of air	Kg/ms	1.8×10^{-5}	1.87×10^{-5}
Diffusion coefficient	m^2/s	1.95×10^{-5}	2.07×10^{-5}

In order to calculate the discrete particle body forces, gravity was activated and the inlet boundary conditions were set according to Table 5.1. Once a converged solution was obtained for the continuous phase the discrete phase model with continuous phase interaction could be activated and the source terms set to update after every ten continuous phase iterations.

The injections could now be defined using the data obtained with the following procedure:

- The inlet speed and angle of each drop trajectory was determined using the three spray nozzle simulation codes as described in Chapter 4 which assumes either constant y velocity, constant speed or constant angle for each trajectory.
- The inlet condition for each trajectory was calculated to obtain a water distribution which corresponds to the experimental data measured in Test no.6 along the x-axis.
- The drop diameters were assumed to be uniform based on the Sauter mean diameter of 3.25 mm as measured for Test no.6 conditions.

These values were then used to define a number of concentric cones with initial spray angles, spray speeds and mass flows as calculated above. These injected cones then formed the spray model that was solved in conjunction with the continuous phase. To model the spray nozzles in up spray, a similar procedure was followed except that the input values for spray angle and spray speed was calculated using the up spray version of the spray simulation codes described in Chapter 4.

The three different FLUENT spray models generated using the three different spray simulation codes described in Chapter 4 will hereafter be called constant y velocity CFD, constant angle CFD and constant speed CFD.

5.3 Comparison of FLUENT single nozzle simulation results to experimental data

To validate the FLUENT spray models developed, the experimental test rig described in Chapter 2 was simulated with a single nozzle installed in the test section under the same conditions at which the tests were conducted. The results were compared to corresponding experimental data gathered in the test rig.

The spray models were developed using data from Test no.6 conducted without counterflow air. To model the effect of counterflow air on the spray models, the test section was subsequently modelled with 3 m/s counterflow air and the predicted water distribution data compared to corresponding experimental data of Test no.7 measured along the x-axis as shown in Figure 5.1.

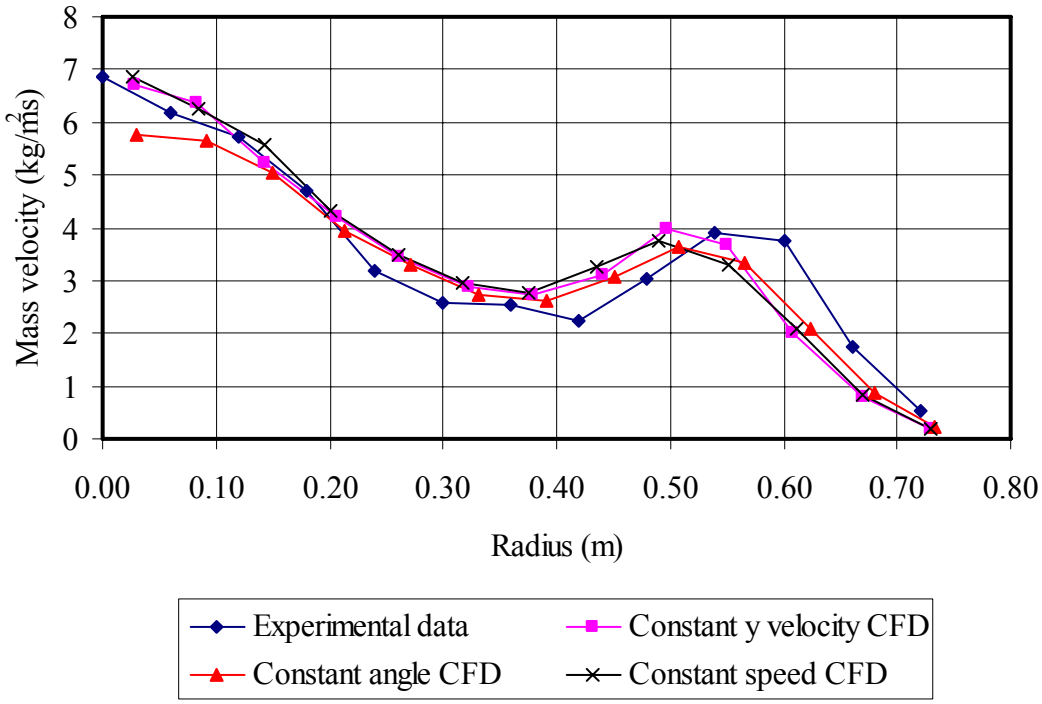

Figure 5.1 Predicted and measured water distributions in 3m/s counterflow air.

From Figure 5.1 it can be seen that the three FLUENT spray models over predict the water distribution trough at radius 0.2 – 0.5 m and then under predict the water distribution peak at radius 0.5 – 0.72 m. This was also the case when comparing the spray simulation codes with experimental data in Chapter 4. Since interaction between the spray and the continuous phase was modelled in the FLUENT spray models, which was not the case in the previous spray simulation codes, there seems to be another effect not accounted for which causes the water distribution peaks to shift radially outward. Both the FLUENT spray models and spray simulation codes do not model the effect of water sheets and high density of drops due to break up near the nozzle outlet as was observed with real nozzles. These effects could cause the continuous phase to open the drop trajectories even more than what was predicted with the FLUENT spray models and spray simulation codes.

It was decided to use the constant speed CFD model for the simulations following hereafter since all three FLUENT spray models gave more or less the same results, but it was assumed the constant speed CFD model is the closest representation of an actual nozzle.

5.4 Single spray nozzle modelling results

The constant speed CFD model was used to simulate a single nozzle in down and up spray in 3 m/s counterflow air and the average water outlet temperature, mass evaporated, total heat transfer rate and pressure drop was calculated. This was then compared to the constant speed spray simulation code.

Figure 5.2 shows the down spray drop trajectory pattern and flow velocity vectors on a plane that cuts through the middle of the down spraying nozzle. Only one half of the spray pattern is shown. The water flow rate, counterflow air velocity and nozzle height simulated were the same as for Test no.7. It can be seen from Figure 5.2 that the air flow vectors are deflected by the down spraying water drops and that a zone of recirculation is formed directly above the nozzle. The drop particles and air velocity vectors are coloured according to velocity magnitude.

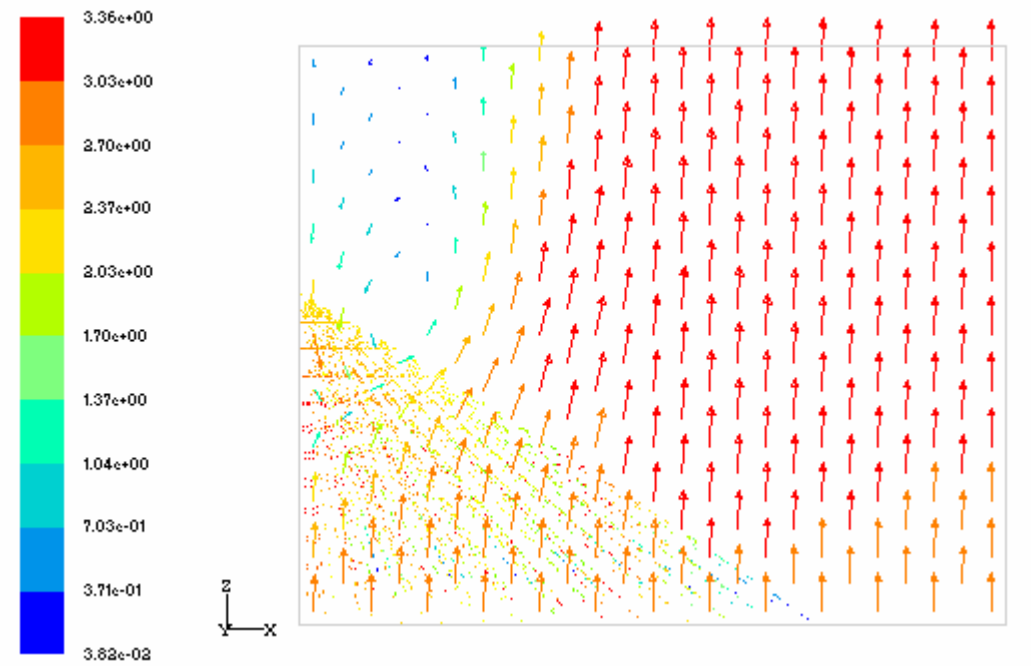

Figure 5.2 Single nozzle down spray drop trajectories and air velocity vectors.

Figure 5.3 shows the up spray drop trajectory pattern and flow velocity vectors on a plane that cuts through the middle of the up spraying nozzle. Only one half of the spray pattern is shown. The water flow rate and counterflow air velocity was the same as for the down spray simulation, but the nozzle height was simulated to be level with

the fill (fill packed between the pipes) and the spray height simulated to be 1 m above the fill. It can be seen from Figure 5.3 that the air velocity vectors close to the nozzle are accelerated by the water drops being sprayed upwards and then slowed down by the cloud of drops at their turning point. There is an area of low air velocity above the spray zone but no recirculation occurs as with the down spray model. The drop particles and air velocity vectors are coloured according to velocity magnitude.

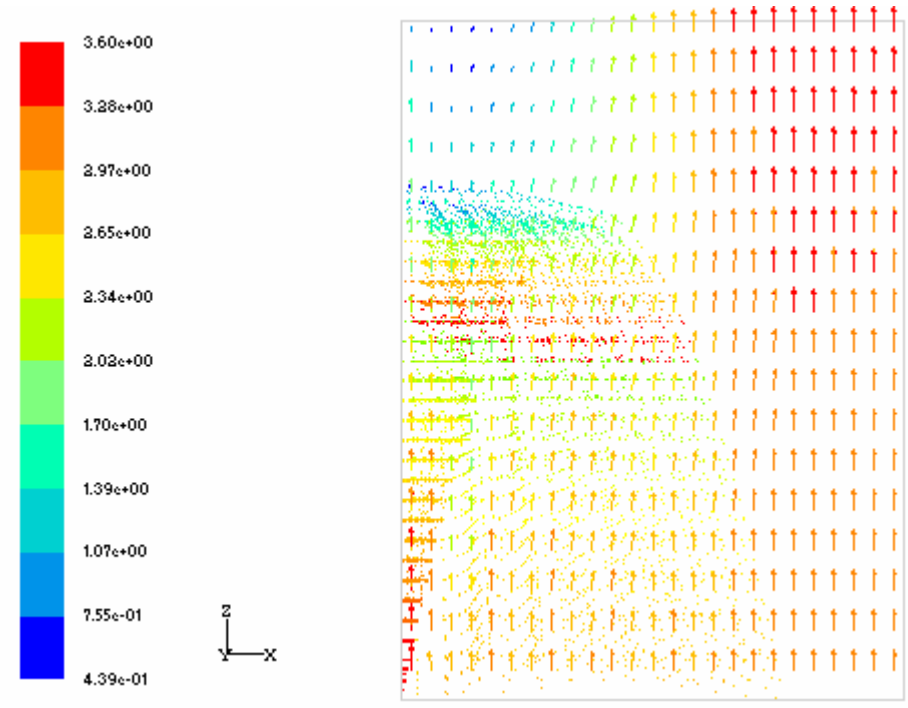

Figure 5.3 Single nozzle up spray drop trajectories and air velocity vectors.

In Table 5.3 the results obtained from the FLUENT spray model and the spray simulation code are given for up and down spray at the two conditions listed in Table 5.1. As described in Chapter 4, the spray simulation code does not simulate the interaction between the drops and the continuous air phase, as is done by FLUENT. It can therefore be seen that the spray simulation code over predicts the total pressure drop, water temperature change, evaporation rate and total heat transfer rate for both up and down spray when compared to the FLUENT simulations. The spray simulation code can however still be used as a check for the FLUENT simulations and for comparing different simulated spray nozzle conditions.

Table 5.3 Modelled up and down spray results for a single nozzle.

	No	Units	Down spray CFD	Down spray code	Up spray CFD	Up spray code
Pressure loss coefficient	1 2	-	0.181 0.178	0.215 0.215	0.333 0.326	0.467 0.471
Pressure drop	1 2	Pa	0.98 0.93	1.16 1.12	1.80 1.70	2.52 2.46
Water temperature difference	1 2	K	0.71 0.27	0.77 0.31	3.38 1.30	4.63 1.86
Evaporation rate	1 2	kg/s	0.0044 0.0017	0.0048 0.0019	0.0209 0.0079	0.0287 0.0116
Total heat transfer rate	1 2	kW	13.345 5.168	14.447 5.845	63.521 24.420	86.932 34.999

When comparing the up spraying and the down spraying CFD simulation results, there was an increase of 84% for condition no.1 and 83% for condition no.2 in the total pressure drop over the spray zone. This increase in pressure drop can be attributed to the increased spray zone height and residence time of the drops. The average water outlet temperature of the up spraying nozzle was 2.67 K and 1.03 K lower than the down spraying nozzle for conditions no.1 and no.2 respectively. The mass evaporated per second and the water temperature difference increased by a factor of 4.76 for condition no.1 and 4.81 for condition no.2 when spraying upwards due to the increased contact time that the drop had with the air. Furthermore approximately 80% of the overall water temperature change was due to mass transfer. When comparing condition no.2 to no.1 it can be seen that the total pressure drops are smaller due to lower air density. The mass evaporated and water temperatures changes are also smaller due to increased air temperature as well as relative humidity.

5.5 Spray nozzle grid modelling results

To simulate grids of four up and down spraying nozzles, the FLUENT spray models used for the single nozzle up and down spray simulations were used. The nozzles were spaced 0.9 m apart with the down spraying nozzles simulated for a nozzle height

of 0.47 m and the up spraying nozzles level with the fill (fill packed between the pipes). The nozzle spacing of 0.9 m was calculated using the superpositioning code to give a fairly uniform water distribution between the spray nozzles as discussed in Chapter 4. Both the up and down spray simulations were simulated at counterflow air velocities of 1.5 and 3 m/s for the conditions listed in Table 5.1.

Figure 5.4 shows the down spray drop trajectory patterns and flow velocity vectors on a plane that cuts through the centrelines of two of the down spraying nozzles. It can be seen from Figure 5.4 that the air flow in between the nozzles is accelerated and that there is a recirculation zone directly above the nozzles. This is caused by the higher flow resistance at the nozzle outlet due to the higher drop concentration in this region. The increased air velocity between the nozzles causes a higher drag on the drops, forcing the spray diameter to increase. This results in an increased overlapping region in between the nozzles and thus causes a higher water mass velocity in this region. This explains why the superpositioning code results discussed in Chapter 4 under predicted the water distribution in the region in between the grid of nozzles when using single nozzle data.

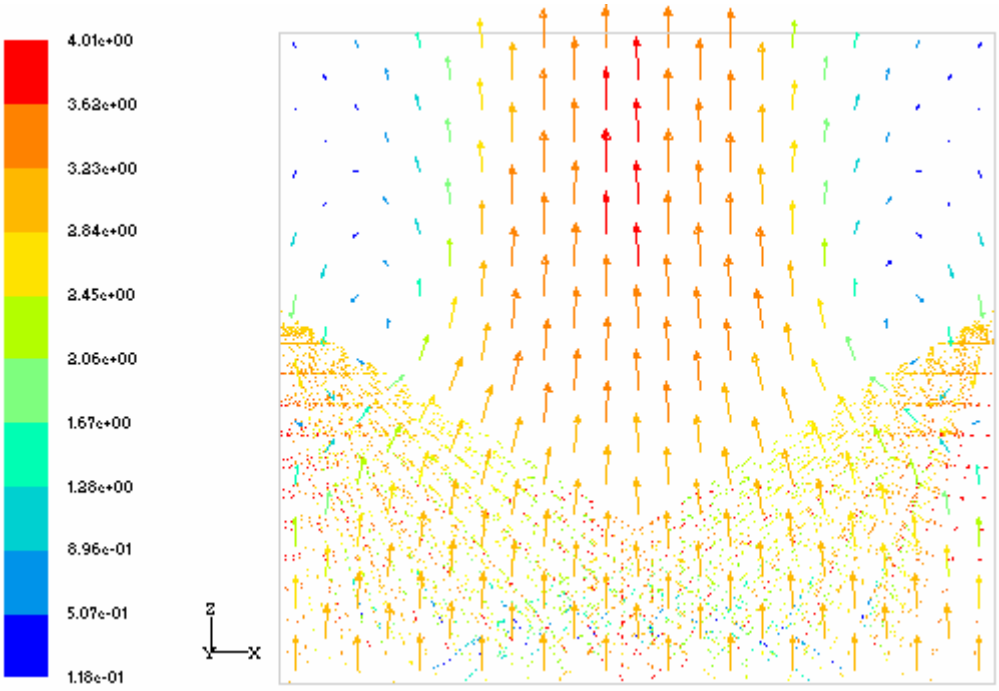

Figure 5.4 Drop trajectories and air velocity vectors for a grid of down spraying nozzles.

Figure 5.5 shows the up spray drop trajectory patterns and flow velocity vectors on a plane that cuts through the centreline of two of the up spraying nozzles. The flow directly above the nozzle is accelerated by the upward spraying drops and then decelerated by the cloud of drops at their turning point, causing a region of lower flow velocity above the nozzles. Air flow between the nozzles is however not accelerated to the same extent as observed with the down spraying nozzles and a more uniform velocity profile is therefore obtained. There is also no region of recirculation above the spray nozzles as observed in down spray.

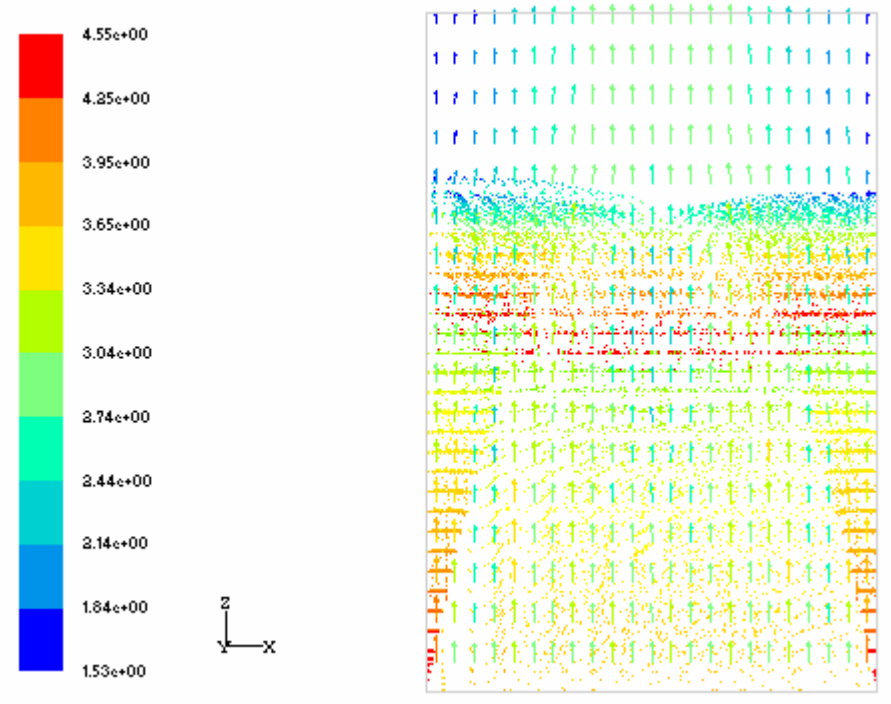

Figure 5.5 Drop trajectories and air velocity vectors for a grid of up spraying nozzles.

In Table 5.4 the up and down spraying nozzles in grid arrangement can be compared for two different counterflow air velocities and the conditions as given in Table 5.1. The pressure drop over the spray zone increased for both the up and down spraying grid of nozzles when compared to the single nozzle data in Table 5.3 since the air could not bypass the spray zone. Similar to the trends observed for single nozzles, pressure drop increased as the counterflow air velocity increased, pressure drop over the up spraying nozzles was larger than over the down spraying nozzles due to increased spray zone height and drop residence time and the evaporation rate, drop temperature change and total heat transfer rate increased with up spray as well as with an increase in air velocity for both up and down spray. There was an increase of 10%

in water temperature difference for the grid of up spraying nozzles with 3 m/s counterflow air when compared to the single nozzle data for both conditions no.1 and 2. This can be attributed to the more uniform velocity profile achieved with a grid of up spraying nozzles than obtained for single nozzles. This was not the case for down spraying nozzles. The other trends are similar to those obtained for single nozzles discussed above.

Table 5.4 Predicted performance of a grid of up and down spraying nozzles.

	No.	Units	Down spray	Down spray	Up spray	Up spray
Counterflow	1	m/s	1.5	3	1.5	3
air velocity	2		1.5	3	1.5	3
Pressure loss	1	-	2.089	0.776	3.474	1.785
coefficient	2		2.061	0.762	3.418	1.747
Pressure drop	1	Pa	2.82	4.19	4.69	9.64
	2		2.69	3.98	4.46	9.12
Water temperature	1	K	0.644	0.716	2.757	3.723
difference	2		0.249	0.278	1.066	1.426
Evaporation rate	1	kg/s	0.0040	0.0044	0.0171	0.0230
	2		0.0015	0.0017	0.0066	0.0088
Total heat	1	kW	12.112	13.479	51.879	70.062
transfer rate	2		4.686	5.217	20.037	26.811

5.6 Comparison of CFD results and experimental data for four nozzle grids

The FLUENT simulations of four nozzles spraying in grid arrangement were compared to experimental data and the Merkel number and pressure loss coefficient of the spray zone calculated.

Using data presented by Cale (1982) the pressure loss coefficient over the spray zone according to Kröger (2004) is expressed as a function of water and air mass velocity and spray nozzle height:

$$K_{sp} = L_{sp}\left(\frac{0.4G_w}{G_a} + 1\right) \qquad (5.2)$$

The total pressure drop over the spray zone is defined as:

$$\Delta p_{tsp} = K_{sp} \frac{1}{2} \rho_a v_a^2 \text{ , Pa} \tag{5.3}$$

The spray zone data presented by Lowe and Christie (1961) is correlated by Kröger (2004) to give the Merkel number as a function of water and air mass velocity and spray zone height:

$$\frac{h_{dsp} a_{sp} L_{sp}}{G_w} = 0.2 L_{sp} \left(\frac{G_a}{G_w} \right)^{0.5} \tag{5.4}$$

To compare the Merkel number calculated with equation (5.4) with the CFD data, the Merkel equation is used to determine the Merkel number from the water inlet and outlet temperatures and air properties as calculated by FLUENT. The Merkel equation is defined by:

$$\frac{h_{dsp} a_{sp} L_{sp}}{G_w} = \int_{T_{wo}}^{T_{wi}} \frac{c_{pw} dT_w}{(i_{masw} - i_{ma})} \tag{5.5}$$

In Table 5.5 the FLUENT up and down spray models for grid arrangements are compared to experimental data at counterflow air velocities of 1.5 and 3 m/s and the conditions in Table 5.1. When comparing the results it should be remembered that, seen from the side, the grid of up spraying nozzles formed a spray zone with a more or less uniform height of 1 m while the grid of down spraying nozzles formed a spray zone with conical peaks and troughs in-between, thus not having a uniform spray thickness. The FLUENT simulations over predicted the pressure drop for all the cases except one. At 3 m/s the simulations was within 10% of the experimental data for both conditions no.1 and 2 but at 1.5 m/s the pressure drop was over predicted in the order of 50 and 100% for up and down spray respectively. When comparing the Merkel number calculated from the FLUENT results to the Merkel number calculated using equation (5.4) at condition no.1, it was found that for up spray the differences were within 1 and 6% respectively and for condition no.2 within 10 and 20%. However for all the down spray cases the Merkel number was significantly under predicted. This could be due to the non-uniform spray thickness described above and the short contact time between drop and air for the down spraying nozzles. These

effects are not taken into account by the correlation and causes the over prediction of the Merkel number.

Table 5.5 Predicted and experimental performance of a grid of up and down spraying nozzles.

	No.	Units	Down spray	Down spray	Up spray	Up spray
Counterflow	1	m/s	1.5	3	1.5	3
air velocity	2		1.5	3	1.5	3
Pressure loss	1	-	1.050	0.760	2.235	1.617
coeff. Eqn (5.2)	2		1.070	0.770	2.277	1.639
Pressure loss	1	-	2.089	0.776	3.474	1.785
coeff. FLUENT	2		2.061	0.762	3.418	1.747
Pressure drop	1	Pa	1.42	4.10	3.02	8.73
Eqn (5.3)	2		1.40	4.02	2.97	8.56
Pressure drop	1	Pa	2.82	4.19	4.69	9.64
FLUENT	2		2.69	3.98	4.46	9.12
Merkel no.	1	-	0.0535	0.0757	0.1138	0.1610
Eqn (5.4)	2		0.0526	0.0744	0.1119	0.1583
Merkel no.	1	-	0.0219	0.0241	0.1147	0.1514
FLUENT, Eqn (5.5)	2		0.0198	0.0218	0.1016	0.1330

5.7 Conclusions

The procedure followed to model a single or grid of up and down spraying nozzles using CFD was presented. The spray models developed were compared to experimental data and found to under predict the effect of counterflow air on the water distribution due to the fact that water sheets and high density of drops near the nozzle outlet were not modelled. Single nozzles in up and down spray were compared and the up spray water temperature difference was 2.67 K and 1.03 K lower compared to down spray for conditions no.1 and 2. Of the overall water temperature change, approximately 80% was due to mass transfer. Grids of up and down spraying nozzles were simulated and the results compared. Again the up spraying nozzles had a bigger water temperature change than the down spraying nozzles due to longer drop contact

time with the air. There was an increase of 10% in water temperature change for the grid of up spraying nozzles in 3 m/s counterflow air when compared to the single nozzle simulations. Comparing the spray nozzle grid simulations to experimental data it was found that for all the up spray simulations the Merkel number was within 20%. This was however not the case for the grid of down spraying nozzles. For 3 m/s counterflow air the predicted pressure drop was within 10% but for 1.5 m/s over predicted by 50 to 100%.

6. IDEAL AND REAL SPRAY NOZZLE CHARACTERISTICS

6.1 Introduction

Experimental nozzle data as measured in the test rig was analysed in preceding chapters. In this chapter, nozzle data and characteristics in general are discussed in relation to ideal nozzle performance bearing in mind that ideal nozzle characteristics, towards which real nozzle characteristics should strive, are theoretical and not always practically achievable.

6.2 Ideal nozzle characteristics

The ideal nozzle characteristics can be discussed under the headings: nozzle design, drops and water distribution. These characteristics are as follows:

Nozzle design:

1. Nozzles should be resistant to chemical attack from chemicals in the cooling tower water.
2. Nozzles should be resistant to abrasion and clogging due to insoluble or suspended particles in the cooling water, in particular the small Taprogge balls used to clean the condenser tubes.
3. Nozzles should be invertible and give ideal behaviour in up and down spray.
4. Low water and air side pressure drop over the ideal nozzles.
5. Nozzles should be easy to replace, install and maintain in the cooling tower environment.
6. Changes in water flow rate or air flow velocity should not affect the nozzle performance characteristics.

Drops:

7. Drops to have a uniform diameter.
8. The drop size should be big enough after evaporation not to be entrained into the counterflow air in the cooling tower (order of 1 – 2 mm).
9. Drop mass fraction to be uniform in the spray zone.

10. Water leaving the nozzle should immediately form drops, therefore there should be no sheet or ligament formation at the nozzle exit.
11. There should be no collision between drops to prevent drop coalescence.
12. Drops should all have the same contact time with the air which should be as long as possible.
13. Change in water flow rate or air flow velocity should not affect the drop size.

Water distribution:

14. Water distribution should be uniform over the whole area where it enters the fill to allow uniform wetting of the fill.
15. No water seepage from the nozzles down the water distribution pipes supports, causing localized water steams.
16. Water distribution on the fill should be a perfect square to allow the nozzles to be placed in a square grid.
17. Nozzles to be placed such that there is no overlapping and there are no gaps in the overall water distribution onto the fill.
18. Changes in water flow rate or air flow velocity should not affect the water distribution.

By striving to fulfil these characteristics the maximum heat transfer rate and optimal performance of a spray nozzle in a cooling tower installation can be achieved.

6.3 Real nozzle characteristics

Data gathered in this study for the two medium and two low pressure cooling tower spray nozzles is presented in Table 6.1 and can be evaluated and compared to characteristics of an ideal nozzle given above. The medium and low pressure nozzles have different ranges of application in different types of cooling towers and this should be kept in mind when doing the comparison.

Table 6.1 Ideal and real nozzle characteristics.

Nozzle characteristic	Unit	Ideal	No.1	No.2	No.3	No.4
Nozzle design:						
1. Chemical attack resistant	-	Yes	Not investigated in thesis			
2. Clogging resistant	-	Yes	Not investigated in thesis			
3. Invertible	-	Yes	No	No	Yes	Yes
4. Required pressure head	m	Low	1.5-7	1.5-6	0.5-1.5	0.5-1.5
5. Maintainability	-	Easy to maintain				
6. Effect of changes in flow rates	-	None	Changes nozzle characteristics			
Drops:						
7. Uniform diameter	mm	Yes	0.5-8	0.5-8	0.5-12	0.5-16
8. Sauter mean diameter	mm	0.75	3.2	3.2	7.4	7.5
9. Drop concentration uniformity	-	Uniform	Not uniform			
10. Immediate drop formation	-	Yes	Sheet and ligament formation			
11. Probability drop collision	-	None	Low	Low	High	High
12. Contact time	s	Long	0.1	0.1	0.7	0.7
13. Effect of changes in flow rates	-	None	Changes drop diameter			
Water distribution:						
14. Uniform distribution	-	Yes	Relatively		Not uniform	
15. Seepage from nozzle	-	No	No	No	Yes	Yes
16. Square spray pattern	-	Yes	Nearly		No	
17. Spray overlapping	-	No	Yes			
18. Effect of changes in flow rates	-	None	Changes water distribution			

Nozzle design:

The nozzle's resistance to clogging as well as against chemical and insoluble particle attack should be tested in the cooling tower environment. Nozzle no.1 and 2 are designed for down spray while nozzles no. 3 and 4 are invertible, nozzle spacing would however change when inverted. Pressure is one of the driving forces for breaking the water stream into small drops and is dependent on the type of nozzle and it's application. This is an important factor when considering pumping cost. All of the tested nozzles were easy to install but maintaining them would be dependent on the

specific cooling tower environment. The nozzles were affected by a change in water and air flow rate due to a change in nozzle characteristics.

Drops:

The real nozzles did not generate drops of uniform diameter. The drop sizes produced by the medium pressure nozzles did however have a smaller diameter range than the low pressure nozzles. Smaller drops cool faster than big ones but have less mass and therefore only a small number of large drops would overshadow the advantage of having small drops. A high density of drops is located near the nozzle outlet where the drops are close together and the density decreases as the drops spread out over a wider area. This effect was the most significant for the medium pressure nozzles. The formation of sheets and ligaments was observed for nozzles no.3 and 4 directly below or above the nozzle depending on spray direction and decreases the heat transfer rate. When nozzles no.3 and 4 are used in up spray, the chances of drop collision is increased since drop trajectories cross. The drop contact time for al the drops are not the same since the trajectories and velocities differ. The contact time for up spraying nozzles no.3 and 4 is also longer than for the down spraying nozzles and will increase the heat transfer from the drops. Drop characteristics were affected by a change in water and air flow rate since drop characteristics changed with flow rate.

Water distribution:

The water distribution generated by nozzles no.1 and 2 is relatively uniform but nozzles no.3 and 4 generate non uniform water distributions radially and circumferentially. With the low pressure nozzles in up spray, water spilled over the supply pipe and the support structure, not forming drops and thus reducing heat transfer. Nozzles no.1 and 2 strive to generate a square spray pattern which is achieved only marginally. Nozzles no.3 and 4 generate a circular spray pattern, jagged along the edges, which varies between and over the diffuser ring supports. By means of overlapping spray patterns, fairly uniform water distributions could be obtained with the medium pressure nozzles, especially nozzle no.1. Water distribution characteristics were affected by a change in flow rates since this affected the water distribution.

Figure 6.1 shows the cumulative mass fraction against the absolute drop initial angle, measured from the horizontal plane, for the three spray simulation codes in up and down spray, with a uniform water distribution. The cumulative mass fraction is defined as the sum of the water mass sprayed, divided by the total mass of water. For the peripheral trajectory the cumulative mass fraction is 1. It can be seen from the figure that the initial drop angle range for up spray is 12˚ and 57˚ for down spray. For the 13 equally spaced trajectories on fill level, 55% of the total mass water was sprayed in the 5 outermost trajectories.

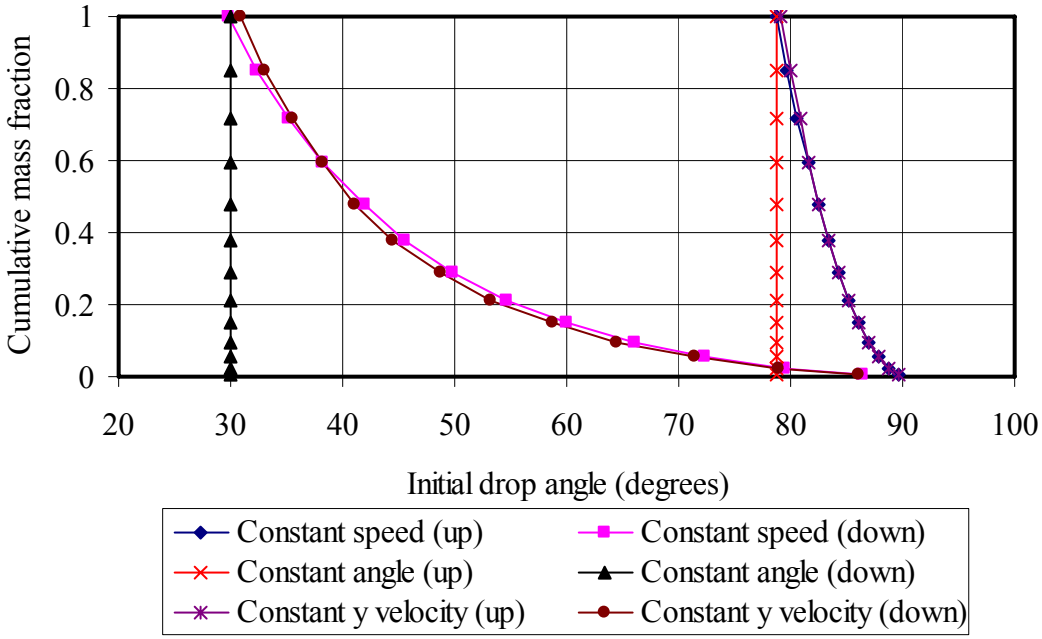

Figure 6.1 Cumulative mass fraction and initial drop angle for spray simulation codes.

6.4 Conclusion

Ideal nozzle characteristics were given towards which real nozzle characteristics should strive. Ideal nozzle characteristics were compared in general to data gathered from low and medium pressure nozzles and the findings discussed. It is evident that there is room for improvement in real nozzle design in all fields, however this is easier said than done due to harsh operating conditions, physical constraints and financial implications.

7. CONCLUSION

In this thesis, cooling tower spray nozzle performance characteristics such as the water distribution onto the fill material, drop size distribution, air side pressure drop, water head loss and mass and heat transfer in the spray zone were investigated. The aim of the project was to provide a method to evaluate and simulate the performance characteristics of new and existing cooling tower spray nozzle installations. The project objectives are given in Chapter 1.

In Chapter 2, the design requirements for a cooling tower test rig, spray nozzle system, water distribution measurement system and drop size measurement system were established and the equipment built to measure the water and drop size distributions of spray nozzles. All the design requirements were met with the exception of low pressure nozzle water distribution tests and drop size distribution tests in counterflow air where the results were influenced by the equipment. Test procedures were also developed to ensure repeatability of the results obtained.

In Chapter 3, flow characteristics, water distribution and drop size distribution tests were done on two medium pressure and two low pressure single spray nozzles. The flow characteristic data was found to compare well with the manufacturers' data. The water distribution tests for the medium pressure nozzles showed that the water distribution produced was not circular, but also not square as claimed. The low pressure spray nozzles produced highly non-uniform water distributions in both radial and circumferential directions. The effect of counterflow air on the medium pressure nozzles were investigated and found to be small, causing a diameter change of less then 10% in down spray, since the drop velocities are high. The effect of increased water flow rate and nozzle height was found to offset the water mass velocity proportionately. A grid of four medium pressure nozzles was tested and counterflow air found to have a smoothing effect on the water distribution, reducing peaks and troughs. The drop size distributions for the medium pressure nozzles had a smaller diameter range than the low pressure nozzles as well as smaller Sauter mean diameters in the order of 3.3 mm and 7.4 mm respectively. By increasing drop travel distance and velocity, the drop diameter decreases.

In Chapter 4, a computer code was developed that superimposes the water distribution data of a single nozzle to predict the water distribution of a grid of four nozzles. The code was found to predict the water distribution trend for tests without counterflow air but failed to predict certain trends in tests with counterflow air. Another computer code was developed to model sprays produced by single nozzles using one of three approaches namely: constant drop y velocity, constant drop speed and constant drop angle. These three approaches were all found to under predict the outward radial movement of the water distribution peak by 5% in counterflow air but predicted the effect of nozzle height on the water distributions satisfactorily when compared to experimental data using the Sauter mean diameter to simulate drop diameter. Simulations predicted that the spray diameter in counterflow air for up spraying nozzles increased by 10% more compared to down spraying nozzles.

In Chapter 5, CFD models were developed and used to simulate single as well as four nozzle grids. The CFD models were compared to the single nozzle computer code and experimental data. The CFD code under predicted the effect of counterflow air on the water distribution of a single nozzle using Sauter mean diameter to simulate drop diameter. The CFD models for four nozzle grids in up and down spray were compared to correlations of experimental data and the up spray models found to predict pressure drop within 50 % and Merkel number within 20%. The experimental correlations for down spray were found to over predict the CFD models since it did not make provision for the unevenness of the spray zone and the higher drop velocities simulated in down spray. Spraying upwards was found to increase the heat transfer rate, evaporation rate and pressure drop over the spray zone compared to down spray.

In Chapter 6 an ideal spray nozzle was described and the tested spray nozzle's performance characteristics compared to this. The ideal nozzle serves as a reference for nozzle design and for evaluation of existing spray nozzles and spray nozzle systems.

A continuation of this work should look into the design of medium and low pressure cooling tower spray nozzles and the use of and refinement of CFD spray models in cooling tower simulations.

REFERENCES

Bellagamba, B, Dinelli, G, Tognotti, L and Zanelli, S, 1988, *Water Distribution in Cooling Towers: Characterization of Industrial Spray Nozzles*, 6th IAHR Cooling Tower Workshop, Pisa, Italy.

Cale, S A, 1982, *Development of Evaporative Cooling Packing, Commission of European Communities*, Report EUR 7709 EN, Luxembourg.

Cengel, Y A and Boles, M A, 2002, *Thermodynamics: An Engineering Approach*, McGraw-Hill, New York.

Clift, R, Grace, J R and Weber, M E, 1978, *Bubbles, Drops and Particles*, Academic Press Inc., New York.

Fay, H P and Hesse, G, 1984, *Application of Up Spray Type Water Distribution Systems in Cooling Towers*, Cooling Tower Institute Annual Meeting, New Orleans, Louisiana.

Gilliland, E R, 1934, *Diffusion Coefficients in Gaseous Systems*, Ind. Eng. Chem., Vol. 26, pp. 681.

Incropera, F P and De Witt, D P, 2002, *Fundamentals of Heat and Mass Transfer*, John Wiley & Sons, New York.

Kröger, D G, 2004, *Air-Cooled Heat Exchangers and Cooling Towers: Thermal-Flow Performance Evaluation and Design*, Pennwell Corp., Tulsa, OK, VSA.

Li, J and Kawano, H, 1995, *Simulating Water Drop Movement from Noncircular Sprinkler Nozzles*, Journal of Irrigation and Drainage Engineering, Vol. 121, No. 2, pp. 152 – 158.

Lowe, H J and Christie, D G, 1961, *Heat Transfer and Pressure Drop Data on Cooling Tower Packings, and Model Studies of the Resistance of Natural Draught Towers to Airflow*, Intern. Development in Heat Transfer, Part V, ASME, New York.

Miura, K, Miura, T and Ohtani, S, 1977, *Heat and Mass Transfer to and from Droplets*, AIChE Symposium Series, Vol. 73, No.163, pp. 95 – 102.

Moussiopoulos, N and Ernst, G, 1987, *Thermal Performance of Spray Cooling Ponds at Zero Wind Velocity*, Journal of Heat Transfer, Vol. 109, pp. 212 – 217.

Nonnenmacher, S and Piesche, M, 2000, *Design of Hollow Cone Pressure Swirl Nozzles to Atomize Newtonian Fluids*, Chemical Engineering Science, Vol. 55, No. 19, pp. 4339 – 4348.

Ranz, W E and Marshall, W R, 1952, *Evaporation from Drops*, Chemical Engineering Progress, Vol. 48, No. 3, pp. 141 – 146.

Terblanche, R, 2005, *Optimization of a Measurement Technique for Evaluation of Drop Size Distribution in a Wet Cooling Tower Test Rig*, B.Eng final year project, University of Stellenbosch.

Thacker, J E, 1997, *Design of Medium Pressure Nozzles for Cooling Towers*, MScIng. Thesis, University of Stellenbosch.

Tognotti, L, Zanelli, S, Bellagamba, B, Mattachini, F and Lotti, G, 1991, *Characterization and Performance of Spray Nozzles for Water Distribution in Cooling Towers*, NIST, Vol. 813, pp. 787 – 795.

Turton, R and Levenspiel, O, 1986, *A Short Note on the Drag Correlation for Spheres*, Powder Technology, Vol. 47, pp. 83 – 86.

White, F M, 1999, *Fluid Mechanics*, WCB/McGraw-Hill, Singapore.

APPENDIX A
CALIBRATION OF MEASUREMENT EQUIPMENT

The cooling tower test rig as described in Chapter 2 can be used for a variety of different tests. Calibrations applicable to the tests conducted in this project are discussed below.

A.1 Pressure transducer calibration

The water and air mass flow rates were obtained by measuring the pressure differences over two different venturi flow meters, the location of which are shown in Figure 2.1. An electronic pressure transducer was used to measure the pressure difference over the water venturi and a water micro manometer (Betz) for the air venturi. For the water pressure difference a FOXBORO pressure transducer, shown in Figure G.3, model 843 DP-H2I with reference number 536 3210 EW with a range of 0-75 kPa was used. For the air pressure difference a Van Essen Betz micro manometer, reference number 12453 with a range of 0-5 kPa was used. The micro manometer needed no calibration.

The FOXBORO pressure transducer was calibrated by means of a mercury manometer. By plotting the manometer pressure readings and output voltages from the pressure transducer on a graph, as seen in Figure A.1, a calibration curve could be obtained by means of a linear curve fit given by equation (A.1).

$$p_w = 15.996 V_{wp} - 16.006, \text{ kPa} \qquad \text{(A.1)}$$

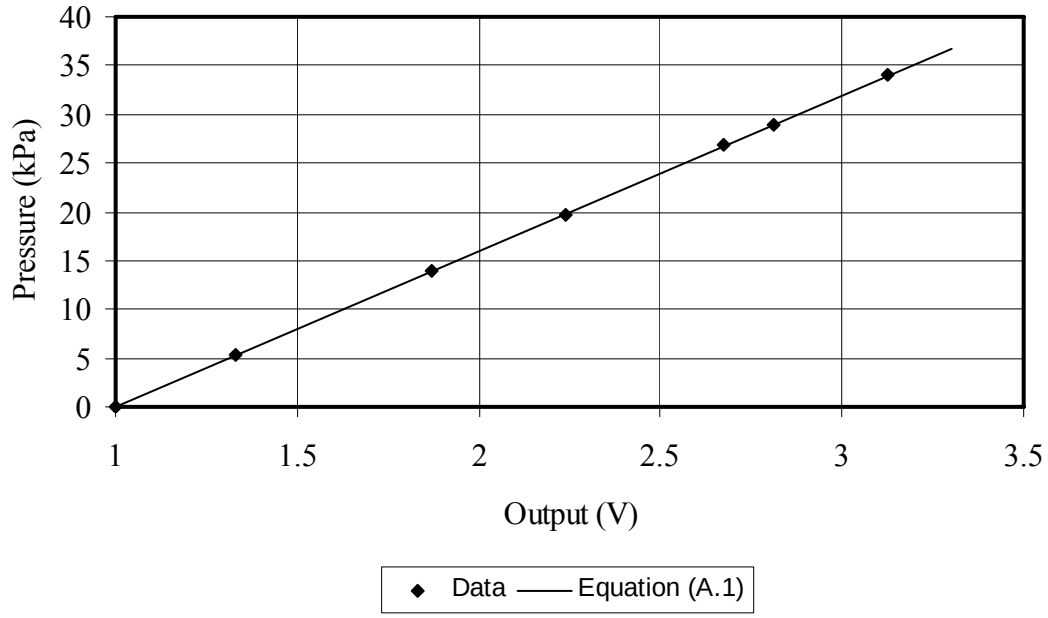

Figure A.1 Pressure transducer calibration curve.

A.2 Anemometer calibration

The anemometer used for calibrating the air mass flow rate through the cooling tower test rig was calibrated in a low speed wind tunnel providing a uniform velocity profile.

A Pitot static tube and a water micro manometer (Betz) were used to measure the air stream velocity. These measurements were confirmed by using another Pitot static tube. The velocity profile in the test section was measured by doing a traverse with the Pitot static tube and was found to be uniform. The anemometer was then placed in the test section and the output voltage from the anemometer recorded at different air velocities. From this a linear calibration curve, equation (A.2), was obtained as shown in Figure A.2.

$$v_a = 15.01V, \text{ m/s} \qquad (A.2)$$

Equation (A.2) was checked by recalibrating the anemometer in another wind tunnel following two approaches. For both approaches the anemometer was placed inside a nozzle installed at the wind tunnel inlet. For the one approach the same Pitot static tube was used as before, placed upstream of the anemometer in the parallel section of

the nozzle. Again the velocity profile were tested and confirmed to be uniform. The results are plotted in Figure A.2.

The other approach used the nozzle contraction instead of the Pitot static tube to measure the air velocity. The same procedure as for the previous two calibration tests were followed and the results are plotted in Figure A.2.

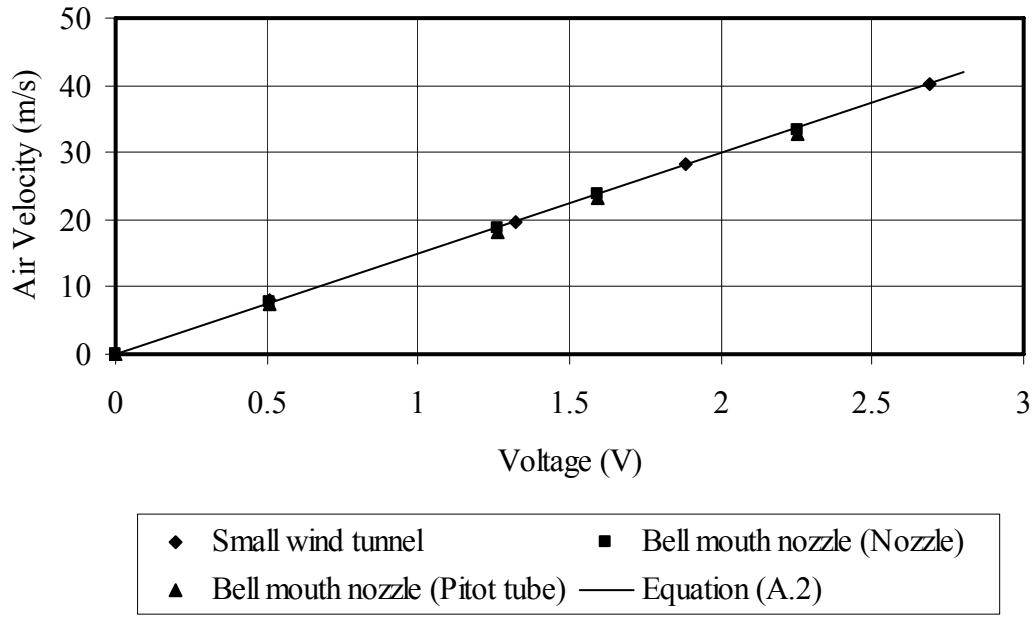

Figure A.2 Anemometer calibration curve.

Sample calculations for a calibration point using the Pitot static tube and the nozzle contraction to measure air velocity are given below.

Water micro manometer (Pitot static tube)	$\Delta h_{Pitot} = 33.6$ mm
Water micro manometer (Nozzle)	$\Delta h_{Nozzle} = 35$ mm
Ambient temperature	$T_a = 291.65$ K
Atmospheric pressure	$p_a = 102100$ Pa
Anemometer voltage	V = 1.59 V

Pitot static tube pressure difference:

$$\Delta p_{Pitot} = \rho_w g \Delta h_{Pitot} = 998 \times 9.81 \times 0.0336 = 329 \text{ Pa} \quad \text{(A.3)}$$

Nozzle pressure difference:

$$\Delta p_{Nozzle} = \rho_w g \Delta h_{Nozzle} = 998 \times 9.81 \times 0.035 = 342.6 \text{ Pa} \quad \text{(A.4)}$$

Air density:

$$\rho_a = \frac{p_a}{287 \cdot T_a} = \frac{102100}{287 \times 291.65} = 1.22 \ \text{kg/m}^3 \qquad \text{(A.5)}$$

According to White (1999) the Bernoulli equation can be applied directly to Pitot static tubes in low Mach numbers flows (incompressible flows).

Velocity calculated with Pitot static tube:

$$v_{Pitot} = \sqrt{\frac{2\Delta p_{Pitot}}{\rho_a}} = \sqrt{\frac{2 \times 329}{1.22}} = 23.22 \ \text{m/s} \qquad \text{(A.6)}$$

The elliptical nozzle used has a discharge coefficient C_n to correct the velocity. According to Kröger (2004) the discharge coefficient for an elliptical nozzle with Reynolds > 350000 is 0.994 which is within the Reynolds number range that the tests were conducted in.

Velocity calculated with the nozzle:

$$v_{Nozzle} = C_n \sqrt{\frac{2\Delta p_{Nozzle}}{\rho_a}} = 0.994 \sqrt{\frac{2 \times 342.6}{1.22}} = 23.46 \ \text{m/s} \qquad \text{(A.7)}$$

From Figure A.2 it can be seen that the data obtained using the elliptical nozzle is slightly below that measured in the small wind tunnel. In the calibration tests with the nozzle, the anemometer propeller was close to the sides of the nozzle. This could have led to some boundary effects around the anemometer propeller as a winding sound was observed that might have caused losses when compared to the small wind tunnel tests. Taking all of this into consideration it was decided to use the calibration curve, equation (A.2), obtained from the small wind tunnel data.

A.3 Calibration of the water flow venturi

The water mass flow rate was obtained from a pressure drop measurement over a venturi flow meter, the location of which is shown in Figure 2.1 and G.3. To calibrate the venturi, a tank and stop watch approach was used to determine the corresponding flow rate at a certain pressure drop measurement over the venturi. The water mass flow rate from the pumps was adjusted by means of a control valve. This control

valve was set to a certain flow rate and once the differential pressure reading stabilised, the tank outlet valve was closed, the stop watch started and the time was recorded for the water to pass two marks on the tank. Knowing the filling time of a known volume of water, the water mass flow rate could be calculated and plotted as a function of the pressure transducer pressure reading. By repeating this for different flow rates a calibration curve for the water mass flow rate against the pressure drop over the venturi could be plotted.

A Perspex pipe was installed upstream of the venturi. Swirl was observed in the pipe when a small amount of air was injected into the flow downstream of the venturi. A flow straightener (honeycomb) was placed in the pipe. The test was repeated to determine the effect of the flow straightener on the calibration data. Figure A.3 shows that the results remain unchanged.

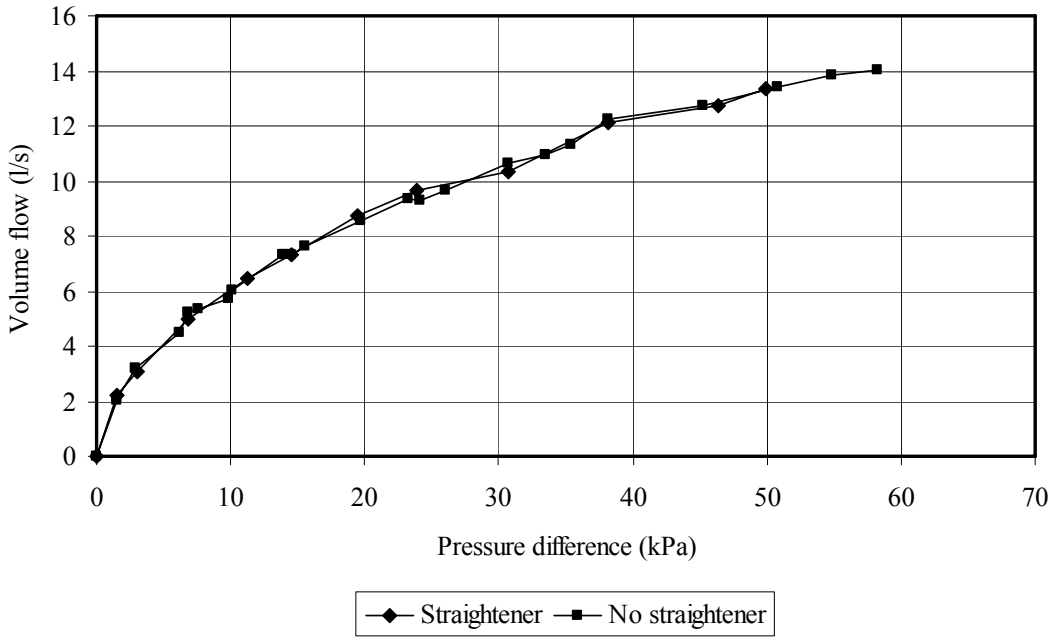

Figure A.3 Calibration data with and without a flow straightener upstream of the venturi.

To confirm the water flow rate determined with the tank and stop watch, the mass flow rate was predicted using theory taken from White (1999) that is based on the Bernoulli equation. The theory uses a discharge coefficient C_n in the Reynolds number range of 1.5×10^5 to 2×10^6. Since the water flow rate of the system can fall below this Reynolds number range only the calibration points within this range were

calculated. In Figure A.4 the theoretically predicted and measured calibration water flow rates are shown. A sample calculation for one measurement is given below.

Water pressure transducer reading $V = 2.627$ V

Diameter at venturi throat $d_{vt} = 0.041$ m

Diameter pipe $d_{pipe} = 0.069$ m

Venturi pressure difference:

$$\Delta p_w = 15.996V\text{-}16.006 = 15.996\times 2.627\text{-}16.006 = 26.023 \text{ kPa} \quad \text{(A.1)}$$

Contraction ratio:

$$\beta = \frac{d_{vt}}{d_{pipe}} = \frac{0.041}{0.069} = 0.594 \quad \text{(A.8)}$$

Throat area:

$$A_{vt} = \pi\left(\frac{d_{vt}}{2}\right)^2 = \pi\left(\frac{0.041}{2}\right)^2 = 0.00132 \text{ m}^2 \quad \text{(A.9)}$$

Discharge coefficient:

$$C_n = 0.9858 - 0.196\cdot\beta^{4.5} = 0.9858 - 0.196\times 0.594^{4.5} = 0.967 \quad \text{(A.10)}$$

Volume flow rate:

$$\begin{aligned} Q &= C_n A_{vt}\left[\frac{2(\Delta p_w)/\rho_w}{1-\beta^4}\right]^{0.5} \\ &= 0.967\times 0.00132\times\left[\frac{2\times(26023)/998}{1-0.594^4}\right]^{0.5} \quad \text{(A.11)} \\ &= 0.00985 \text{ m}^3/\text{s} \end{aligned}$$

It can be seen from Figure A.4 that the measured and theoretically calculated data correlate well. It was however decided to do the calibration of the venturi with the measured data by fitting a fifth order polynomial equation curve fit through the data, also shown in Figure A.4 and given by equation (A.12). The pressure difference is in kPa and the flow rate in l/s.

$$Q = 1.73\times10^{-7}\Delta p_w^5 - 2.915\times10^{-5}\Delta p_w^4 + 1.819\times10^{-3}\Delta p_w^3 - 5.363\times10^{-2}\Delta p_w^2 + 9.511\times10^{-1}\Delta p_w + 4.887\times10^{-1},\ l/s \quad (A.12)$$

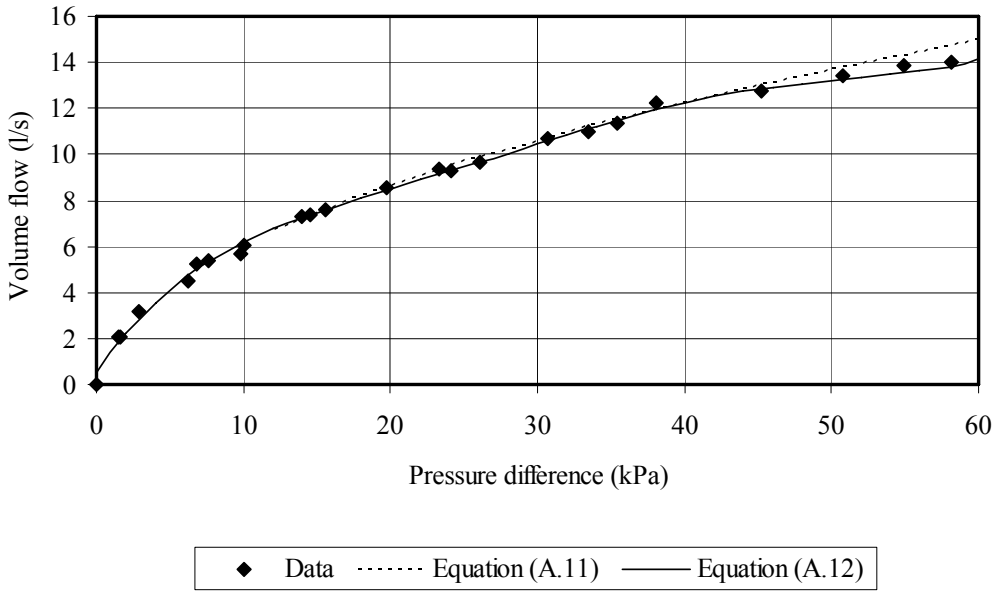

Figure A.4 Water flow rate calibration curve and equation (A.11) based on Bernoulli-Venturi theory.

A.4 Calibration of the air flow venturi

The air flow rate through the test section was measured using a venturi flow meter, shown in Figure G.4, placed before the fan diffuser as is shown in Figure 2.1. Measuring the pressure difference between the venturi throat and the upstream plenum chamber, venturi theory is used to determine the air flow rate through the test section.

The velocity profile in the venturi throat was checked with a hand held hot wire anemometer and found to be uniform within reasonable limits and the effect of velocity distribution on the propeller anemometer and differential pressure measurements is therefore considered negligible. The effect of different pressure tapping point locations on the differential pressure measurement was investigated. Initially, the tapping points were located in the plenum corners. It was however not clear what the effect of recirculation in the corners may be on the upstream pressure

measurement, so the tapping points were relocated to the centreline of the plenum. Differences in the pressure readings were small and since the velocity was calculated using the square root of the pressure, as shown in equation (A.20), the difference in velocity was negligible and it was decided to place the pressure points in the corners. Figure A.5 shows the pressure readings taken in the corners and middle of the plenum chamber.

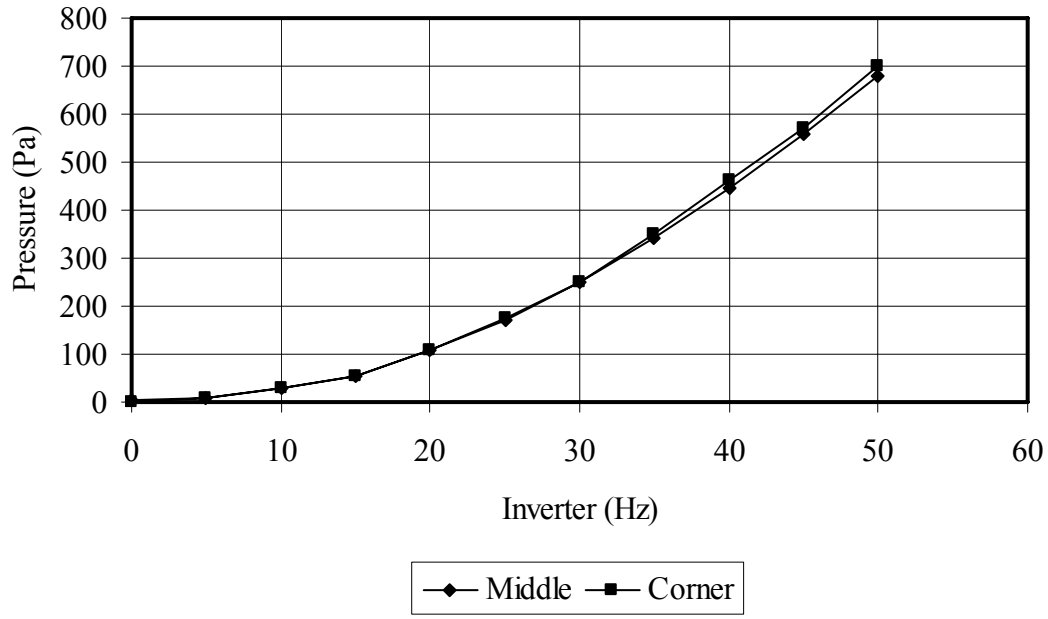

Figure A.5 Pressure readings taken in the plenum chamber.

To calibrate the venturi the calibrated anemometer was placed in the throat of the venturi and the pressure difference over the venturi was measured. The air velocity was measured with the anemometer and also calculated with the pressure difference over the venturi. The results could then be plotted for different fan speeds. According to Kröger (2004) the discharge coefficient for an elliptical nozzle is 0.994 in the Reynolds number range that the tests were conducted in. In this case the inlet conditions to the venturi are not ideal as there may be vortices and regions of recirculation due to plenum chamber size, drift eliminators and the close proximity of the fan blades, and therefore a calibration correction factor C_n was determined. Sample calculation for one calibration point is shown below.

Atmospheric pressure	$p_a = 102000$ Pa
Air temperature in plenum	$T_a = 288.85$ K
Anemometer voltage	$V_{anemometer} = 1.09$ V

Water micro manometer reading $\Delta h = 17.7$ mm

Air density:

$$\rho_a = \frac{p_a}{287 \cdot T_a} = \frac{102000}{287 \times 288.85} = 1.23 \text{ kg/m}^3 \quad \text{(A.13)}$$

Venturi pressure difference:

$$\Delta p_a = \rho_w g \Delta h = 998 \times 9.81 \times 0.0177 = 173.29 \text{ Pa} \quad \text{(A.14)}$$

Velocity measured by means of anemometer:

$$v_{anemometer} = 15.01 \cdot V_{anemometer} = 15.01 \times 1.09 = 16.36 \text{ m/s} \quad \text{(A.2)}$$

Plenum frontal area:

$$A_{pl} = L \cdot W = 1.5 \times 1 = 1.5 \text{ m}^2 \quad \text{(A.15)}$$

Venturi throat frontal area:

$D_{vt} = 0.455$ m

$$A_{vt} = \pi \left(\frac{D_{vt}}{2} \right)^2 = \pi \left(\frac{0.455}{2} \right)^2 = 0.1626 \text{ m}^2 \quad \text{(A.16)}$$

The air velocity in the plenum chamber is a function of the area ratio of venturi throat and plenum areas and the venturi throat velocity.

$$v_{pl} = \left(\frac{A_{vt}}{A_{pl}} \right) v_{vt} \quad \text{(A.17)}$$

This area ratio can now be substituted into Bernoulli's equation and v_{pl} eliminated.

$$\kappa = 1 - \left(\frac{A_{vt}}{A_{pl}} \right)^2 = 1 - \left(\frac{0.1626}{1.5} \right)^2 = 0.988 \quad \text{(A.18)}$$

$$v_{vt} = \left(\frac{2 \cdot \Delta p_a}{\rho_a \kappa} \right)^{0.5} \quad \text{(A.19)}$$

This velocity is multiplied by the calibration correction factor to obtain the velocity in the venturi throat. A calibration correction factor of 0.96 was obtained by dividing the

anemometer velocity by the velocity as determined from the pressure difference over the venturi and taking the average of all the points measured in that calibration test. The velocity in the throat is then given by:

$$v_{vt} = c_n \left(\frac{2 \cdot \Delta p_a}{\rho_a \kappa} \right)^{0.5} = 0.96 \cdot \left(\frac{2 \times 173.29}{1.23 \times 0.988} \right)^{0.5} = 16.21 \ \text{m/s} \qquad \text{(A.20)}$$

To check this calibration an air mass balance between the venturi throat and the rain zone test section was done using a handheld propeller anemometer placed at different grid positions in the rain zone test section. From this traverse, the velocity profile in the rain zone test section could be established from which the air mass flow is obtained. This is compared to the mass flow as calculated from the pressure difference measured over the venturi and the anemometer in the venturi. No fill was placed in the test section and no inlet bell mouth was present during the test. Table A.1 shows the mass flow obtained using the three different methods as well as the deviations of each mass flow when compared to the mass flow as calculated with the anemometer in the venturi.

Table A.1 Mass flow balance using three different methods.

	Mass flow	Deviation
Units	Kg/s	%
Mass flow calculated with anemometer	5.78	0
Mass flow calculated without calibration correction factor using Δp	6.03	4.1
Mass flow calculated with anemometer traverse	5.52	-4.7

The mass flow calculated by using the velocity calculated with the pressure difference over the venturi without the calibration correction factor was 4.1% higher than the mass flow obtained by using the velocity obtained with the anemometer in the venturi. This confirms the calibration correction factor of 0.96. The mass flow obtained by using the anemometer traverse was 4.7% lower than the mass flow obtained by means

of the anemometer in the venturi. This could be due to the coarseness of the grid used in the rain zone section and the instabilities in the flow in the rain zone section corners as the test were done with no inlet bell mouth and fill material.

A.5 Calibration of the water drop size measurement system

Drop size tests were done at two different distances from the spray nozzles. For the drop size tests conducted at a distance of 1.25 m from the spray nozzle the same test set-up was used as described by Terblanche (2005) and shown in Figure G.6. The calibration for these tests did not change and the reader is referred to Terblanche (2005).

For the tests conducted at a distance of 0.7 m from the spray nozzle the calibration of the closest boundary had to be redone since this boundary was now also inclined at 30˚ and not perpendicular as in the first scenario. A schematic of the set-up is shown in Figure A.6.

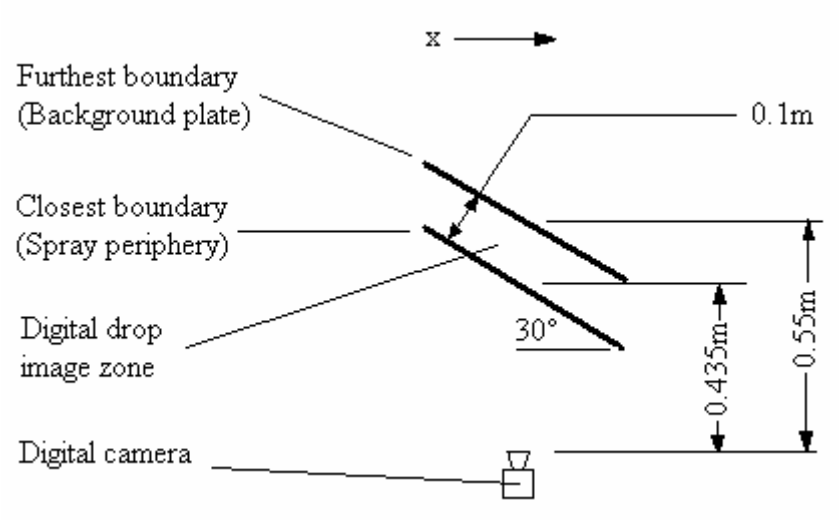

Figure A.6 Water drop size measurement equipment calibration (0.7 m).

The same calibration procedure was followed as described by Terblanche (2005) using a grid divided into uniform blocks placed at an angle of 30˚, with the centre of the grid 0.435 m away from the camera lens. From the image taken the blocks could be counted and the distance across the image calculated. Using geometry the distance from the camera to the furthest and closest point on the image could be calculated as 0.482 and 0.393 m respectively. The grid was then placed at both these distances and

images taken respectively. From these images the number of millimetres per pixel could be counted. All the calibrations were done with 640 x 480 pixel digital images. For the calibration the pixels in the x direction were used as one measuring unit. From the calibration data the following calibration curves could be set up for the further and closer boundaries.

Furthest boundary (Terblanche, 2005):

$$y = - 0.000075x + 0.313 \text{ mm/pixel} \quad \text{(A.21)}$$

Closest boundary:

$$y = - 0.000078125x + 0.25 \text{ mm/pixel} \quad \text{(A.22)}$$

APPENDIX B
THERMOPHYSICAL PROPERTIES OF FLUIDS

Thermophysical properties taken from Kröger (2004).

B.1 Thermophysical properties of dry air from 220K to 380 K at atmospheric pressure (101325 Pa)

Density:

$$\rho_a = \frac{p_a}{287 \cdot T}, \text{ kg/m}^3 \tag{B.1}$$

Specific heat:

$$c_{pa} = 1.045356 \times 10^3 - 3.161783 \times 10^{-1}\, T + 7.083814 \times 10^{-4}\, T^2 - 2.705209 \times 10^{-7}\, T^3, \text{ J/kgK} \tag{B.2}$$

Dynamic viscosity:

$$\mu_a = 2.287973 \times 10^{-6} + 6.259793 \times 10^{-8}\, T - 3.131956 \times 10^{-11}\, T^2 + 8.15038 \times 10^{-15}\, T^3, \text{ kg/sm} \tag{B.3}$$

Thermal conductivity:

$$k_a = -4.937787 \times 10^{-4} + 1.018087 \times 10^{-4}\, T - 4.627937 \times 10^{-8}\, T^2 + 1.250603 \times 10^{-11}\, T^3, \text{ W/mK} \tag{B.4}$$

Thermal diffusivity:

$$\alpha_a = \frac{k_a}{\rho_a \cdot c_{pa}}, \ \text{m}^2/\text{s} \tag{B.5}$$

Prandtl number:

$$Pr_a = \frac{\mu_a}{\rho_a \cdot \alpha_a} \tag{B.6}$$

B.2 Thermophysical properties of saturated water vapour from 273.15K to 380K

Vapour pressure:

$$p_v = 10^z, \text{ Pa} \qquad \text{(B.7)}$$

$$\begin{aligned} z &= 10.79586(1 - 273.16/T) + 5.02808 \log_{10}(273.16/T) \\ &\quad + 1.50474 \times 10^{-4}[1 - 10^{-8.29692\{(T/273.16)-1\}}] \\ &\quad + 4.2873 \times 10^{-4}[10^{4.76955(1 - 273.16/T)} - 1] + 2.786118312 \end{aligned}$$

Specific heat:

$$\begin{aligned} c_{pv} &= 1.3605 \times 10^3 + 2.31334\,T - 2.46784 \times 10^{-10}\,T^5 \\ &\quad + 5.91332 \times 10^{-13}\,T^6, \text{ J/kgK} \end{aligned} \qquad \text{(B.8)}$$

B.3 Thermophysical properties of mixtures of air and water vapour

Humidity ratio:

$$w = \left(\frac{2501.6\text{-}2.3263(T_{wb}\text{-}273.15)}{2501.6\text{+}1.8577(T\text{-}273.15)\text{-}4.184(T_{wb}\text{-}273.15)}\right)\left(\frac{0.62509p_{vwb}}{p_a\text{-}1.005p_{vwb}}\right) - \left(\frac{1.00416(T\text{-}T_{wb})}{2501.6\text{+}1.8577(T\text{-}273.15)\text{-}4.184(T_{wb}\text{-}273.15)}\right) \qquad \text{(B.9)}$$

Enthalpy of the air-vapour mixture per unit mass of dry air:

$$i_{ma} = c_{pa}(T - 273.15) + w[i_{fgwo} + c_{pv}(T - 273.15)], \text{ J/kg dry air} \qquad \text{(B.10)}$$

Specific heats are evaluated at (T + 273.15)/2 and the latent heat i_{fgwo} is evaluated at 273.15 K i.e. $i_{fgwo} = 2.5016\text{x}10^6$ J/kg

B.4 Thermophysical properties of saturated water liquid from 273.15K to 380K

Density:

$$\begin{aligned} \rho_w &= (1.49343 \times 10^{-3} - 3.7164 \times 10^{-6}T + 7.09782 \times 10^{-9}T^2 \\ &\quad - 1.90321 \times 10^{-20}T^6)^{-1}, \text{ kg/m}^3 \end{aligned} \qquad \text{(B.11)}$$

Specific heat:

$$c_{pw} = 8.15599 \times 10^{3} - 2.80627 \times 10\,T + 5.11283 \times 10^{-2}\,T^{2} - 2.17582 \times 10^{-13}\,T^{6},\ \text{J/kgK} \qquad \text{(B.12)}$$

Latent heat of vaporisation :

$$i_{fgw} = 3.4831814 \times 10^{6} - 5.8627703 \times 10^{3}\,T + 12.139568\,T^{2} - 1.40290431 \times 10^{-2}\,T^{3},\ \text{J/K} \qquad \text{(B.13)}$$

APPENDIX C

SAMPLE CALCULATION FOR VELOCITY, TRAJECTORY AND TEMPERATURE CHANGE OF A DROP INJECTED AT AN ANGLE INTO UPWARD FLOWING AIR

C.1 Input data

Ambient air drybulb temperature	$T_a = 293$ K
Ambient air wetbulb temperature	$T_{wb} = 286$ K
Atmospheric pressure	$p_a = 101325$ Pa
Absolute vertical air velocity	$v_a = 2.5$ m/s
Drop diameter	$d = 3$ mm
Drop temperature	$T_d = 313$ K
Drop absolute speed at injection point	$v_d = 3$ m/s
Drop injection angle from the horizontal plane	$\theta = -35^{\circ}$
Position co-ordinates at injection point	$(x, y) = (0, 0)$
Code time step	$\Delta t = 0.01$ s

C.2 Thermophysical properties of fluids

Thermophysical properties of fluids were calculated using the equations in Appendix B.

Density of air	$\rho_a = 1.205$ kg/m^3	(B.1)
Specific heat of air	$c_{pa} = 1006.7$ J/kgK	(B.2)
Dynamic viscosity of air	$\mu_a = 1.815 \times 10^{-5}$ kg/ms	(B.3)
Thermal conductivity of air	$k_a = 25.7 \times 10^{-3}$ W/mK	(B.4)
Thermal diffusivity of air	$\alpha_a = 2.117 \times 10^{-5}$ m^2/s	(B.5)
Prandtl number of air	$Pr_a = 0.711$	(B.6)
Vapour pressure at air wetbulb temperature	$p_{vwb} = 1.482 \times 10^3$ Pa	(B.7)
Vapour pressure at drop temperature	$p_{vd} = 7.318 \times 10^3$ Pa	(B.7)
Humidity ratio of air	$w_a = 0.0064$ kg/kg dry air	(B.9)

Density of water	$\rho_w = 996.7$ kg/m^3	(B.11)
Specific heat of water	$c_{pw} = 4.177 \times 10^3$ J/kgK	(B.12)
Latent heat of vaporization	$i_{fgw} = 2.407 \times 10^6$ J/kg	(B.13)

The diffusion coefficient between air and water vapour is given by:

$$D = \frac{0.3 \times 0.04357 \cdot T_a^{1.5}}{33.14 \cdot p_a} = \frac{0.3 \times 0.04357 \times 293^{1.5}}{33.14 \times 101325} = 1.952 \times 10^{-5} \text{ m}^2/\text{s} \qquad (4.21)$$

Schmidt number of air:

$$Sc_a = \frac{\mu_a}{\rho_a D} = \frac{1.815 \times 10^{-5}}{1.205 \times 1.952 \times 10^{-5}} = 0.771 \qquad (4.22)$$

C.3 Drop velocity and trajectory

The drop trajectory was determined by calculating the absolute velocity components in the x- and y directions for each time step and integrating the velocity with respect to time in both directions.

For the first time step the drop x and y direction absolute velocities were calculated from the initial drop absolute velocity and drop injection angle.

$$v_{dx} = v_d \cos(\theta) = 3 \cos(-35^\circ) = 2.457 \text{ m/s} \qquad (4.5)$$

$$v_{dy} = v_d \sin(\theta) = 3 \sin(-35^\circ) = -1.721 \text{ m/s} \qquad (4.6)$$

The air velocity relative to the drop was calculated using the x- and y drop absolute velocity components and the absolute vertical air velocity.

$$v_{ax} = -v_{dx} = -2.457 \text{ m/s} \qquad (4.7)$$

$$v_{ay} = v_a - v_{dy} = 2.5 - (-1.721) = 4.221 \text{ m/s} \qquad (4.8)$$

$$v_{ad} = \left(v_{ax}^2 + v_{ay}^2\right)^{0.5} = \left(-2.457^2 + 4.221^2\right)^{0.5} = 4.884 \text{ m/s} \qquad (4.9)$$

The relative air velocity was used to calculate the Reynolds number and drag coefficient.

$$Re = \frac{\rho_a v_{ad} d}{\mu_a} = \frac{1.205 \times 4.884 \times 0.003}{1.815 \times 10^{-5}} = 973 \tag{4.10}$$

$$\begin{aligned} C_D &= \frac{24(1+0.173Re^{0.657})}{Re} + \frac{0.413}{(1+16300Re^{-1.09})} \\ &= \frac{24(1+0.173 \times 973^{0.657})}{973} + \frac{0.413}{(1+16300 \times 973^{-1.09})} \\ &= 0.458 \end{aligned} \tag{4.11}$$

The x- and y drop relative velocities were then used to calculate the relative velocity angle Φ.

$$\Phi = \text{atan}\left(\frac{v_{ay}}{v_{ax}}\right) = \text{atan}\left(\frac{4.221}{-2.457}\right) = 120.2^{\circ} \tag{4.12}$$

The total drag force acting on the drop could also be calculated.

$$\begin{aligned} F_D &= 0.5\rho_a v_{ad}^2 C_D A_{fr} = 0.5 \times 1.205 \times 4.884^2 \times 0.458 \times \pi \times \frac{0.003^2}{4} \\ &= 4.652 \times 10^{-5} \text{ N} \end{aligned} \tag{4.13}$$

Knowing the relative velocity angle, which is the same as the drag force angle, the x and y components of the drag could be determined from:

$$F_{Dx} = F_D \cos(\Phi) = 4.652 \times 10^{-5} \cos(120.2^{\circ}) = -2.34 \times 10^{-5} \text{ N} \tag{4.14}$$

$$F_{Dy} = F_D \sin(\Phi) = 4.652 \times 10^{-5} \sin(120.2^{\circ}) = 4.02 \times 10^{-5} \text{ N} \tag{4.15}$$

The differential equations of motion for the x and y directions were solved using a first order Euler integration scheme with respect to time to calculate the new drop velocities in the x and y directions.

x direction:

$$\frac{dv_{dx}}{dt} = \frac{F_{Dx}}{m_d} = \frac{F_{Dx}}{\rho_w \pi \frac{d^3}{6}} = \frac{-2.34 \times 10^{-5}}{996.7\pi\left(\frac{0.003^3}{6}\right)} = -1.66 \text{ m/s}^2 \tag{4.3}$$

$$v_{dx}^{i+1} = v_{dx}^{i} + \frac{dv_{dx}}{dt} \cdot \Delta t = 2.457 - 1.66 \times 0.01 = 2.441 \text{ m/s} \tag{C.1}$$

y direction:

$$\frac{dv_{dy}}{dt} = \frac{F_{Dy}}{\rho_w \pi \frac{d^3}{6}} + \frac{\rho_a g}{\rho_w} - g = \frac{4.02\times10^{-5}}{996.7\pi\left(\frac{0.003^3}{6}\right)} + \frac{1.205\times9.81}{996.7} - 9.81$$
$$= -6.945 \text{ m/s}^2 \qquad (4.4)$$

$$v_{dy}^{i+1} = v_{dy}^{i} + \frac{dv_{dy}}{dt}\cdot\Delta t = -1.721 - (6.945\times0.01) = -1.79 \text{ m/s} \qquad (C.2)$$

With the drop velocity components and time step known the drop displacement components could be calculated.

Displacement in x direction:

$$x_d^{i+1} = x_d^{i} + \frac{dx}{dt}\cdot\Delta t = x_d^{i} + \frac{v_{dx}^{i} + v_{dx}^{i+1}}{2}\cdot\Delta t$$
$$= 0 + \left(\frac{2.457+2.441}{2}\right)\times0.01 = 0.0245 \text{ m} \qquad (4.17)$$

Displacement in y direction:

$$y_d^{i+1} = y_d^{i} + \frac{dy}{dt}\cdot\Delta t = y_d^{i} + \frac{v_{dy}^{i} + v_{dy}^{i+1}}{2}\cdot\Delta t$$
$$= 0 + \left(\frac{-1.721-1.790}{2}\right)\times0.01 = -0.0176 \text{ m} \qquad (4.18)$$

From the drop x and y direction displacements respectively, the drop position could be plotted for each time step.

C.4 Drop temperature change

To determine the drop temperature change the change in total internal energy of the drop, due to mass transfer and convective heat transfer was calculated.

The Sherwood number:

$$\begin{aligned} Sh &= 1+\left(\left(1+\frac{1}{Re\cdot Sc_a}\right)^{\frac{1}{3}} Sc_a^{\frac{1}{3}}\right)(0.752Re^{0.472}) \\ &= 1+\left(\left(1+\frac{1}{973\times 0.771}\right)^{\frac{1}{3}} 0.771^{\frac{1}{3}}\right)(0.752\times 973^{0.472}) \\ &= 18.75 \end{aligned} \qquad (4.24)$$

The vapour pressure calculated at the drop temperature was used to calculate the humidity ratio of the air at the drop surface, assuming a relative humidity φ of 100%.

$$w_d = \frac{0.622\varphi p_{vd}}{p_a - \varphi p_{vd}} = \frac{0.622\times 1\times 7.318\times 10^3}{101325 - 1\times 7.318\times 10^3} = 0.0484 \text{ kg/kg dry air} \qquad (4.26)$$

The mass transfer coefficients were calculated using the Sherwood number and diffusion coefficient.

$$h_D = \frac{Sh\cdot D}{d} = \frac{18.75\times 1.952\times 10^{-5}}{0.003} = 0.1220 \text{ m/s} \qquad (4.27)$$

The mass transfer coefficient where water is exposed to an air stream is given as:

$$\begin{aligned} h_d &= \frac{2h_D p_a}{R_v(w_d - w_a)(T_d + T_a)}\left(\frac{w_d}{(w_d + 0.622)} - \frac{w_a}{(w_a + 0.622)}\right) \\ &= \left(\frac{2\times 0.1220\times 101325}{461.52(0.0484 - 0.0064)(313+293)}\right)\left(\frac{0.0484}{(0.0484 + 0.622)} - \frac{0.0064}{(0.0064 + 0.622)}\right) \\ &= 0.1305 \text{ kg/m}^2\text{s} \end{aligned} \qquad (4.28)$$

With the mass transfer coefficients known the mass transfer from the drop could be calculated.

$$\begin{aligned} \dot{m}_v &= h_d A_d(w_d - w_a) = 0.1305\times\pi\times 0.003^2(0.0484 - 0.0064) \\ &= 1.55\times 10^{-7} \text{ kg/s} \end{aligned} \qquad (4.29)$$

The Nusselt number was calculated and used to calculate the convective heat transfer coefficient.

$$Nu = 2 + 0.6Re^{\frac{1}{2}}Pr_a^{\frac{1}{3}} = 2 + 0.6\times 973^{\frac{1}{2}}\times 0.711^{\frac{1}{3}} = 18.71 \quad (4.30)$$

$$h_c = \frac{Nu \cdot k_a}{d} = \frac{18.71\times 25.7\times 10^{-3}}{0.003} = 160.1 \ W/m^2K \quad (4.31)$$

The differential equation of temperature was solved using a first order Euler integration scheme with respect to time and the new drop temperature calculated.

$$\begin{aligned}\frac{dT_d}{dt} &= \frac{\left(-\dot{m}_v i_{fgw} - h_c A(T_d - T_a)\right)}{\left(m_d c_{vw}\right)} \\ &= \frac{\left(-1.55\times 10^{-7}\times 2.407\times 10^{6} - 160.1\times\pi\times d^2(313 - 293)\right)}{\left(1.409\times 10^{-5}\times 4.177\times 10^{3}\right)} \\ &= -7.877 \text{ K/s}\end{aligned} \quad (4.20)$$

$$T_d^{i+1} = T_d^i + \frac{dT_d}{dt}\cdot\Delta t = 313 + \left(-7.877\times 0.01\right) = 312.92 \text{ K} \quad (C.3)$$

Repeating these calculations for all the time steps the drop temperature change and mass transfer is calculated over a required period of time.

APPENDIX D

SAMPLE CALCULATION FOR A WATER DISTRIBUTION TEST IN THE COOLING TOWER TEST RIG

A sample calculation is done for one of the measurement cups on the measurement beam as described in Chapter 2 to determine the water mass velocity for a single point during a water distribution test conducted as described in Chapter 2. The following data was measured during a test:

Ambient temperature	$T_a = 295$ K
Atmospheric pressure	$p_a = 102100$ Pa
Air venturi water micro manometer reading	$\Delta h = 41$ mm
Water pressure transducer voltage output	$V_{wp} = 1.626$ V
Sample time	$\Delta t = 60$ s
Volume of water in measurement cylinder	$V_{cyl} = 0.0005$ m^3

The air flow rate through the cooling tower test rig and water flow rate to the spray nozzles in the test section was calculated as follows:

Pressure difference over air venturi flow meter:

$$\Delta p_a = \rho_w g \Delta h = 997 \times 9.81 \times 0.041 = 401 \text{ Pa} \qquad \text{(D.1)}$$

Air density:

$$\rho_a = \frac{p_a}{287 \cdot T_a} = \frac{102100}{287 \times 295} = 1.206 \text{ kg/m}^3 \qquad \text{(D.2)}$$

Air velocity in air venturi flow meter throat:

$$v_{vt} = c_n \left(\frac{2 \cdot \Delta p}{\rho_a \times 0.988} \right)^{0.5} = 0.96 \cdot \left(\frac{2 \times 401}{1.206 \times 0.988} \right)^{0.5} = 24.9 \text{ m/s} \qquad \text{(A.20)}$$

Venturi throat cross sectional area:

$D_{vt} = 0.455$ m

$$A_{vt} = \pi\left(\frac{D_{vt}}{2}\right)^2 = \pi\left(\frac{0.455}{2}\right)^2 = 0.1626 \text{ m}^2 \quad \text{(D.3)}$$

Cooling tower test rig test section frontal area:

$$A_{fr} = L \cdot W = 1.5 \times 1 = 1.5 \text{ m}^2 \quad \text{(D.4)}$$

Air velocity in tests section:

$$v_a = \frac{A_{vt} v_{vt}}{A_{fr}} = \frac{0.1626 \times 24.9}{1.5} = 2.7 \text{ m/s} \quad \text{(D.5)}$$

Pressure difference over water venturi flow meter:

$$\Delta p_w = 15.996 V_{wp} - 16.006 = 15.996 \times 1.626 - 16.006 = 10 \text{ kPa} \quad \text{(A.1)}$$

Water flow rate to spray nozzles:

$$\begin{aligned} Q &= 1.73\times10^{-7}\Delta p_w^5 - 2.915\times10^{-5}\Delta p_w^4 + 1.819\times10^{-3}\Delta p_w^3 - 5.363\times10^{-2}\Delta p_w^2 \\ &\quad + 9.511\times10^{-1}\Delta p_w + 4.887\times10^{-1} \\ &= 1.73\times10^{-7}\times10^5 - 2.915\times10^{-5}\times10^4 + 1.819\times10^{-3}\times10^3 - 5.363\times10^{-2}\times10^2 \\ &\quad + 9.511\times10^{-1}\times10 + 4.887\times10^{-1} \\ &= 6.18 \text{ l/s} \end{aligned}$$

(A.12)

The mass velocity in the fill material in the test section was calculated as follows:

Average volume flow rate into one measuring cup collected in a measurement cylinder:

$$Q_{cyl} = \frac{V_{cyl}}{\Delta t} = \frac{0.0005}{60} = 8.33\times10^{-6} \text{ m}^3/\text{s} \quad \text{(D.6)}$$

Area of measurement cup:

$$A_{cup} = \pi\left(\frac{d_{cup}}{2}\right)^2 = \pi\left(\frac{0.04}{2}\right)^2 = 1.257\times10^{-3} \text{ m}^2 \quad \text{(D.7)}$$

Average mass velocity measured with one measurement cup:

$$G_w = \frac{Q_{cyl}\rho_w}{A_{cup}} = \frac{8.33\times10^{-6}\times998}{1.257\times10^{-3}} = 6.61 \text{ kg/m}^2\text{s} \qquad \text{(D.8)}$$

APPENDIX E

PROCEDURE FOLLOWED TO DETERMINE THE MEASUREMENT CUP DIAMETER

Thacker (1997) used a measurement beam with measurement cup diameter 0.045m spaced 0.08 m apart. It was decided that the resolution obtained with this spacing was too coarse for the tests to be conducted in this project and a new measurement cup diameter and cup spacing was calculated.

In Figure E.1 a measurement cup at the edge of the spray area is shown. According to the manufacturer's data sheet for a medium pressure full cone nozzle the maximum spray angle, θ for a nozzle to fill height of 0.4 m and spray area diameter on the fill of 1.2 m is 56.3˚ from the vertical. The biggest particle to enter the measurement cup at this angle was chosen to be 20 mm since water drops are normally smaller than this. Using geometry, the angle Φ was calculated to be 1.59˚. Knowing the total angle, nozzle height and spray diameter, the measurement cup diameter x could be calculated from equation (E.1).

$$x = 0.4\tan(\theta+\Phi) - 0.6 = 0.4\tan(56.3+1.59) - 0.6 = 0.0374 \text{ m} \qquad \text{(E.1)}$$

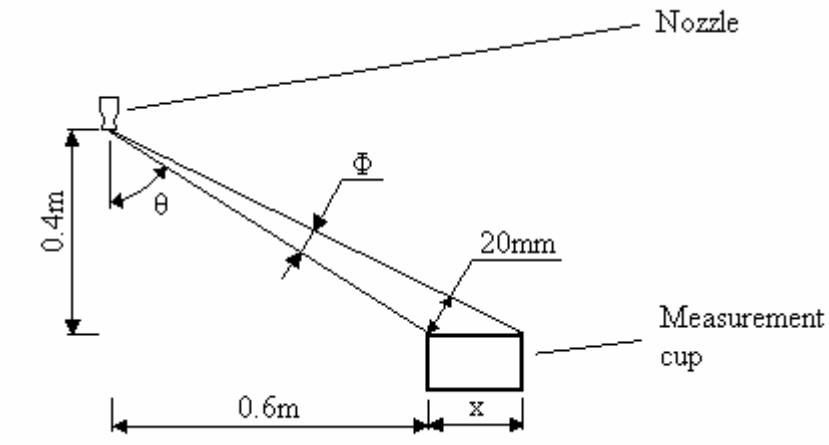

Figure E.1 Schematic of measurement cup diameter calculation.

It was decided to use standard 40 mm PVC tubing and the edges of the measurement cups were sharpened to provide a catchment diameter of 40 mm. The measurement cups were then spaced at 60 mm on the measurement beam since this provided a sufficiently fine measurement resolution for the nozzle's water distribution to be tested. Figure G.5 shows a photograph of the measurement beam.

APPENDIX F
SAMPLE CALCULATION FOR MERKEL NUMBER AND PRESSURE LOSS COEFFICIENT

F.1 Spray nozzle conditions

Ambient air drybulb temperature	$T_a = 293$ K
Ambient air wetbulb temperature	$T_{wb} = 286$ K
Atmospheric pressure	$p_a = 101325$ Pa
Absolute vertical air velocity	$v_a = 3$ m/s
Inlet water temperature	$T_{wi} = 313$ K
Outlet water temperature	$T_{wo} = 309.28$ K
Area sprayed	$A = 0.81$ m^2
Mass flow water	$\dot{m}_w = 4.5$ kg/s
Mass flow air	$\dot{m}_a = 2.916$ kg/s
Height sprayed	$L_{sp} = 1$ m

F.2 Sample calculation for Merkel equation

The Merkel number is calculated using the four point Chebyshev integral and data obtained from the FLUENT spray model simulation as given above.

The specific heat of water is evaluated at the mean water temperature:

$$(T_{wi}+T_{wo})/2 = (313+309.28)/2 = 311.14 \text{ K} \quad \text{(F.1)}$$

$$c_{pwm} = 4177 \text{ J/kgK} \quad \text{(B.12)}$$

The enthalpy differentials are dependent on the following intermediate temperatures:

$$T_{w(1)} = T_{wo}+0.1(T_{wi}-T_{wo}) = 309.28+0.1(313-309.28) = 309.65 \text{ K} \quad \text{(F.2)}$$

$T_{w(2)} = T_{wo} + 0.4(T_{wi} - T_{wo}) = 309.28 + 0.4(313 - 309.28) = 310.77$ K (F.3)

$T_{w(3)} = T_{wo} + 0.6(T_{wi} - T_{wo}) = 309.28 + 0.6(313 - 309.28) = 311.51$ K (F.4)

$T_{w(4)} = T_{wo} + 0.9(T_{wi} - T_{wo}) = 309.28 + 0.9(313 - 309.28) = 312.63$ K (F.5)

The relevant specific heat of air and water vapour are evaluated at:

$(T_{w(1)} + 273.15)/2 = (309.65 + 273.15)/2 = 291.40$ K (F.5)

Specific heat of air $c_{pa(1)} = 1006.7$ J/kgK (B.2)

Specific heat of water vapour $c_{pv(1)} = 1878.1$ J/kgK (B.8)

The pressure of saturated water vapour and the humidity ratio are evaluated at $T_{w(1)}$:

Vapour pressure $p_{vs(1)} = 6106.5$ Pa (B.7)

Humidity ratio of saturated air $w_{s(1)} = 0.0401$ kg/kg dry air (B.9)

Determine the enthalpy of saturated air at $T_{w(1)}$:

$i_{masw(1)} = 139810$ J/kg dry air (B.10)

Determine the enthalpy of air at $T_{w(1)}$:

$$\begin{aligned} i_{ma(1)} &= \dot{m}_w c_{pwm} \left(T_{w(1)} - T_{wo}\right)/\dot{m}_a + i_{mai} \\ &= 4.5 \times 4177 \left(309.65 - 309.28\right)/2.916 + 36231 \\ &= 38631 \text{ J/kg dry air} \end{aligned} \quad \text{(F.6)}$$

Find the difference in enthalpy:

$\Delta i_{(1)} = i_{masw(1)} - i_{ma(1)} = 139810 - 38631 = 101179$ J/kg dry air (F.7)

Repeat the above procedure for the cases of the other three intermediate temperatures:

$\Delta i_{(2)} = 102110$ J/kg dry air (F.7)

$\Delta i_{(3)} = 102970$ J/kg dry air (F.7)

$\Delta i_{(4)} = 104650$ J/kg dry air (F.7)

The four point Chebyshev integral is applied to the Merkel equation:

$$\frac{h_{dsp}a_{sp}L_{sp}}{G_w} = \int_{T_{wo}}^{T_{wi}} \frac{c_{pw}dT_w}{(i_{masw} - i_{ma})} \approx \frac{c_{pwm}(T_{wi}-T_{wo})}{4}\left(\frac{1}{\Delta i_{(1)}}+\frac{1}{\Delta i_{(2)}}+\frac{1}{\Delta i_{(3)}}+\frac{1}{\Delta i_{(4)}}\right)$$
$$= \frac{4177(313-309.28)}{4}\left(\frac{1}{101179}+\frac{1}{102110}+\frac{1}{102970}+\frac{1}{104650}\right)$$
$$= 0.1514$$

(5.5)

The Merkel number calculated using data obtained from the FLUENT spray model simulation was compared to spray zone data presented by Lowe and Christie (1961) and correlated by Kröger (2004) to give the Merkel number as a function of water and air mass velocity and spray zone height.

Water and air mass velocities:

$$G_w = \frac{\dot{m}_w}{A} = \frac{4.5}{0.81} = 5.56 \text{ kg/m}^2\text{s} \quad \text{(F.8)}$$

$$G_a = \frac{\dot{m}_a}{A} = \frac{2.916}{0.81} = 3.6 \text{ kg/m}^2\text{s} \quad \text{(F.9)}$$

Spray zone Merkel equation:

$$\frac{h_{dsp}a_{sp}L_{sp}}{G_w} = 0.2L_{sp}\left(\frac{G_a}{G_w}\right)^{0.5} = 0.2\times1\left(\frac{3.6}{5.56}\right)^{0.5} = 0.1610 \quad \text{(5.4)}$$

F.3 Pressure loss coefficient

Using data presented by Cale (1982) the pressure loss coefficient over the spray zone according to Kröger (1998) may be expressed as a function of water and air mass velocity and spray nozzle height:

$$K_{sp} = L_{sp}\left(\frac{0.4G_w}{G_a}+1\right) = 1\left(\frac{0.4\times5.556}{3.6}+1\right) = 1.617 \quad \text{(5.2)}$$

Density of air:

$\rho_a = 1.2 \text{ kg/m}^3$ (B.1)

The pressure drop over the spray zone is calculated by:

$$\Delta p_{tsp} = 0.5 K_{sp} \rho_a v_a^2 = 0.5 \times 1.617 \times 1.2 \times 3^2 = 8.73 \text{ Pa} \quad (5.3)$$

The pressure drop over the spray zone, Δp_{tsp} = 9.64 Pa, is used to calculate the pressure loss coefficient:

$$K_{sp} = \frac{2\Delta p_{tsp}}{\rho_a v^2} = \frac{2 \times 9.64}{1.2 \times 3^2} = 1.785 \quad (5.3)$$

APPENDIX G
PHOTOGRAPHS

Figure G.1 Photograph of low and medium pressure nozzles.

Figure G.2 Photograph of commercially available low pressure nozzles.

Figure G.3 Photograph of water flow venturi and pressure transducer.

Figure G.4 Photograph of fan and air flow venturi nozzle.

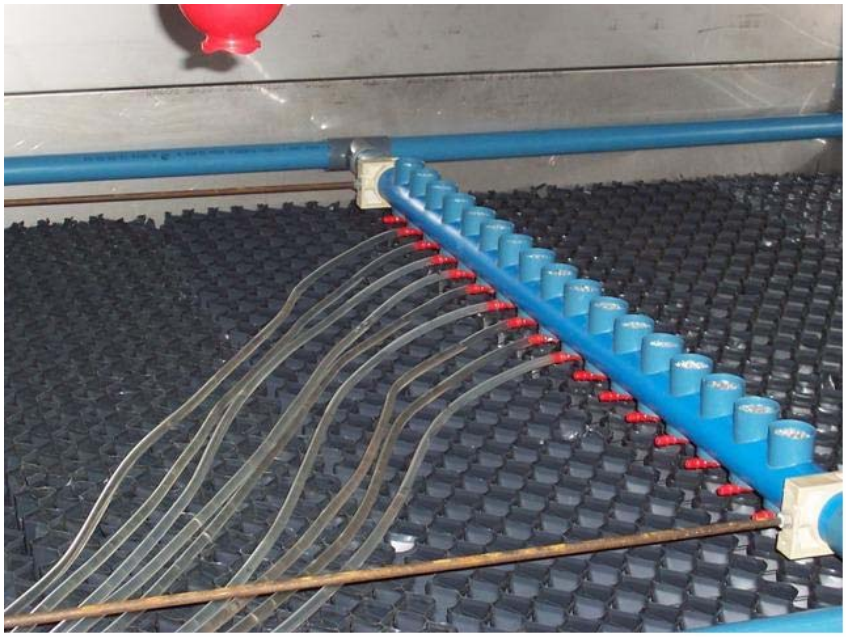

Figure G.5 Photograph of measurement beam.

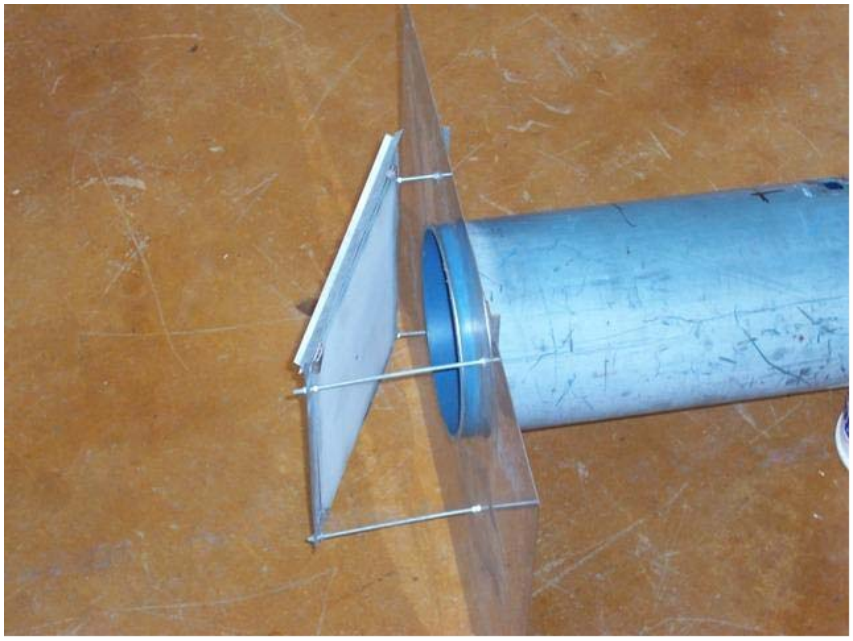

Figure G.6 Photograph of drop size measurement system.